

UNCLASSIFIED

AD NUMBER
AD475412
NEW LIMITATION CHANGE
TO Approved for public release, distribution unlimited
FROM Distribution: Further dissemination only as directed by U.S. Naval Postgraduate School, Monterey, CA, 1965 or higher DoD authority.
AUTHORITY
USNPS ltr, 21 Jan 1969

THIS PAGE IS UNCLASSIFIED

1965

475412

UNITED STATES NAVAL POSTGRADUATE SCHOOL



THESIS

AN ANALYSIS OF GROUND EROSION
CAUSED BY JET DOWNWASH IMPINGEMENT

* * * * *

David V. Shuter

This document may be further distributed by any holder only with specific prior approval of the U. S. Naval Postgraduate School (Code 035).

**AN ANALYSIS OF GROUND EROSION
CAUSED BY JET DOWNWASH IMPINGEMENT**

by

David V. Shuter

Captain, United States Marine Corps

Submitted in partial fulfillment of
the requirements for the degree of

**MASTER OF SCIENCE
IN
AERONAUTICAL ENGINEERING**

**United States Naval Postgraduate School
Monterey, California**

1 9 6 5

AN ANALYSIS OF GROUND EROSION
CAUSED BY JET DOWNWASH IMPINGEMENT

by

David V. Shuter

This work is accepted as fulfilling
the thesis requirements for the degree of

MASTER OF SCIENCE

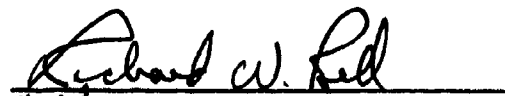
IN

AERONAUTICAL ENGINEERING

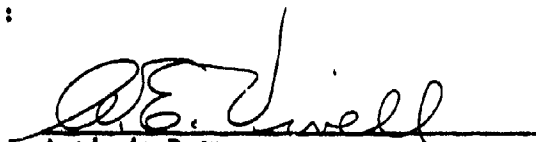
from the

United States Naval Postgraduate School


Faculty Advisor


Chairman
Department of Aeronautics

Approved:


Academic Dean

ABSTRACT

Recent interest in military VTOL/STOL aircraft employing unprepared landing sites has led to interest in the problem of landing surface erosion. Surface erosion is caused by the aerodynamic forces on ground particles existing within the flow field of an impinging jet. The inviscid flow field is discussed and the viscous ground boundary layer is analyzed utilizing both theory and available experimental data. A mathematical model of the process of entrainment of ground particles is constructed. Erosion rates in the form of erosion profiles are predicted for selected jet configuration and types of terrain. A criterion for entrainment, due to both lift and drag, was found and presented for selected distances from the jet centerline.

TABLE OF CONTENTS

Section	Title	Page
1.	Introduction	1
2.	History of the Problem	3
3.	The Flow Field	4
4.	The Ground Boundary Layer	6
5.	Analysis of Aerodynamic Forces Within the Boundary Layer	10
6.	Particle Entrainment and Incipient Erosion Rates	19
7.	Results and Conclusions	20
8.	Bibliography	89
Appendix	FORTTRAN Program	91

LIST OF ILLUSTRATIONS

Table		Page
I.	Nozzle Configurations and Radial Stations	23
II.	Types of Terrain Covered by Analysis	24
Figure		
1.	Flow Field Model of Circular Impinging Jet	25
2.	Variation of Inviscid Velocity with Radial Station	26
3.	Velocity Profile of Boundary Layer Near Stagnation	27
4.	Ground Plane Static Pressure Distribution	28
5.	Velocity Profiles of Laminar and Transition Boundary Layer	29
6.	Velocity Profile of Turbulent Boundary Layer	37
7.	Comparison of Shear Lift Force by Sphere and Cylindrical Methods	39
8.	Critical Particle Size for Drag Entrainment, Jet Velocity = 65 ft/sec, Nozzle Height = One Nozzle Diameter	40
9.	Critical Particle Size for Lift Entrainment, Jet Velocity = 65 ft/sec, Nozzle Height = One Nozzle Diameter	48
10.	Critical Particle Size for Drag Entrainment, Jet Velocity = 65 ft/sec, Nozzle Height = Four Nozzle Diameters	58
11.	Critical Particle Size for Lift Entrainment, Jet Velocity = 65 ft/sec, Nozzle Height = Four Nozzle Diameters	66
12.	Incipient Erosion Rate, Jet Velocity = 65 ft/sec, Nozzle Height = 1/2 Nozzle Diameter	67
13.	Incipient Erosion Rate, Jet Velocity = 500 ft/sec, Nozzle Height = 1/2 Nozzle Diameter	74
14.	Incipient Erosion Rate for Lift Entrainment, Jet Velocity = 500 ft/sec	81
15.	Boundary Layer Thickness of Laminar Boundary Layer	88

NOTATION

E	erosion rate - ft/sec ²
C _D	coefficient of drag
C _F	coefficient of skin friction
D _N	nozzle diameter - ft.
d	particle diameter - in.
F	force - lb.
L _w	lift force due to the effect of the ground - lb.
L _s	lift force due to shear - lb.
m	mass - lb sec ² /ft.
N	rotational flow parameter = $U_L/\omega_0 r_c$
N _R	Reynolds number = $U_L d \rho/\mu$
n	number of strips used in strip analysis
P _s	static pressure on the ground lb/ft ² .
q	shear velocity - ft/sec.
R	radial distance from jet centerline - ft.
r	radius of particle - in.
T	kinetic energy - ft lb.
U	velocity parallel to the ground - ft/sec.
V	velocity perpendicular to the ground - ft/sec.
x	coordinate parallel to the ground
y	coordinate perpendicular to the ground
y _{1/2}	vertical distance at which $U = \frac{U_{max}}{2}$ in turbulent boundary layer
z	height of nozzle above the ground - ft.
ρ	density - lb sec ² /ft ⁴ .
μ	viscosity - lb sec/ft ² .

- Θ angle measured from center of particle
- ω_0 vorticity
- δ boundary layer thickness

Subscripts

- crit. value at boundary layer transition
- J indicates value associated with jet
- L value at local point on the particle
- a property of air
- I value in inviscid flow
- p value associated with a particle
- c measurements made on cylinder in strip analysis
- s static
- A ambient
- n measurement made on a strip
- w value associated with effect of wall constraint
- S value associated with shear effect

1. Introduction.

The increasing interest in, and use of, VTOL aircraft and other vehicles with vertically directed fans and jets, particularly in military operations, has brought about concern for the deterioration of unprepared or soft landing sites. The downwash impingement caused by these aircraft results in a radially developed viscous flow field on the ground, producing forces adequate to cause entrainment of the ground particles. The reasons for concern with this problem are numerous. In addition to possible damage to the aircraft itself and the erosion of the landing surface there are the accompanying hazards to ground personnel, damage to ground support equipment, poor visibility afforded the pilot, and the violation of the military concept of concealment. The present study was designed to construct a mathematical model of the ground erosion process to allow prediction of the initial erosion rates for various types of terrain for various nozzle velocities and geometries. Previous work [1, 14, 15, 22, 23, 25] on the problem of erosion due to downwash impingement has been primarily an experimental examination of the problem with small scale jets.

The critical mechanism in the erosion process is the interaction of the ground boundary layer and the terrain particles. An analysis of this mechanism requires an understanding of the viscous mixing problem of a finite free jet, with the inviscid flow field extending radially from the jet center line as a result of the presence of the ground plane. An analysis of the phenomenon which produces entrainment of the ground particles is basically a study of the aerodynamic forces which exist in the ground boundary layer, as they are affected both by the decaying inviscid flow field above the boundary layer and by the constraint of the

ground surface. In analyzing the boundary layer forces available theory was utilized whenever possible, but since the radially developed boundary layer runs the gamut of stagnation point flow to turbulent flow and then complete decay, there are areas for which no theory or exact solution exists. To fill these holes, experimental data were used. Where exact solutions were used for the velocity profiles within the boundary layer, verification was made with experimental results if data existed.

The analysis was restricted to single jets of uniform dynamic pressure loading and circular cross-section under "no wind" conditions shown diagrammatically in Fig. 1. An axi-symmetric boundary layer was assumed, acting over a terrain of uniform particle size and density. Table I indicates the various combinations of nozzle characteristics and radial stations that were analyzed. The prediction of erosion rates is necessarily restricted to incipient motion, since the secondary effect of random collision is not readily treated by analysis and because the constantly changing shape of the ground surface is not accounted for as a continuing process. Although this work is restricted to consideration of uniform jets only, previous experiments by Morse [23] indicate that the dynamic pressure distribution due to downwash from rotor blades and ducted fans is similar to that for a uniform jet. The uniformity of the jet or downwash appears to be a critical factor only for ratios of jet altitude to diameter, Z/D_N , less than unity.

2. History of the Problem.

The classic problem of an impinging jet on a normal surface is not new, but its application to the field of VTOL aircraft, of either rotor or jet type, has been generated only within the past several years. The problem of surface erosion resulting from impinging downwash first received attention from Kuhn [14]. Kuhn's work was experimental employing small scale test equipment to make dynamic pressure distribution surveys. An experiment was conducted by fixing the nozzle dynamic pressure and raising or lowering it over terrain of known condition. Testing was done with various types of sod, dry and wet dirt, dust, and sand. Similar experimental tests have been conducted more recently by Morse [23].

The most recent work done on this problem is that of Brady and Ludwig [26]. This work consists of extensive experiments to investigate the characteristics of the impinging uniform jet, including both the inviscid flow and the ground boundary layer. Measurements of boundary layer velocity profiles were compared with theory and showed agreement to a limited degree. Some of these experimental results have been used in support of the present work. Vidal [28] has given an insight into the aerodynamic forces existing within the boundary layer.

3. The Flow Field.

In order to consider the mechanism of particle entrainment and ground erosion, a thorough knowledge of the flow field of the impinging jet is required. This flow field can effectively be separated into three regions. The first of these regions exists regardless of the presence of the ground surface, and is the region of viscous decay immediately external to the jet nozzle. Viscous decay of a free jet is a classical problem under uniform conditions. This region is characterized by the flaring out of the jet as the jet boundary mixes viscously with the stationary field external to it. Introducing a ground surface into the flow field, normal to the jet, does not invalidate the quantitative solution of free jet decay, but restricts its extent of usefulness. Experimentation has shown that the theory of viscous decay of a free jet is adequate for the impinging jet problem for nozzle heights of greater than about eight jet diameters. Since in this work, the interest is in nozzle heights of $Z/D_N < 8$, an additional region of viscous mixing with the stationary boundary must be studied and determined, beginning with the point at which the presence of the ground surface has altered the free jet characteristics. Further study must then be made of the viscous decay of the jet after impingement on the ground plane. To date no satisfactory theoretical method exists for dealing with the entire flow region in three dimensions. This problem may be partially overcome, however, by including the viscous decay region in describing the inviscid flow field.

Knowledge of the inviscid flow field is necessitated by the requirement that the inviscid velocity existing at the upper edge of the ground boundary layer be known. The difficulty in finding a theoretical solution for this region lies in the fact that although the boundary conditions

are well defined, the location of the free streamline is not known. Three dimensional theoretical solutions of this problem are limited to approximate methods. One of these, by LaClere [10], uses an electrolytic analog to determine the shape of the free streamline boundary. In this method the solution of the inviscid flow region was accomplished by relaxation techniques, predicting velocity and pressure distribution. Such a method of solution could be made to approach the exact solution to any desired degree of accuracy.

In the present work an exact solution of the inviscid flow field was not required. It was assumed adequate to use existing experimental data which compared favorably with the limited theoretical analyses available. In most instances it was found that the theoretical solutions were not in good agreement with the experimental data for $R/D_N < 4$. The approximate methods of predicting the characteristics of the inviscid flow region by use of an equivalent inviscid jet of greater diameter and decreasing dynamic pressure, or by replacing the jet with a cylindrical vortex sheet of constant radius extending to the ground, have proven unsatisfactory when compared with experimental data. In view of this, available experimental data were used in this work as a solution to the inviscid flow field. Fig. 2 shows the result of empirical equations fitted to these data.

The third flow region is that of the ground boundary layer. A thorough knowledge of this region was most important to this work as the ground particles are predominately immersed in the boundary layer, and the mechanics of particle movement originate with the aerodynamic forces resulting from the characteristics of the boundary layer.

4. The Ground Boundary Layer.

The key to the entire analysis of ground erosion is the mathematical model used for the boundary layer. Sound theoretical analysis of the boundary layer was used in this study when possible. Experimental results were used whenever the theory was non-existent or was in large disagreement with these results. For effective analysis the boundary layer may be divided into four regions. The first is the stagnation area boundary layer existing adjacent to the jet center line and extending to $R/D_N = .5$ or to a station directly under the original free jet boundary. This area is laminar for the conditions investigated. The solution of this region utilized the Himenez solution [18] for the uniform impinging jet on a perpendicular wall. Experimental results were not available for this region, so that the validity of this solution is not verified but was assumed. The Himenez solution in three dimensional flow, developed by Homann [18] is an exact solution utilizing the Navier-Stokes equations for axisymmetric flows. The solution was developed explicitly for stagnation conditions and the velocity profiles resulting from this have been employed to $R/D_N = 0.5$. The nondimensional velocity profile is shown in Fig. 3.

The second region is the laminar boundary layer extending from the edge of the original jet boundary to the radial station at which transition begins. A complete method of solution for this laminar region, by Smith [19], is well verified by experiment for $Z/D_N = .5$ [26], but gives little insight as to the limit of the laminar region and the beginning of transition. This point has been approximated by Brady and Ludwig [26] from considerations of neutral stability of the laminar boundary layer. A Reynolds Number at which the boundary layer becomes neutrally

stable can be determined [18] and may be converted to a jet nozzle Reynolds Number as a function of $(R/D_N)_{CRIT}$. On this basis the boundary layer becomes unstable at $R/D_N \approx 1.0$ for the jet velocities and nozzle diameters analyzed in this work. In view of this, and the fact that the inviscid velocity generally reaches a peak in the vicinity of $R/D_N = 1.0$ (Fig. 2), the beginning of transition was taken to be $R/D_N = 1.0$.

The transition region is even more difficult to define. Since fully turbulent flow exists theoretically when the pressure gradient on the ground surface is essentially zero, it was assumed that the transition region extended to the station where the pressure gradient could be taken to be negligible. Fig. 4 shows the static pressure distribution near the ground taken from an electrolytic analogy of the entire flow field [10]. The station at which the gradient, $\partial(\frac{P_1 - P_2}{\frac{1}{2} \rho V^2}) / \partial x$, was taken to be zero was $R/D_N = 2.0$. For the laminar and transition regions of the boundary layer experimental results were used to form the velocity profiles. This data, collected by Brady and Ludwig [26] for a limited range of jet velocities indicate that the non-dimensional velocity profile was almost completely independent of the jet velocity. The measurements were taken at nozzle heights in the range $Z/D_N = 0.5$ to 4.0 at four locations and for the radial range of $R/D_N = .5$ to 1.33 at six different stations. These twenty-four configurations are assumed to be fairly representative of the laminar and transition regions and are shown in Figs. 3a through 5h. For purposes of computation, curves were fitted to each group of data.

The fourth region in the boundary layer is the turbulent regime. It was assumed that this region begins at $R/D_N = 2$ as this is the

station at which the pressure gradient is assumed negligible. A limited amount of work has been done on theoretical solutions of turbulent boundary layers. One of these that appears applicable to the impinging jet is that of Glauert [7]. This single solution for velocity profiles in the turbulent boundary layer, assumed valid to $R/D_N = 4$, which is the radial limit of the analysis, has been verified by experimental results at $R/D_N = 1.33$ [26]. The uncertainty as to the characteristics of flow decay limit further extension of the analysis.

Glauert set up the boundary layer equations and found a similarity solution in which the form of the velocity distribution across the jet does not vary along its length. The solution is dependent upon the assumption of an effective eddy viscosity as required to satisfy the law due to Blasius for flow in a pipe as well as Prandtl's hypothesis for free turbulent flow. The first solution is considered to be valid near the ground surface, and the second to be valid above some determined distance from the ground surface. Fig. 6 shows these results in the form of a velocity profile, for the radial distances and nozzle heights considered in the present work. It was found that the shape of the velocity profile was essentially independent of both the radial distance and the nozzle height, but is dependent upon the nozzle Reynolds Number.

The turbulent region is characterized by a velocity profile which approaches a maximum, U_{max} , with increasing y and then decreases with further increase in y . As is shown in Fig. 1 it is expected that the turbulent boundary layer will continue to grow as long as there exists an inviscid upper boundary. Since very little attention has been given to this phenomenon of flow decay, and because of the nature of the turbulent solution, a fictitious boundary layer thickness is assumed for

this region. This is defined to be the thickness that exists at $U = U_{max}$. It was found that the nature of this assumption does not affect the overall results appreciably.

5. Analysis of Aerodynamic Forces Within the Boundary Layer.

The ground boundary layer is a non-uniform flow that is characterized by a large velocity gradient or shear layer extending over a large portion of the thickness. In addition, the ground surface or wall boundary at the base of the flow forms a constraint on the streamlines as they attempt to pass beneath an obstacle bedded in the ground surface.

There are three distinct forces that exist within the boundary layer. These are: 1) Drag due to the horizontal velocity component of the flow; 2) lift due to the proximity of the wall; and 3) lift due to the velocity gradient in the flow. There is no theory available which deals with this problem in general. Therefore it was necessary to piece together an approximate theory for each of the various forces.

Drag Force.

The drag force was the easiest to account for. To simplify the analysis in a non-uniform flow, a strip analysis was made in which the spherical particle was divided into a number of layers and it was assumed that a uniform flow acted upon each layer. Knowing the velocity of the flow on each layer, from the velocity profile, the force on each layer and the summation of horizontal forces were developed. The calculation of the total drag force employed the drag coefficient of cylindrical bodies measured by Hoerner [9]:

$$N_R < 100$$

$$C_D = 30./N_R^{.699}$$

$$100 < N_R < 10^4$$

$$C_D = 1.44/N_R^{.0396}$$

$$N_R > 10^4$$

$$C_D = 1.18$$

In addition to the drag force the skin friction force was calculated for each layer and summed for the particle. The friction force, a result of a minute boundary layer effect on the particle itself, was relatively small but in some cases significant. For spheres in low Reynolds Number flows the skin friction coefficient can be approximated by:

$$C_F = .664 / (N_R)^{1/2}$$

The tendency of the velocity gradient to cause a moment on the particle was neglected.

Lift Due to Wall Proximity.

Theories accounting for the effect of a wall constraint in non-uniform flow do not exist, but this effect was estimated using the existing theory for uniform flow [12]. The effect of the ground surface constraint is to distort the flow over the sphere, crowding the streamlines, causing a negative lift force. The theory is based on kinetic energy considerations, maintaining equilibrium on a sphere in the presence of a wall. For a sphere, in a flow parallel to the wall, an upward force is required to maintain equilibrium, indicating that the sphere must be attracted to the wall.

The method of calculation of this lift force was similar to that of drag. The strip approximation method was used to determine an average local velocity over a particular strip. It was then assumed that this average local velocity was that existing in the vicinity of the stagnation

point, realizing that the stagnation point is shifted toward the region of higher velocities. The lift then becomes a function of the sphere size and the average local velocity, for a particle bedded on the ground plane. The kinetic energy of a sphere in a moving fluid near an infinite fixed wall can be approximated by a first order solution [12]:

$$T = \frac{1}{2} (A V_L^2 + B U_L^2)$$

where:

$$A = \frac{1}{2} m_a (1 + \frac{3}{8} r^3 / y^3)$$

$$B = \frac{1}{2} m_a (1 + \frac{3}{16} r^3 / y^3)$$

m_a = mass of fluid displaced by the sphere.

From Lagrange's equation for equilibrium:

$$d/dt (\partial T / \partial \dot{x}) - \partial T / \partial x = 0$$

If the sphere is to be maintained in equilibrium, the result is a force exerted on the sphere:

$$F_x = d/dt (\partial T / \partial \dot{x}) - \partial T / \partial x$$

$$F_y = d/dt (\partial T / \partial \dot{y}) - \partial T / \partial y$$

Making the substitutions, the force exerted on the sphere in the y or vertical direction becomes:

$$\begin{aligned} F_y &= d/dt (\partial T / \partial V_L) - \partial T / \partial y \\ &= d/dt (A V_L) - \partial / \partial y (\frac{1}{2} A V_L^2 + \frac{1}{2} B U_L^2) \end{aligned}$$

$$F_y = A V_L - (-1/2 V_L^2 \cdot 9/16 m_a r^3 / y^4 - 1/2 U_L^2 \cdot 9/32 m_a r^3 / y^4)$$

Assuming that $V, \dot{V} \ll 1$.

$$F_y = 9/64 U_L^2 m_a r^3 / y^4$$

where:

$$m_a = \rho_a \cdot 4/3 \pi r^3$$

we get:

$$F_y = 3/16 \rho_a U_L^2 \pi r^6 / y^4$$

Assuming that the particle is very close to the ground such that;

$$y - r \ll 1$$

or

$$y \approx r$$

the lift due to the wall constraint becomes:

$$L_w = -3/16 \rho_a U_L^2 \pi r^2$$

For the strip analysis, summation yields:

$$L_w = (-3/16 \rho_a \pi r^2 \sum_n U_{Ln}) / n$$

Lift Due to Velocity Gradient.

There have been a number of theoretical studies of the effects of velocity gradients or shear on aerodynamic forces. Most of these, however, deal either with an unbounded flow or two dimensional flow. In comparing two dimensional solutions with three dimensional solutions it

was noted that the difference is a term in the three dimensional solution describing the lateral component of flow. For the axi-symmetrical case dealt with here, this component was assumed negligible. A solution for non-uniform flow on cylinders by Murray and Mitchell [13] was employed in conjunction with a strip analysis.

In the strip analysis, the particle was divided into layers of circular cylinders situated such that their centers formed a line perpendicular to the flow. Beginning with the final result of Murray and Mitchell, the dimensionless shear velocity on each cylinder was found to be:

$$g' = - \left\{ \sin \theta \left[\cosh (\sin \theta) - \frac{1}{N} \sinh (\sin \theta) \right] \right. \\ \left. + \frac{2}{N} \sum_{n=1}^{\infty} (-1)^n \frac{I_{2n}(1)}{K_{2n}(1)} K'_{2n}(1) \cos (2n \theta) \right. \\ \left. + 2 \sum_{n=0}^{\infty} (-1)^{n+1} \frac{I_{2n+1}(1)}{K_{2n+1}(1)} K'_{2n+1}(1) \sin (2n+1) \theta \right\}$$

where:

$$K'_{2n}(1) = d/da [K_{2n}(a)]_{a=1}$$

$$K'_{2n}(1) = \frac{1}{2} \sum_{r=0}^{n-1} \frac{(-1)^r (n-r-1)!}{r!} (n-2r) (2)^{n-2r-1} (-2)$$

$$+ (-1)^{n+1} \sum_{r=0}^{\infty} \frac{(n/2+r) (1/2)^{n+2r-1}}{r! (n+r)}$$

$$\left\{ \log \frac{1}{2} - \frac{1}{2} [\psi(r+1) + \psi(n+r+1)] \right\}$$

$$+ (-1)^{n+1} \sum_{r=0}^{\infty} \frac{(1/2)^{n+2r}}{r! (n+r)!}$$

and

$$\begin{aligned}\Psi(1) &= \text{Euler's Constant} \\ &= 0.57721567\end{aligned}$$

The dimensional shear velocity is given by:

$$g = g' U_L$$

which is of the form (when squared):

$$g^2 = U_L^2 (A^2 + B^2 + C^2 + 2AB + 2AC + 2BC)$$

Where:

$$A^2 = \sin^2 \theta [\cosh^2 (\sin \theta - 2/N \cosh (\sin \theta) \cdot$$

$$\sinh (\sin \theta) + 1/N^2 \sinh^2 (\sin \theta)]$$

$$B^2 = 4/N^2 \left[\sum_{n=1}^{\infty} (-1)^n \frac{I_{2n}(1)}{K_{2n}(1)} K'_{2n}(1) \right]^2 \left[\sum_{n=1}^{\infty} \cos 2n\theta \right]^2$$

$$C^2 = 4 \left[\sum_{n=0}^{\infty} (-1)^{n+1} \frac{I_{2n+1}(1)}{K_{2n+1}(1)} K'_{2n+1}(1) \right]^2 \left[\sum_{n=0}^{\infty} \sin (2n+1)\theta \right]^2$$

$$2AB = 4/N \left[\sum_{n=1}^{\infty} (-1)^n \frac{I_{2n}(1)}{K_{2n}(1)} K'_{2n}(1) \cos 2n\theta \right] \cdot$$

$$\sin \theta [\cosh (\sin \theta) - 1/N \sinh (\sin \theta)]$$

$$2AC = 4 \left[\sum_{n=0}^{\infty} (-1)^{n+1} \frac{I_{2n+1}(1)}{K_{2n+1}(1)} K'_{2n+1}(1) \sin (2n+1)\theta \right] \cdot$$

$$\sin \theta [\cosh (\sin \theta) - 1/N \sinh (\sin \theta)]$$

$$2BC = \frac{8}{N} \left[\sum_{n=1}^{\infty} (-1)^n \frac{I_{2n}(C)}{K_{2n}(C)} K'_{2n}(C) \cos 2n\theta \right] \cdot$$

$$\left[\sum_{n=0}^{\infty} (-1)^{n+1} \frac{I_{2n+1}(C)}{K_{2n+1}(C)} K'_{2n+1}(C) \sin (2n+1)\theta \right]$$

U_L is the local velocity at the center of each cylinder, and I , K and K' are Bessel functions of the first and second kind, and the derivative of the second kind respectively. N is a flow parameter dependent upon local velocity, radius of the cylinder and the vorticity at the stagnation point, and is defined as: $N = U_L / \omega_0 r_c$. The determination of the flow parameter was approximated since the stagnation point on each cylinder could not be known in advance of the calculations. In order to keep the shear velocity in the direction it was known to flow, a lower bound of $N = 1$ could be established. If ω_0 and U are evaluated at the geometric centers of the cylinders, experimentation has indicated an upper bound of $N = 3$ [13]. After analyzing the computed results of shear velocity with values of N ranging from 1.1 to 10, a value of $N = 1.5$ was accepted as being representative of the physical model.

Having found the shear velocity the lifting force due to shear effect was calculated for each cylinder and summed over the particle. The resulting expression is:

$$L_s = \sum_n -b r_c \frac{\rho}{2} \int_0^{2\pi} (U_{Ln}^2 - g_n^2) \sin \theta d\theta$$

Where:

r_c = radius of cylindrical strips

b = width of strip

n = number of strips

Noting that:

$$\int_0^{2\pi} U_n^2 \sin \theta d\theta = 0$$

We have:

$$L_S = \sum_n b r_c \frac{1}{2} U_n^2 \int_0^{2\pi} (A^2 + B^2 + C^2 + 2AB + 2AC + 2BC) \sin \theta d\theta$$

In evaluating the integral we have:

$$\int_0^{2\pi} 2BC \sin \theta d\theta = 8/N \left[\sum_{n=1}^{\infty} (-1)^n \frac{I_{2n}(1)}{K_{2n}(1)} K'_{2n}(1) \right]$$

$$\left[\sum_{n=0}^{\infty} (-1)^{n+1} \frac{I_{2n+1}(1)}{K_{2n+1}(1)} K'_{2n+1}(1) \right] \left[\sum_{n=1}^{\infty} \int_0^{2\pi} \cos 2n\theta \sin \theta d\theta \right]$$

$$\left[\sum_{n=0}^{\infty} \int_0^{2\pi} \sin (2n+1)\theta \sin \theta d\theta \right] = 0$$

Since the last two integrals are identically zero. Further we may write:

$$\begin{aligned} \int_0^{2\pi} A^2 \sin \theta d\theta &= \int_0^{2\pi} \sin^3 \theta \cosh^2 (s \sin \theta) d\theta \\ &- \frac{2}{N} \int_0^{2\pi} \sin^3 \theta \cosh (s \sin \theta) d\theta \\ &+ \frac{1}{N^2} \int_0^{2\pi} \sin^3 \theta \sinh^2 (s \sin \theta) d\theta \end{aligned}$$

$$\int_0^{2\pi} A^2 \sin \theta d\theta = -2/N \int_0^{2\pi} \sin^3 \theta \cosh(\sin \theta) \sinh(\sin \theta) d\theta$$

Since the first and last integrals are identically zero.

Due to the complexity of the above expressions and the difficulty of integration, it was desired to check this method with another method [29] of a much more approximate nature for calculating the lift due to shear.

The alternate method of calculating lift assumes that the previously discussed lift due to the ground surface constraint is negligible and that the lift forces on the particle can be estimated by using the solution of Hall 8 for a sphere in a two dimensional uniform shear flow. In addition, the approximate method assumes that the sphere rests on a bed of spheres of the same diameter and that the pressure on the bed is the ambient stream static pressure. The lift coefficient then becomes simply a function of the local slope of the velocity profile, the local velocity on the sphere, and the radius of the sphere. In view of the many restrictions placed on this solution it was used only as an order of magnitude check on the other solutions. Fig. 7 shows a comparison of the two solutions.

6. Particle Entrainment and Incipient Erosion Rates.

Only a few of the possible types of terrain to which a mathematical analysis of the erosion rates might be practically applied, were investigated. Uniform particles ranging in size from .003 in. to .125 in. in diameter were investigated. The smallest sizes represent loose dirt and the larger diameters represent sand or sandy gravel, with .125 in. being representative of small gravel type rock. It was assumed that all terrain was without any moisture content. The densities of the particles ranged from 75 lb/ft³ for loose dirt to 125 lb/ft³ for gravel. Table II lists the various terrain particles analyzed.

There are three possibilities for entrainment of the ground particle. The first is that it may have enough lift force on it to be lifted directly from the ground surface into the free stream. The second is that after rolling motion is started due to the drag force, it may be able to gain the additional lift required for entrainment in the free stream. The third is that with many particles rolling at different velocities the random collision of particles that follows will bounce some of them into the inviscid stream. Only incipient motion is within the scope of this work, hence it was assumed that any particle which was moved contributed to the erosion rate.

The net drag force and the net lift force, including both mechanisms of lift, were computed for each of the particles, at each of thirteen radial stations on the ground surface for each of the nozzle configurations studied. To calculate the initial net drag force, the previously mentioned ground surface model of nested particles was assumed using a coefficient of static friction of .

7. Results and Conclusions.

The particle size criteria for lifting entrainment and drag entrainment are shown in Figs. 8, 9, and 10 in which the particle size is plotted versus a load parameter at various stations with jet velocity and jet height as parameters. The load parameter is defined as the particle density divided by the dynamic pressure in the free stream. The lift entrainment criterion predicts that an optimum particle size, the particle size most prone to entrainment, exists for all radial stations and that the critical density increases with radial distance to a certain R/D_N . The optimum particle size for lift entrainment occurs because particles smaller than the optimum are affected by much smaller velocities, and particles larger than optimum are affected more by a flow region where the shear gradient, $\partial u / \partial y$, approaches zero.

The drag criterion indicates that extremely small particles of 0.02 in. diameter or less, up to very high densities will roll on the ground (see Fig. 8). As the particle size is increased the possibility of rolling decreases rapidly up to a particle diameter of 0.03 in. at which size the tendency to roll increases again, since the larger velocities in the boundary layer begin to act on the particle, until an optimum diameter of approximately 0.06 in. is reached. For radial distances less than $R/D_N = .1$, velocities in the boundary layer are not sufficient to move large particles of high density. The range of optimum size particle for drag entrainment of approximately .03 to .09 is consistent for all radial stations. It is of particular significance that the range of optimum particle diameter for both lift and drag is very nearly equal to the boundary layer thickness at the particular radial station being considered.

The incipient erosion rates for selected densities, particle sizes, and nozzle configurations are shown in Figs. 11 and 12. These are found by combining as vectors the incipient horizontal and vertical accelerations of the particles. This was assumed to be proportional to the incipient erosion rate. The erosion rate, normalized by the maximum rate, is plotted versus the nondimensional radial distance. For all configurations and particles the erosion profile is maximum in the area $.5 < R/D_N < 2.0$. The maximum erosion for larger particles occurs near $R/D_N = 1$, and then drops off sharply with increased radial distance. As the particles become smaller a maximum erosion occurs closer to the perimeter of the jet nozzle and a second maximum begins to occur at $R/D_N \approx 1.3$. This occurs after the transition region has begun to form and where the onset of turbulence can affect the particles. Fig. 13 shows the incipient rate of lift entrainment by itself and indicates that, in general, the shape of the erosion profile can be attributed to the lift forces.

The results shown in the graphs represent only a few configurations selected from the large amount of data collected. In viewing all of the results and comparing the many combinations of configurations, it was found that the variation of ground erosion rates was principally a function of the dimensionless radial distance from the jet centerline and the size of the particle for a given nozzle height, Z/D_N . The erosion rate was nearly proportional to the particle density except near the stagnation point, where the erosion rates were very small.

From these results it may be concluded that for ground particles of less than .04 in. diameter the incipient erosion rate has two maximum points. One in the vicinity of the perimeter of the jet nozzle, and the

second at a radial distance approximately two diameters from the stagnation point. For very small particles and low jet velocities the second maximum is the most significant. In all other cases where two maximum points exist, the first is the most significant. For ground particles whose diameters are greater than .04 in. a single maximum point exists near the perimeter of the jet nozzle. As the particle size increases the influence of the turbulent region decreases.

It was concluded that particles of approximately .02 in. diameter or less would entrain due to drag even at very high densities or very low velocities. For particles larger than approximately .02 in., an optimum size of approximately .06 in. exists up to radial distances of four nozzle diameters for drag entrainment. An optimum particle size most susceptible to entrainment due to lift exists in the range of .07 to .12 in. diameter for radial distances up to four nozzle diameters.

Also, it may be concluded that varying the nozzle diameter had very little effect on the dimensionless erosion rate; hence in the final analysis the nozzle diameter was not considered as a parameter. Moreover, while the actual erosion rates were approximately linearly dependent upon the jet velocity, the dimensionless erosion profile appeared to be independent of jet velocity, with the exception of the order of importance of the maximum points.

NONDIMENSIONAL RADIAL DISTANCE FROM JET - R/D_H													
NON-DIMENSIONAL	.05	.1	.2	.3	.4	.5	.667	.83	1.0	1.17	1.33	2.0	4.0
NOZZLE HEIGHT z/D_H	.5									.5	.5		
	1.0									2.0	1.0		
	2.0									4.0	2.0		
	4.0										4.0		
JET VELOCITY V_J - ft/sec	65												
	191												
	500												

TABLE I

NOZZLE CONFIGURATIONS AND RADIAL STATIONS ANALYZED

PARTICLE DENSITY lb/ft ³	PARTICLE SIZE - DIAMETER IN INCHES			
	→.003	→.06	→.2	→.5
75	DUST	LOOSE DIRT AND CLAY	CLAY	CLAY
90				
105		SAND	GRAVEL	GRAVEL
120				
135		SANDY GRAVEL	ROCK	ROCK
150				

TABLE II
TYPES OF TERRAIN COVERED BY ANALYSIS

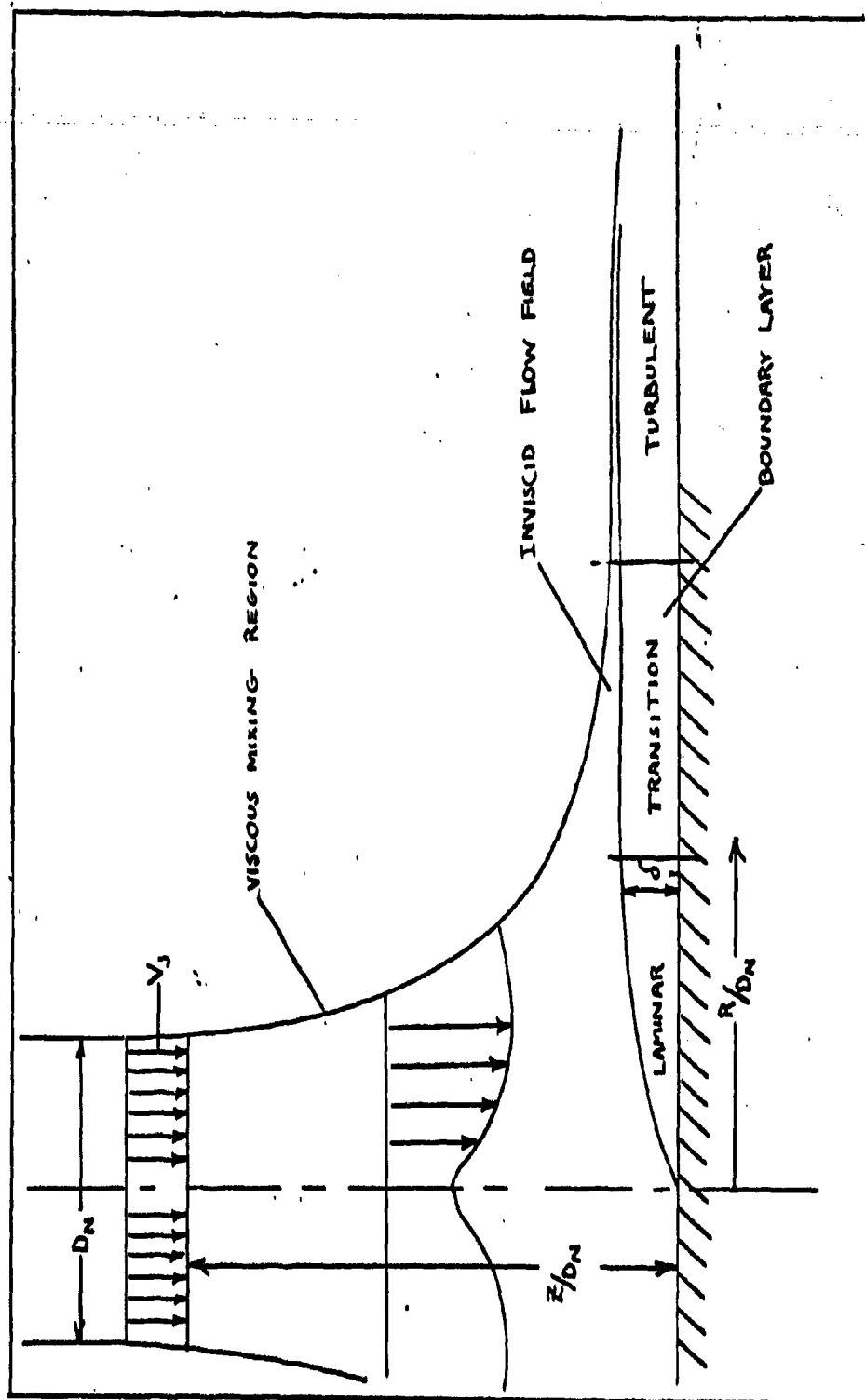


FIGURE 1
FLOW FIELD MODEL OF CIRCULAR IMPINGING UNIFORM JET

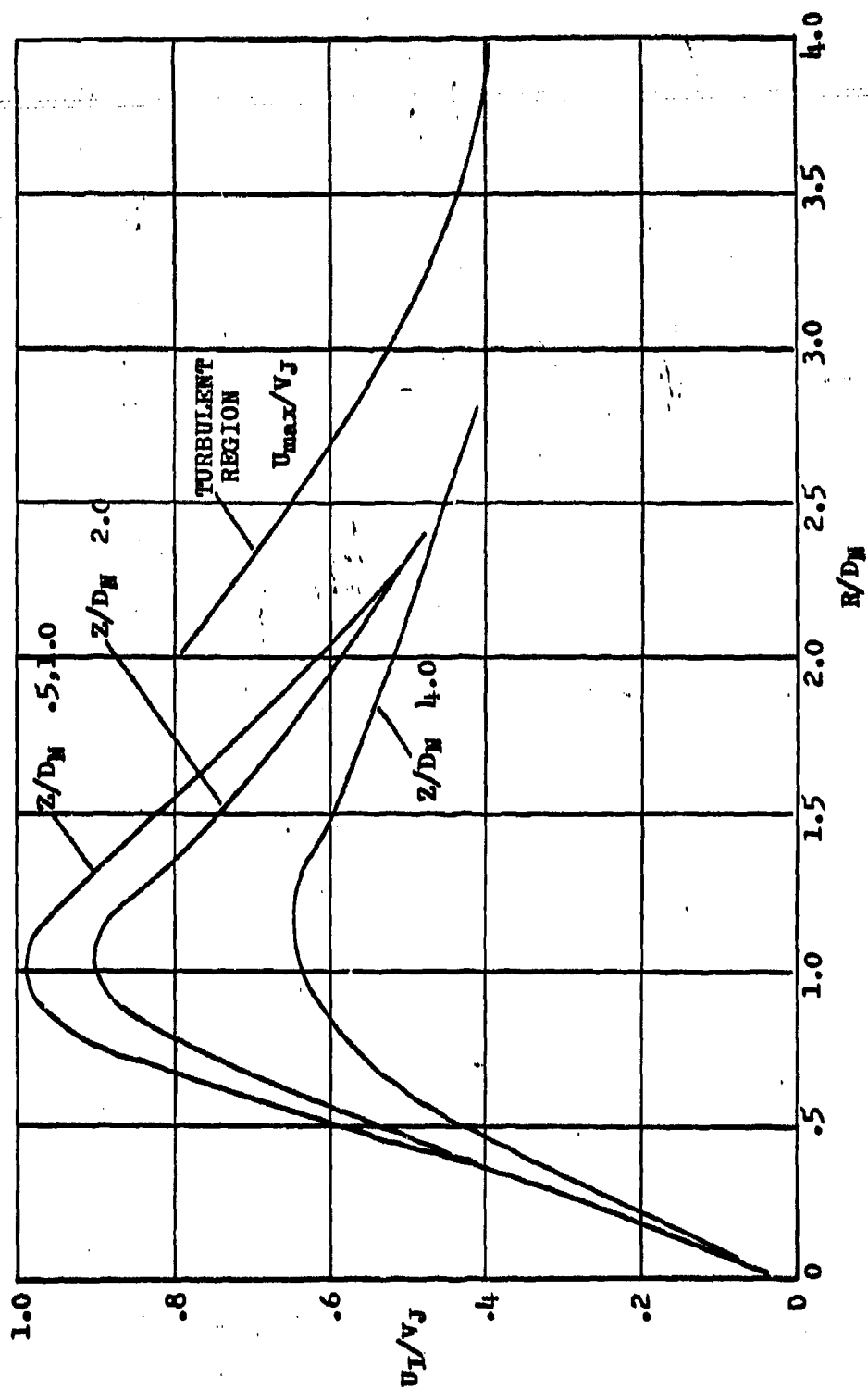


FIGURE 2
VARIATION OF INVISCID VELOCITY WITH RADIAL STATION

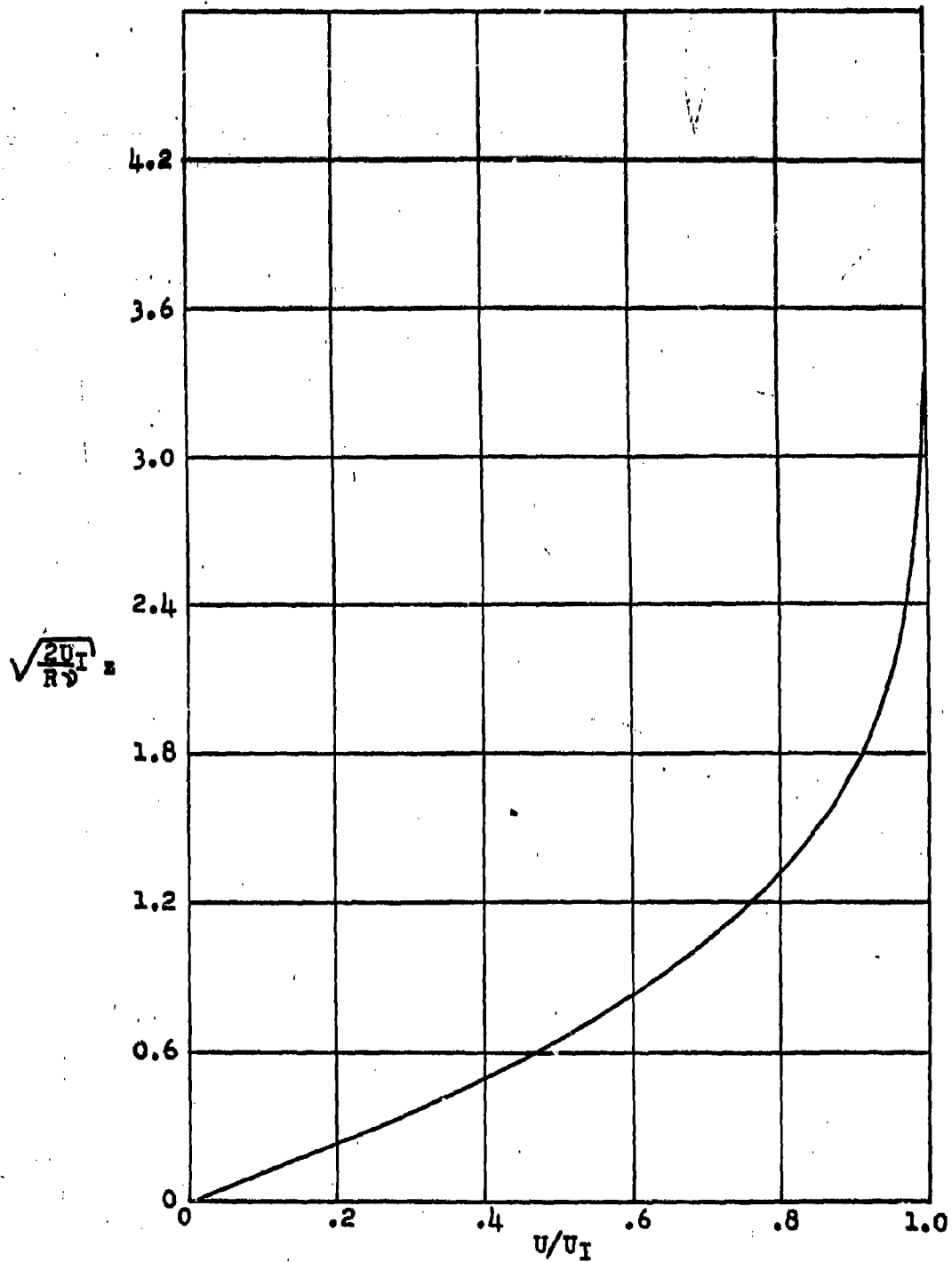


FIGURE 3

VELOCITY PROFILE FOR BOUNDARY LAYER
NEAR STAGNATION POINT

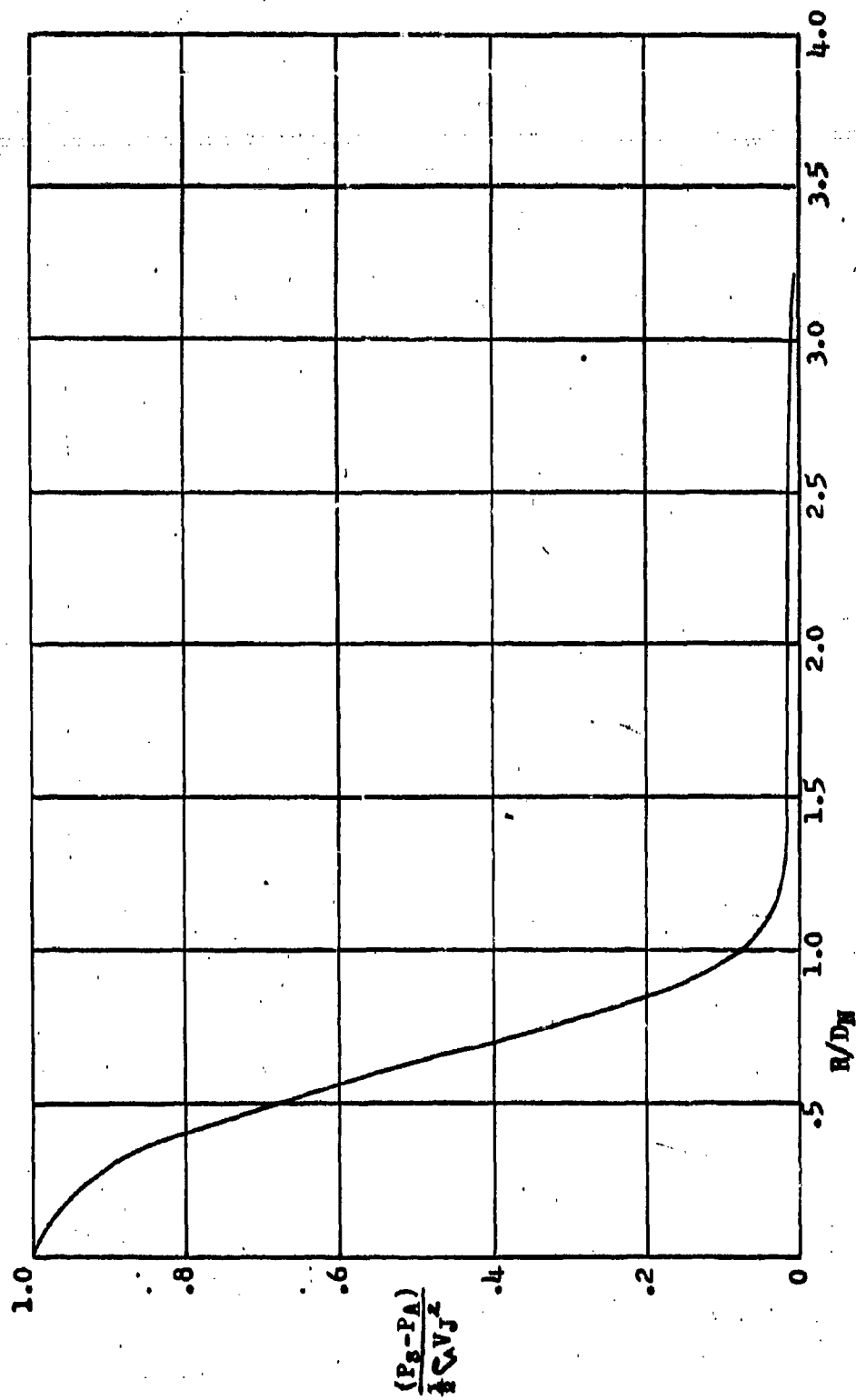


FIGURE 4

GROUPED PLANE STATIC PRESSURE DISTRIBUTION - $z/D_H > .5$

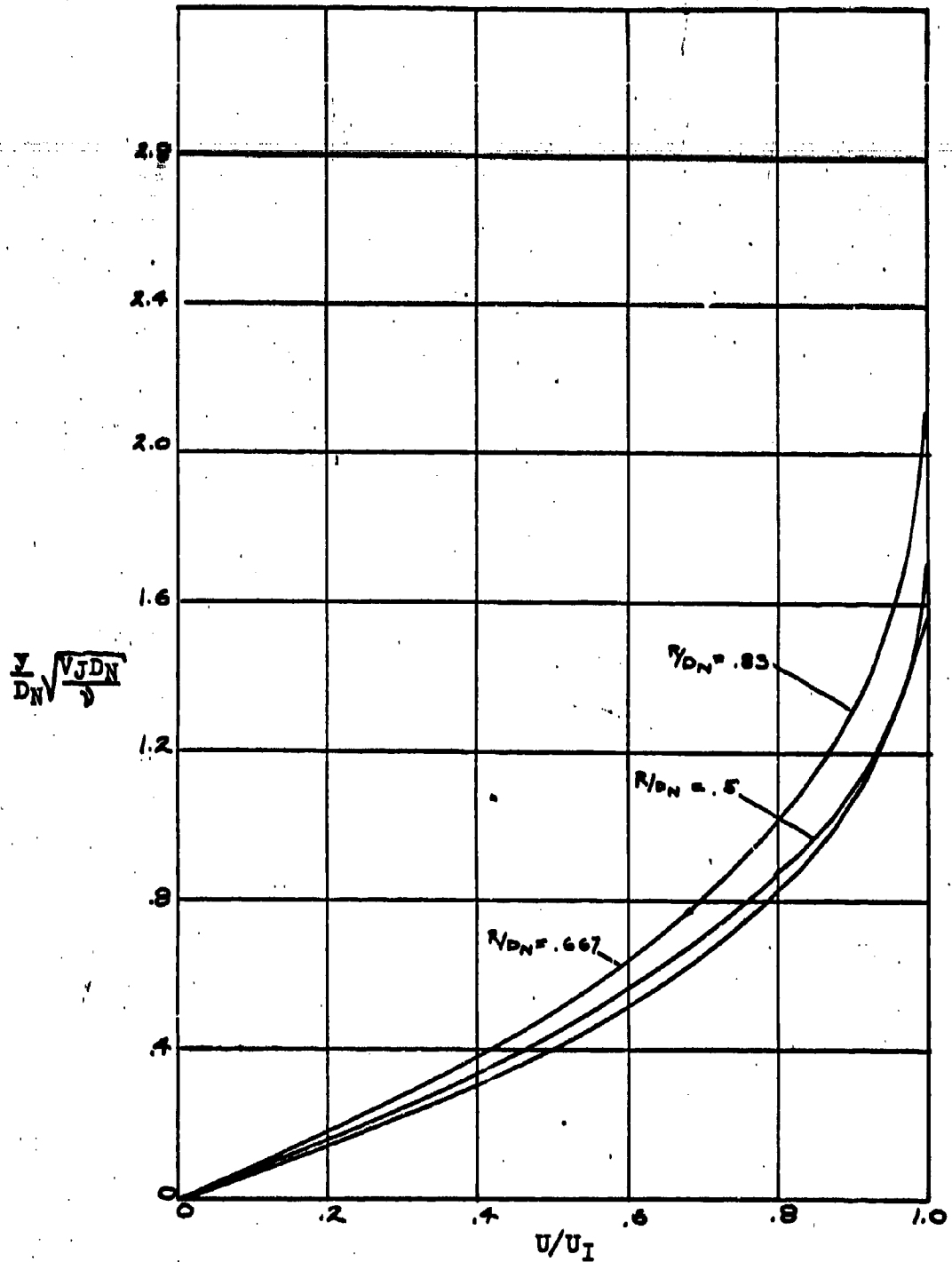


FIGURE 5a

VELOCITY PROFILES OF LAMINAR AND TRANSITION
BOUNDARY LAYER, $z/D_N = .5$

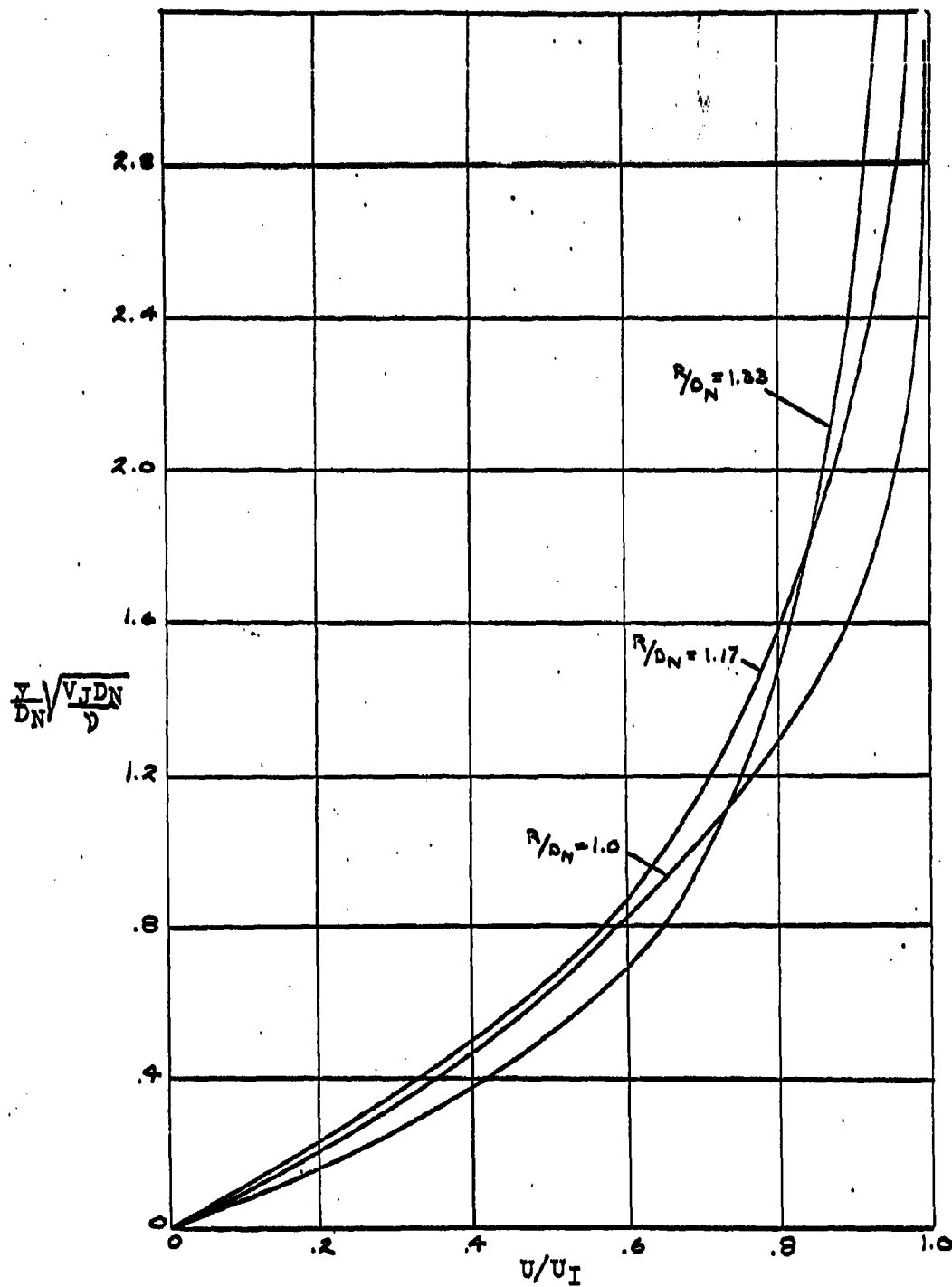


FIGURE 5b
VELOCITY PROFILES FOR LAMINAR AND TRANSITION
BOUNDARY LAYER, $z/D_N = .5$

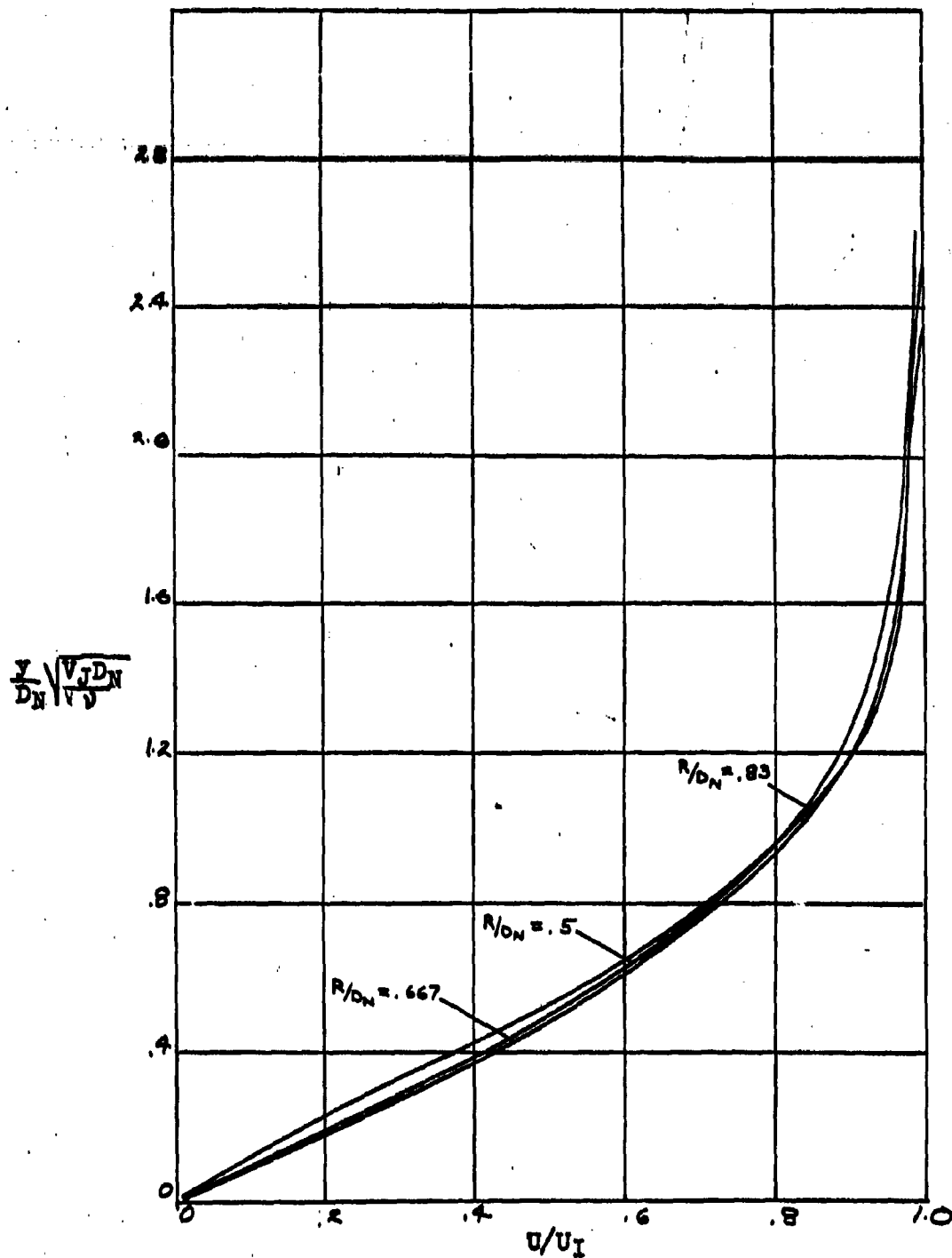


FIGURE 50

VELOCITY PROFILES FOR LAMINAR AND TRANSITION
BOUNDARY LAYER, $z/D_N = 1.0$

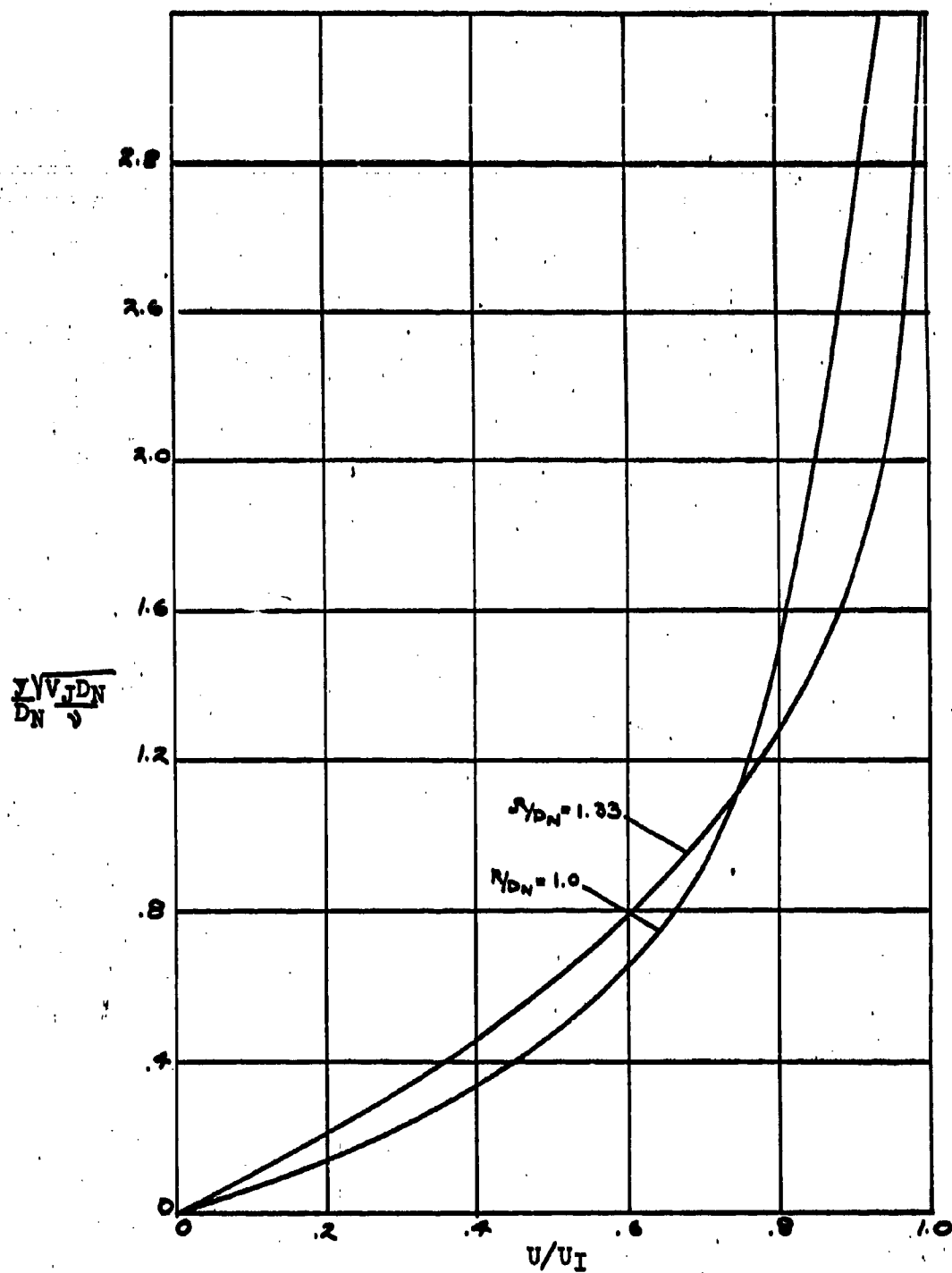


FIGURE 5d

VELOCITY PROFILES OF LAMINAR AND TRANSITION
BOUNDARY LAYER, $z/D_N = 1.0$

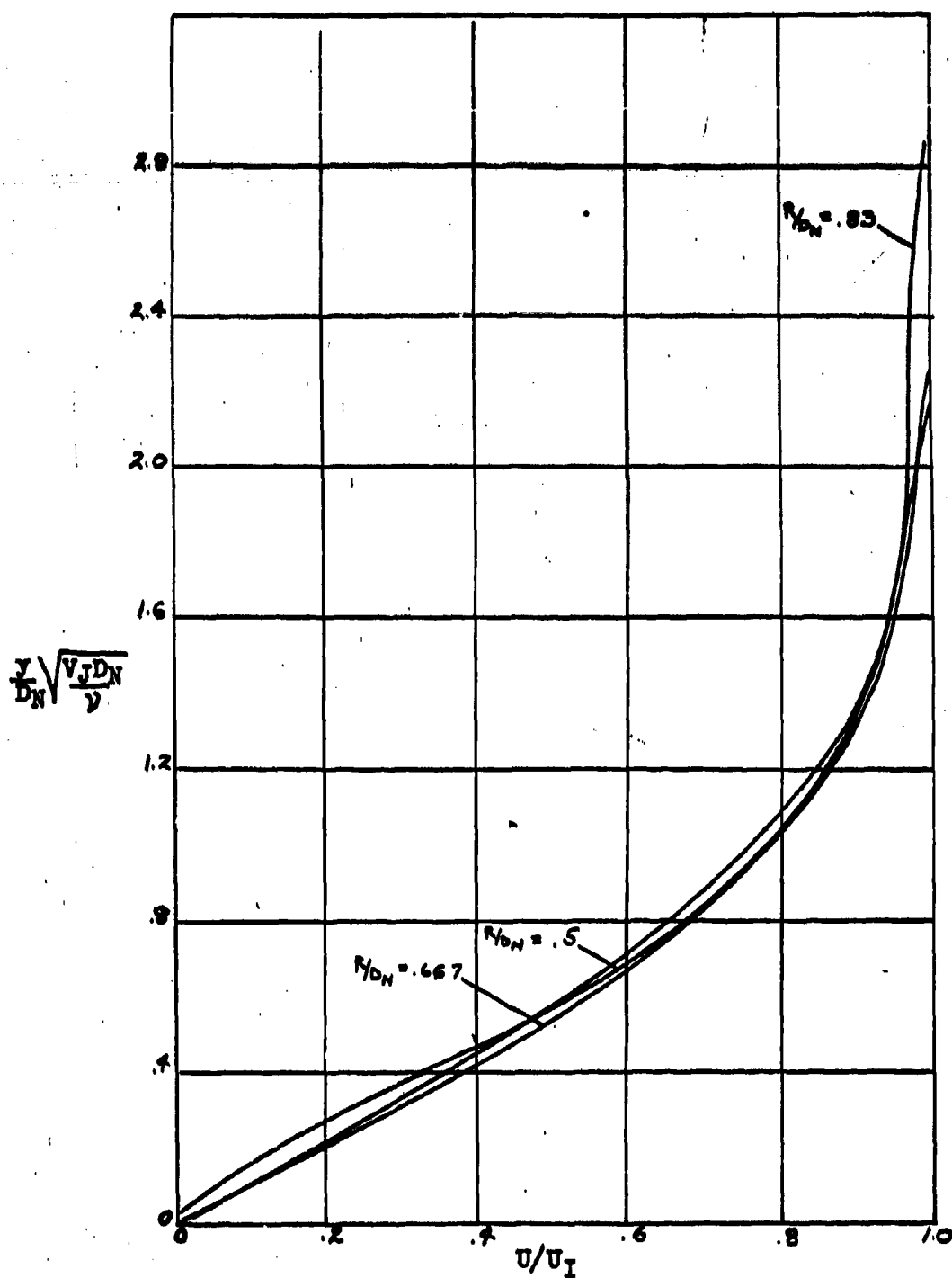


FIGURE 5e

VELOCITY PROFILES FOR LAMINAR AND TRANSITION
BOUNDARY LAYER, $z/D_N = 2.0$

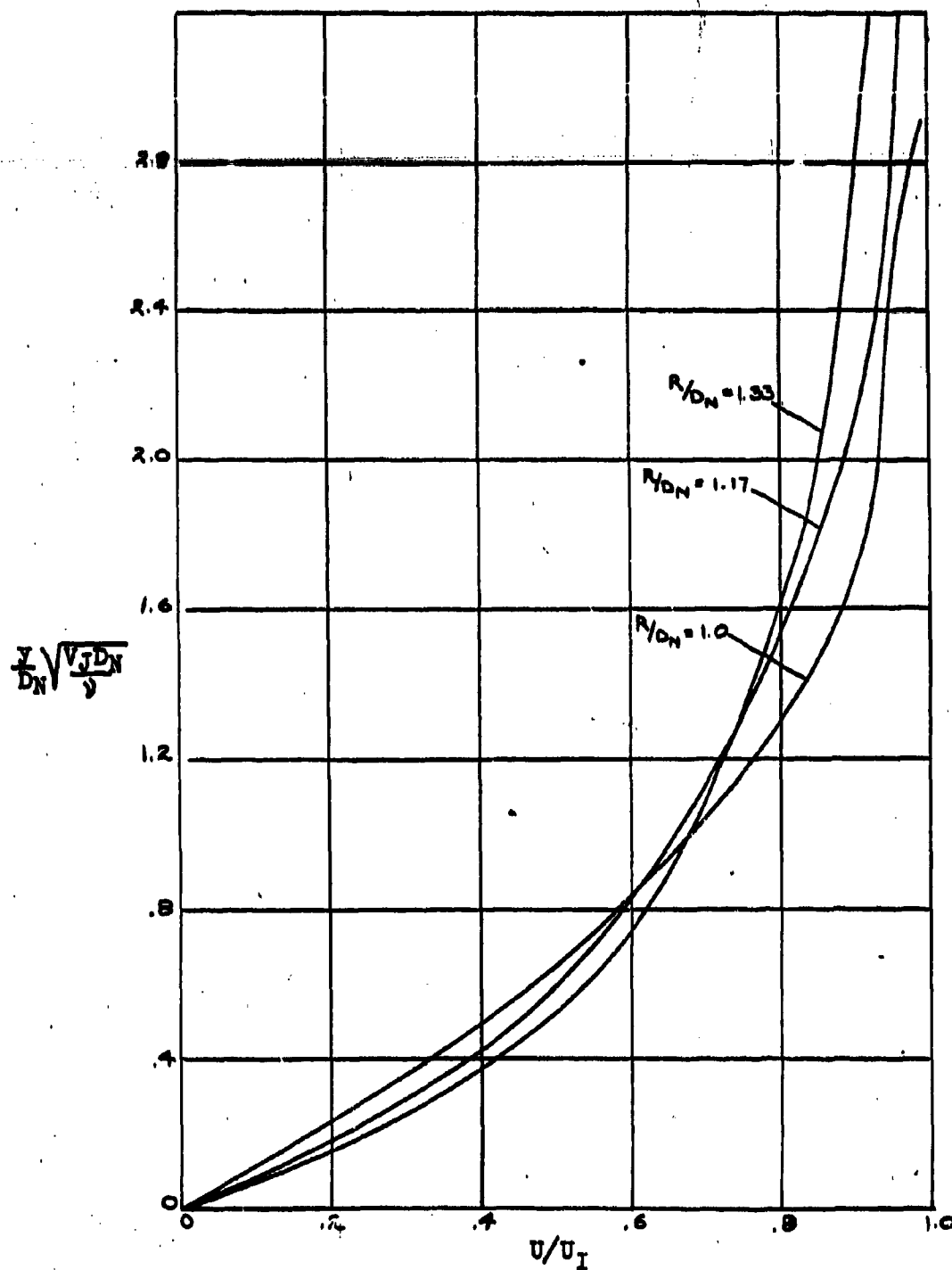


FIGURE 5f

VELOCITY PROFILES OF LAMINAR AND TRANSITION
BOUNDARY LAYER, $z/D_N = 2.0$

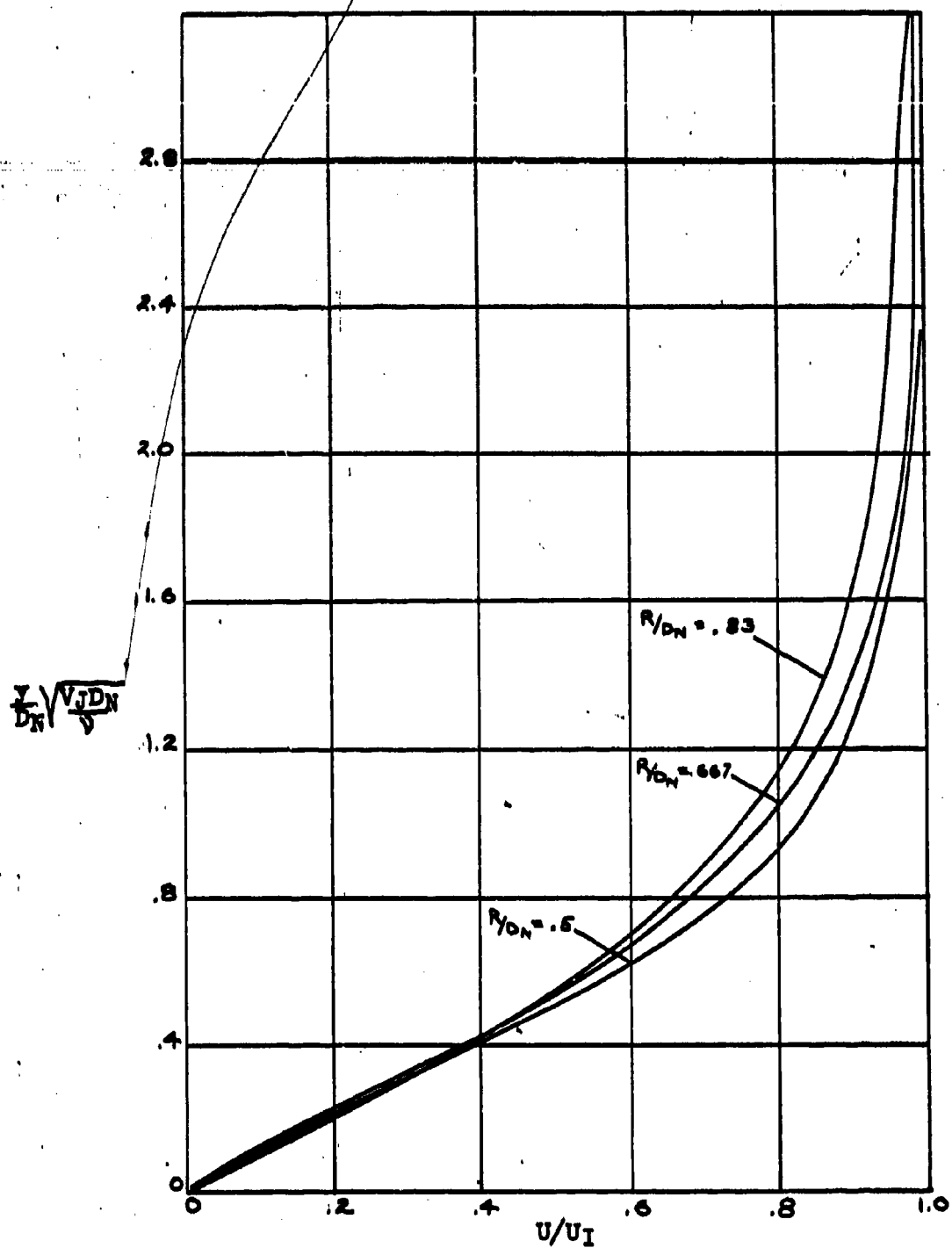


FIGURE 5g

VELOCITY PROFILES OF LAMINAR AND TRANSITION
BOUNDARY LAYER, $Z/D_N = 4.0$

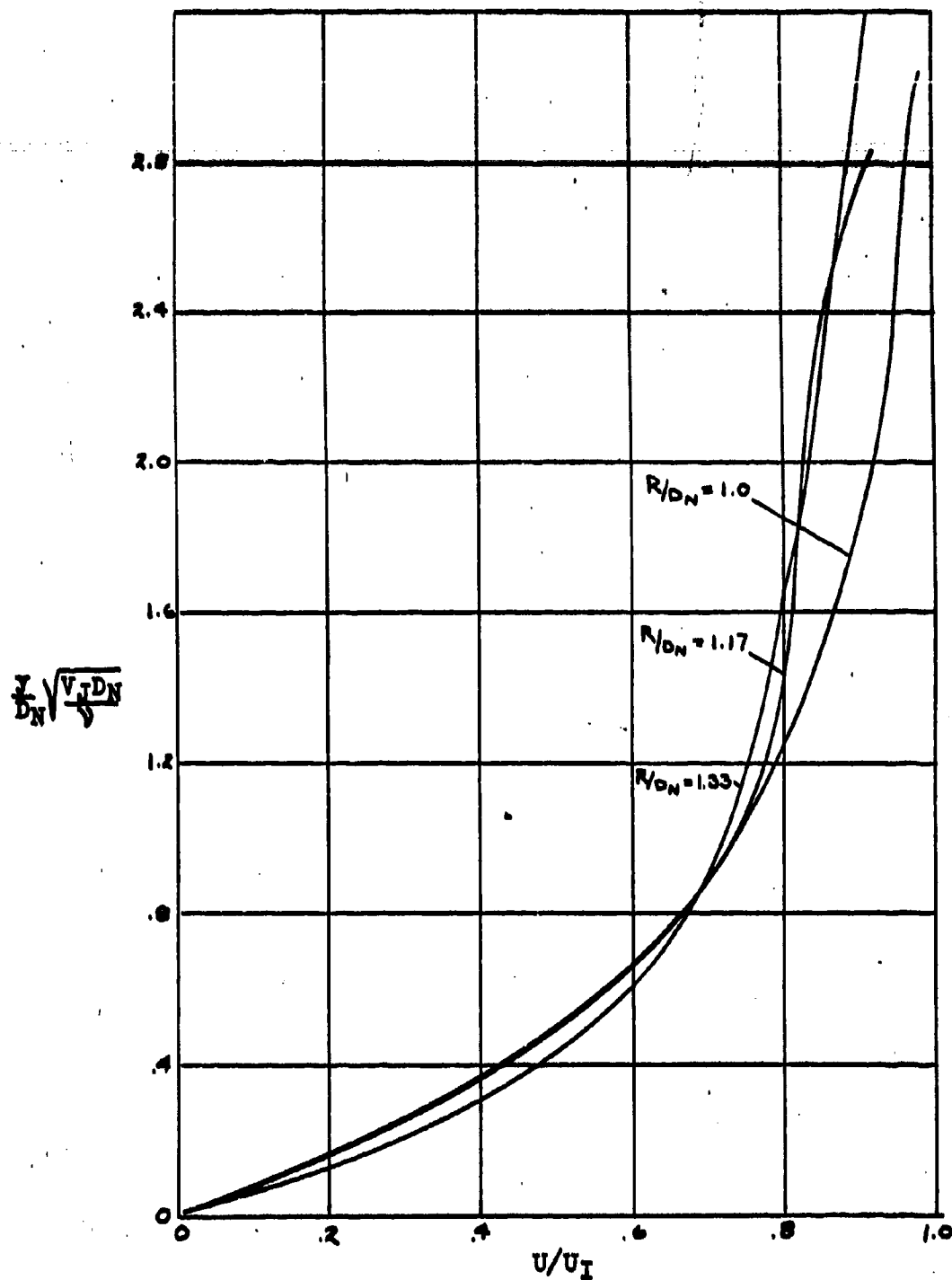


FIGURE 5h

VELOCITY PROFILES FOR LAMINAR AND TRANSITION
BOUNDARY LAYER, $z/D_N = 4.0$

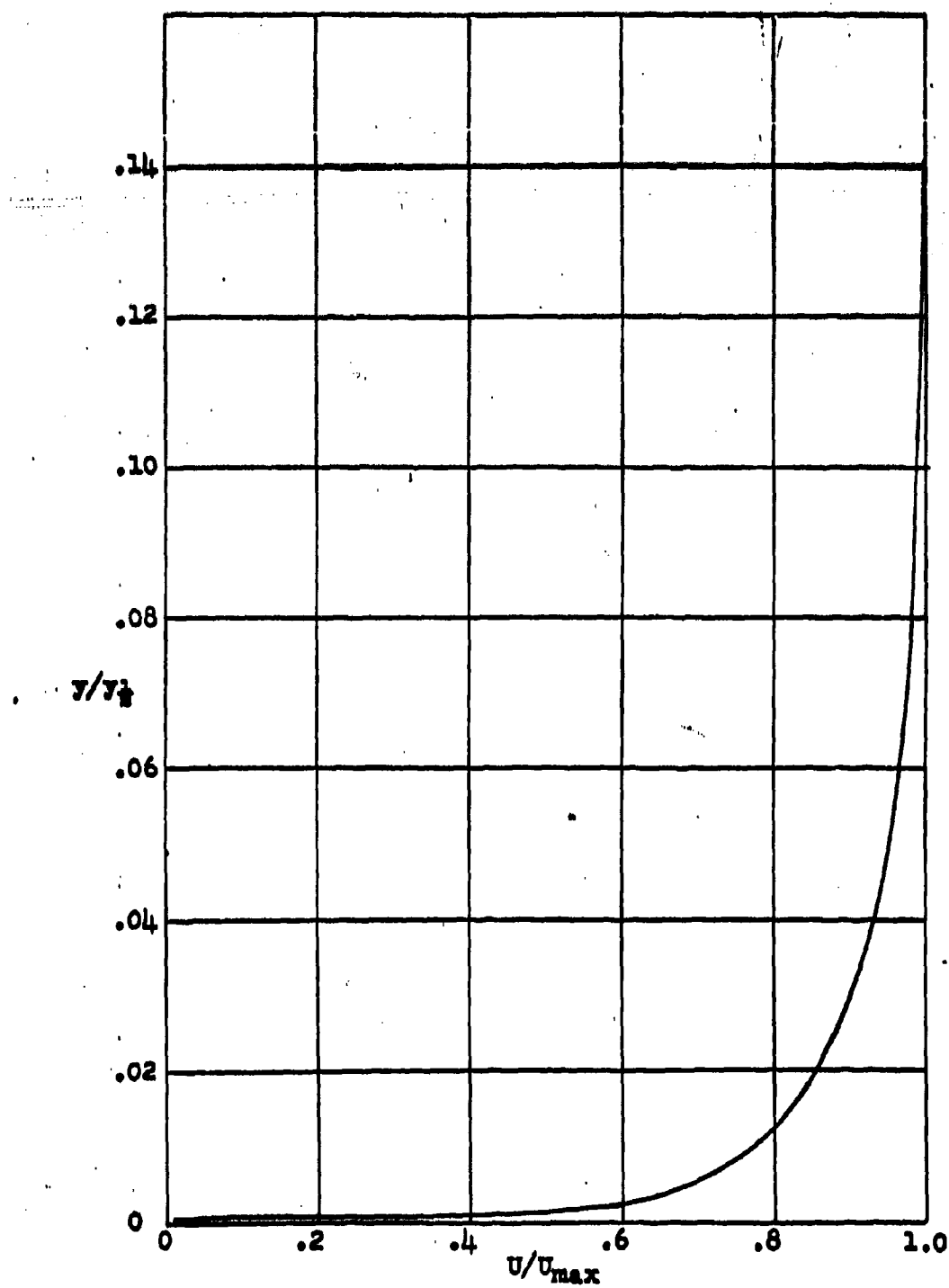


FIGURE 6a

VELOCITY PROFILE OF TURBULENT
BOUNDARY LAYER - INNER LAYER

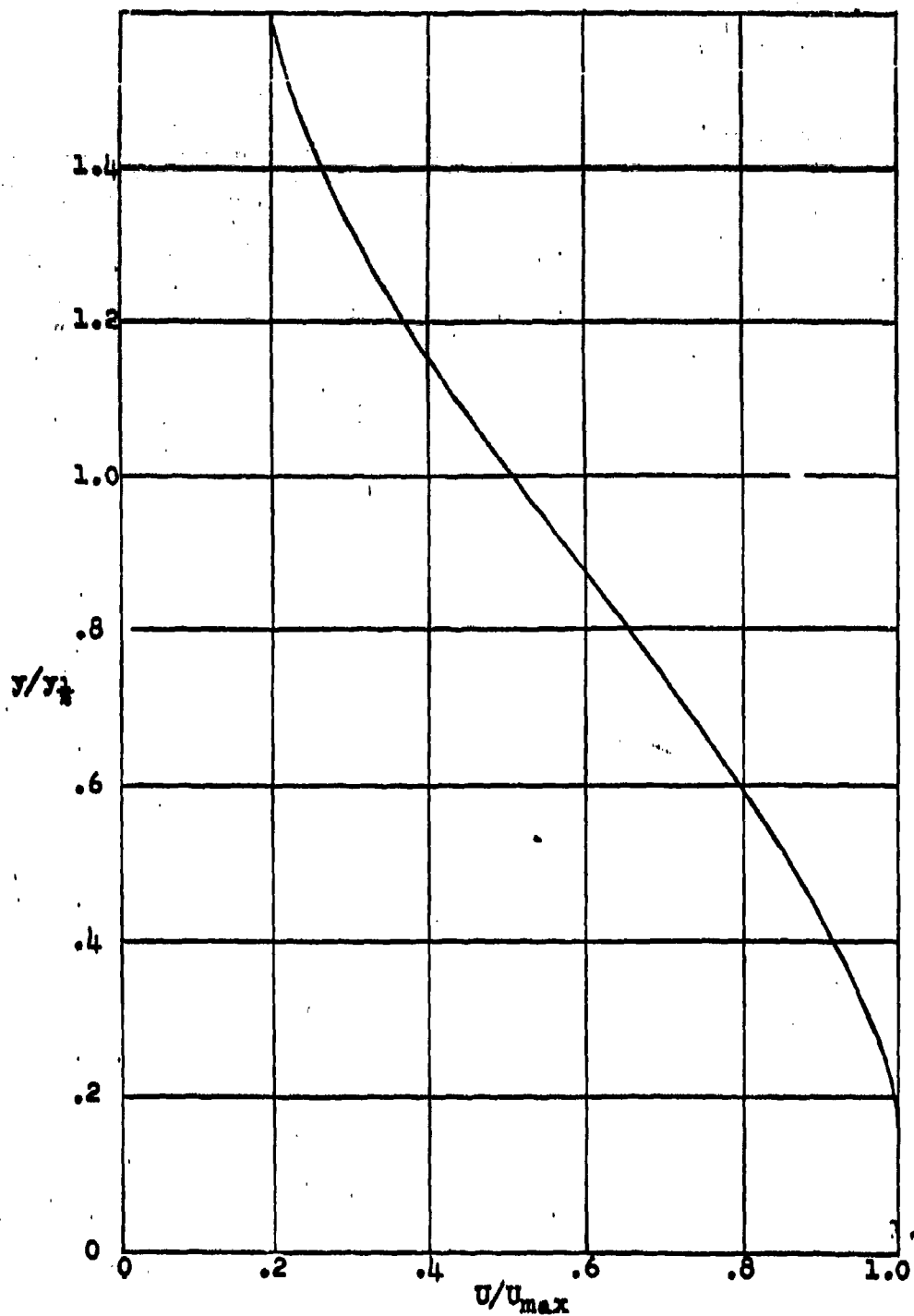


FIGURE 6b

VELOCITY PROFILE OF TURBULENT
BOUNDARY LAYER - OUTER LAYER

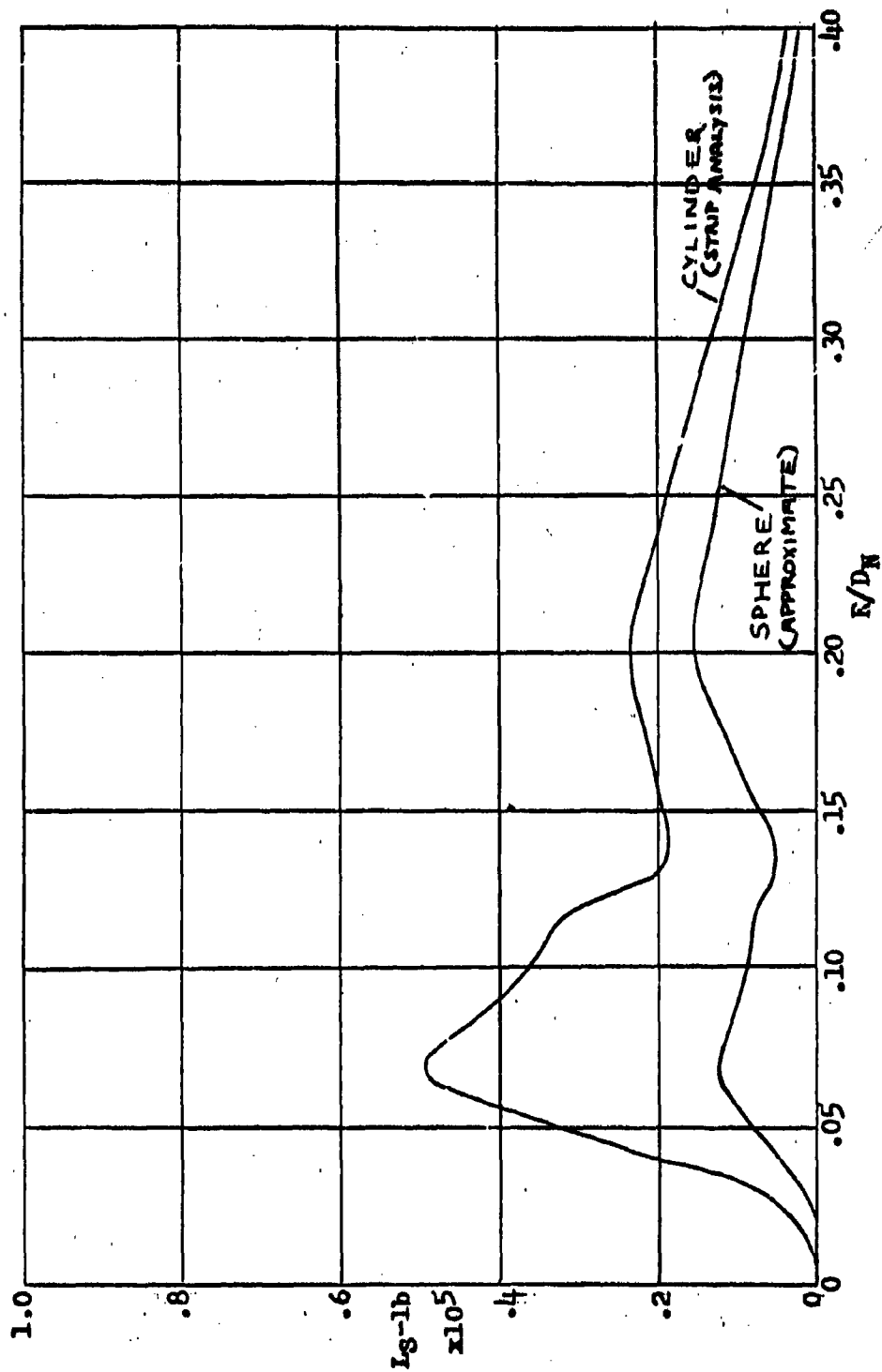


FIGURE 7

COMPARISON OF SHEAR LIFT FORCE BY
CYLINDER AND SPHERE METHODS

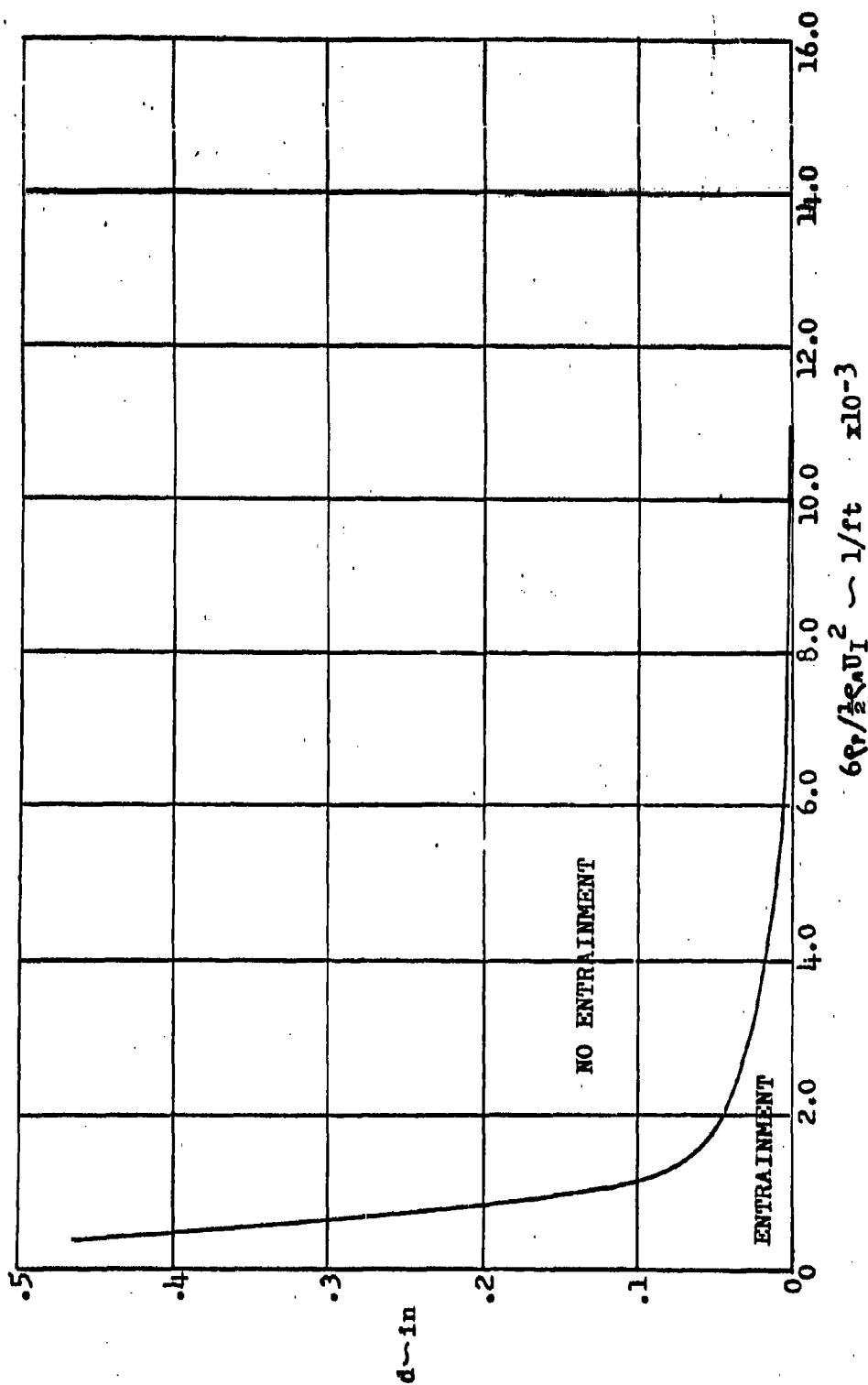


FIGURE 8a

CRITICAL PARTICLE SIZE FOR DRAG ENTRAINMENT

$V_J = 65$ ft/sec, $Z/D_N = 1$, $R/D_N = .05$

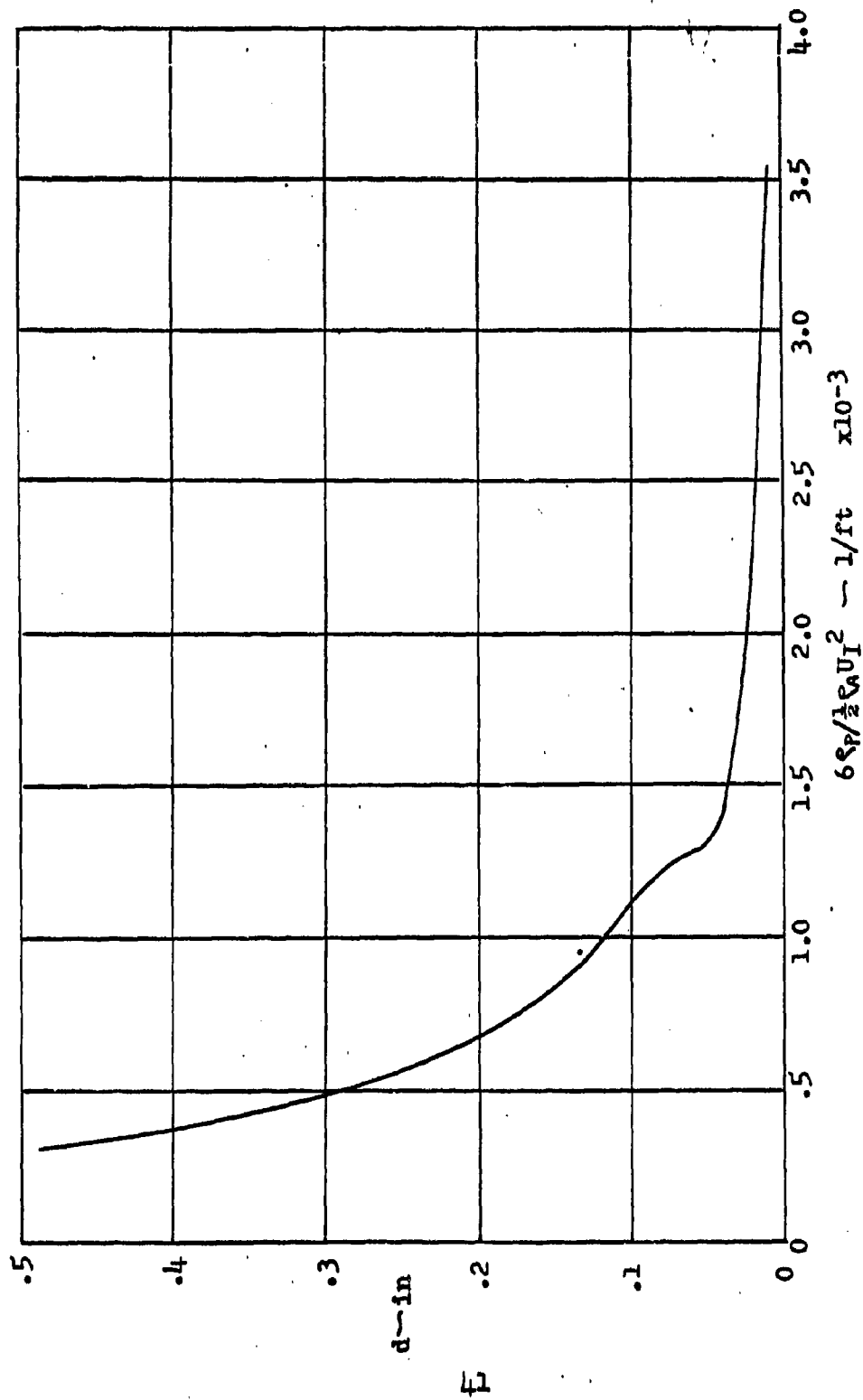


FIGURE 8b

CRITICAL PARTICLE SIZE FOR DRAG ENTRAINMENT
 $V_J = 65 \text{ ft/sec}$, $Z/D_N = 1$, $R/D_N = 1$

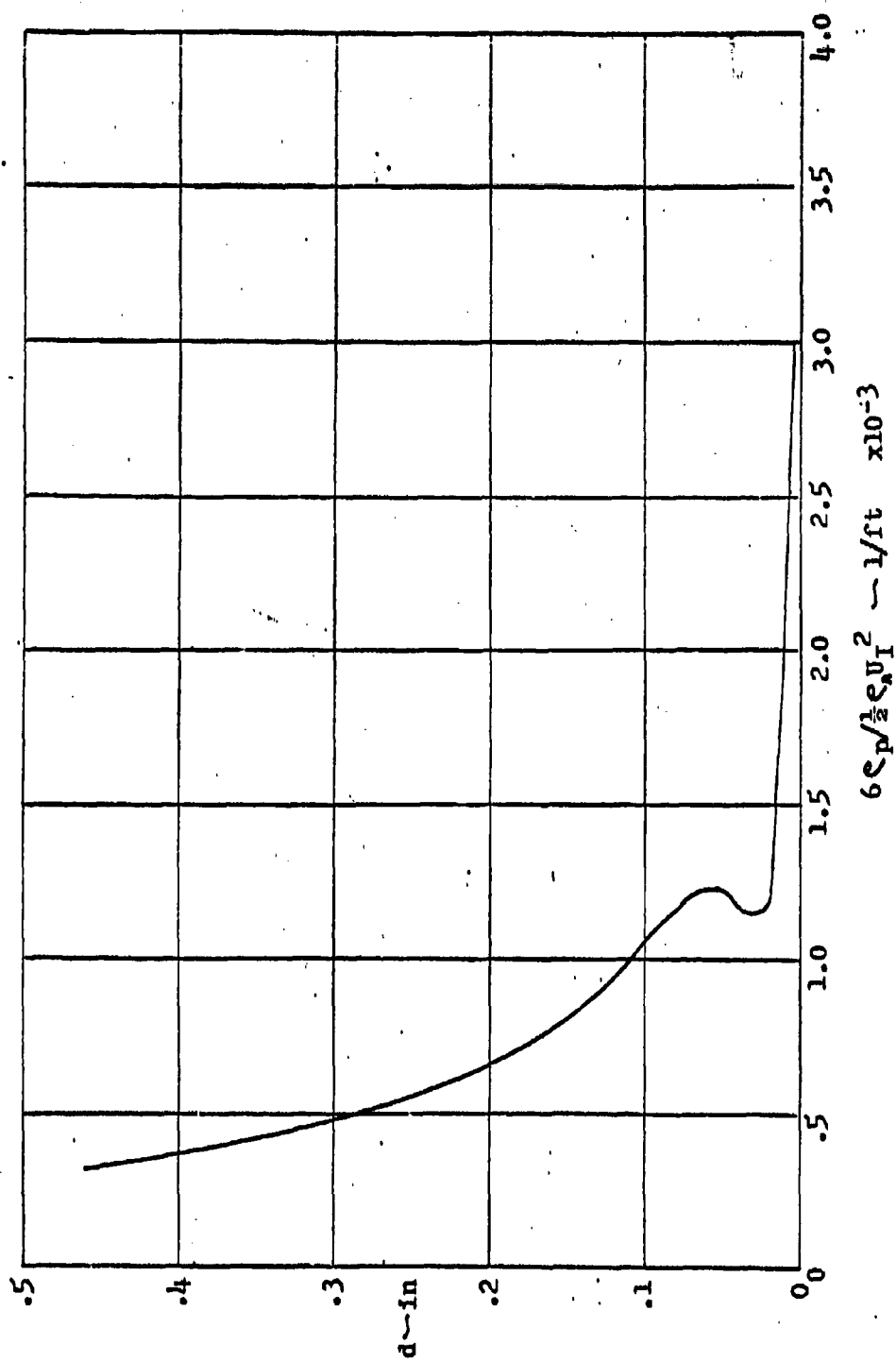


FIGURE 8c

CRITICAL PARTICLE SIZE FOR DRAG ENTRAINMENT
 $V_J = 65$ ft/sec, $Z/DH = 1$, $R/DH = .2$

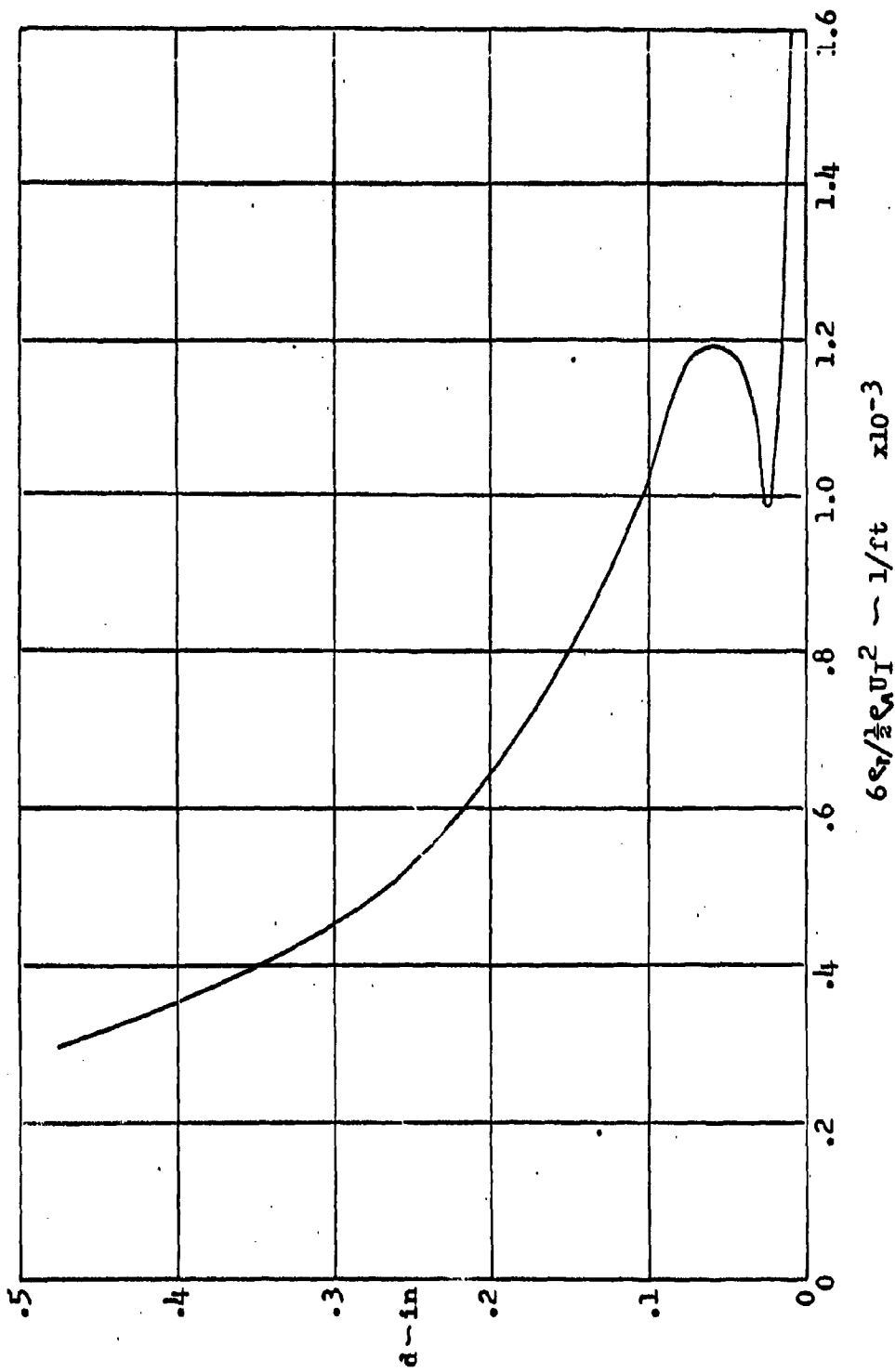


FIGURE 8d

CRITICAL PARTICLE SIZE FOR DRAG ENTRAINMENT
 $V_J = 65$ ft/sec, $Z/D_N = 1$, $R/D_N = .3$

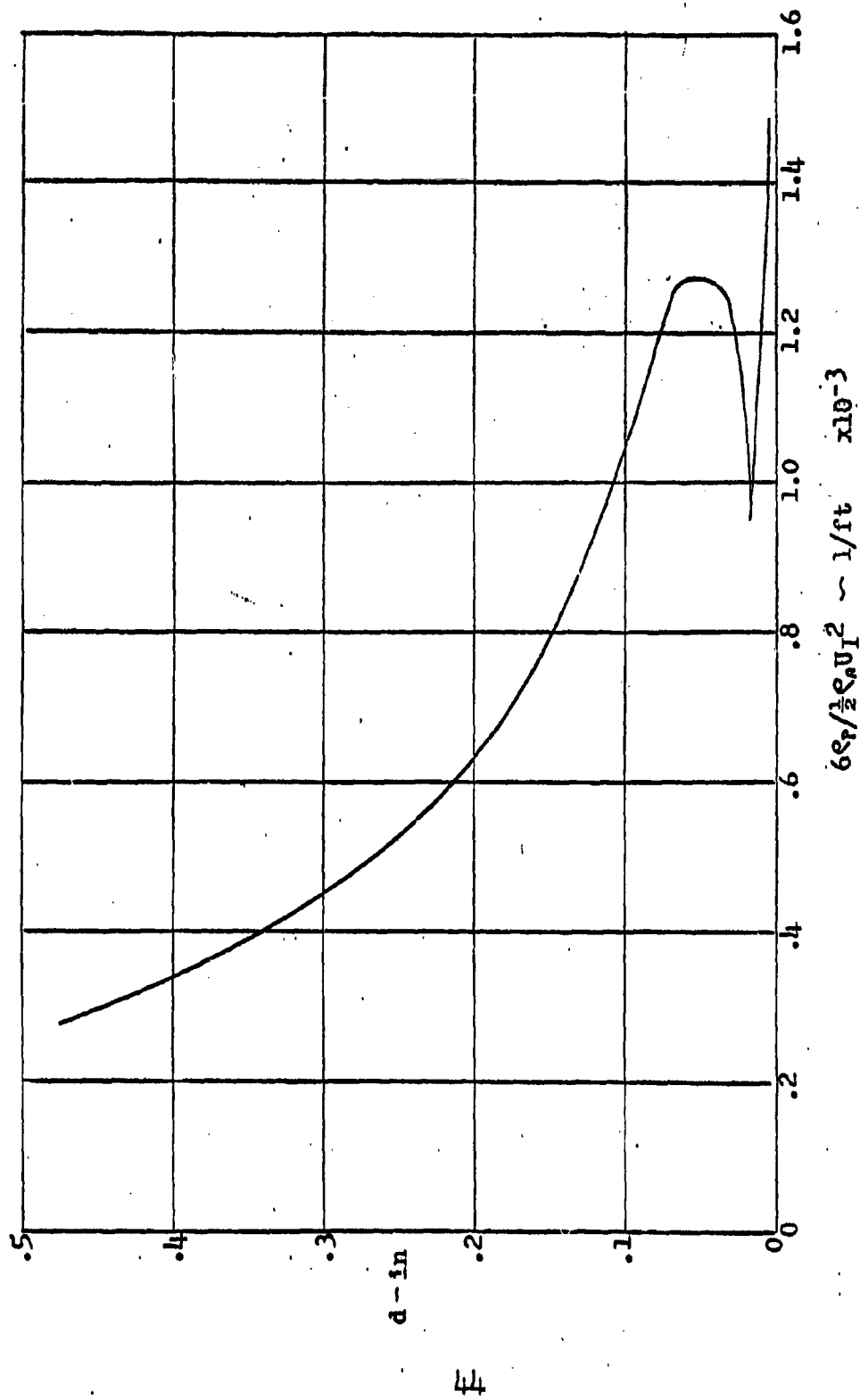


FIGURE 80

CRITICAL PARTICLE SIZE FOR DRAG ENTRAINMENT
 $V_J = 65$ ft/sec, $Z/D_H = 1$, $R/D_H = .4$

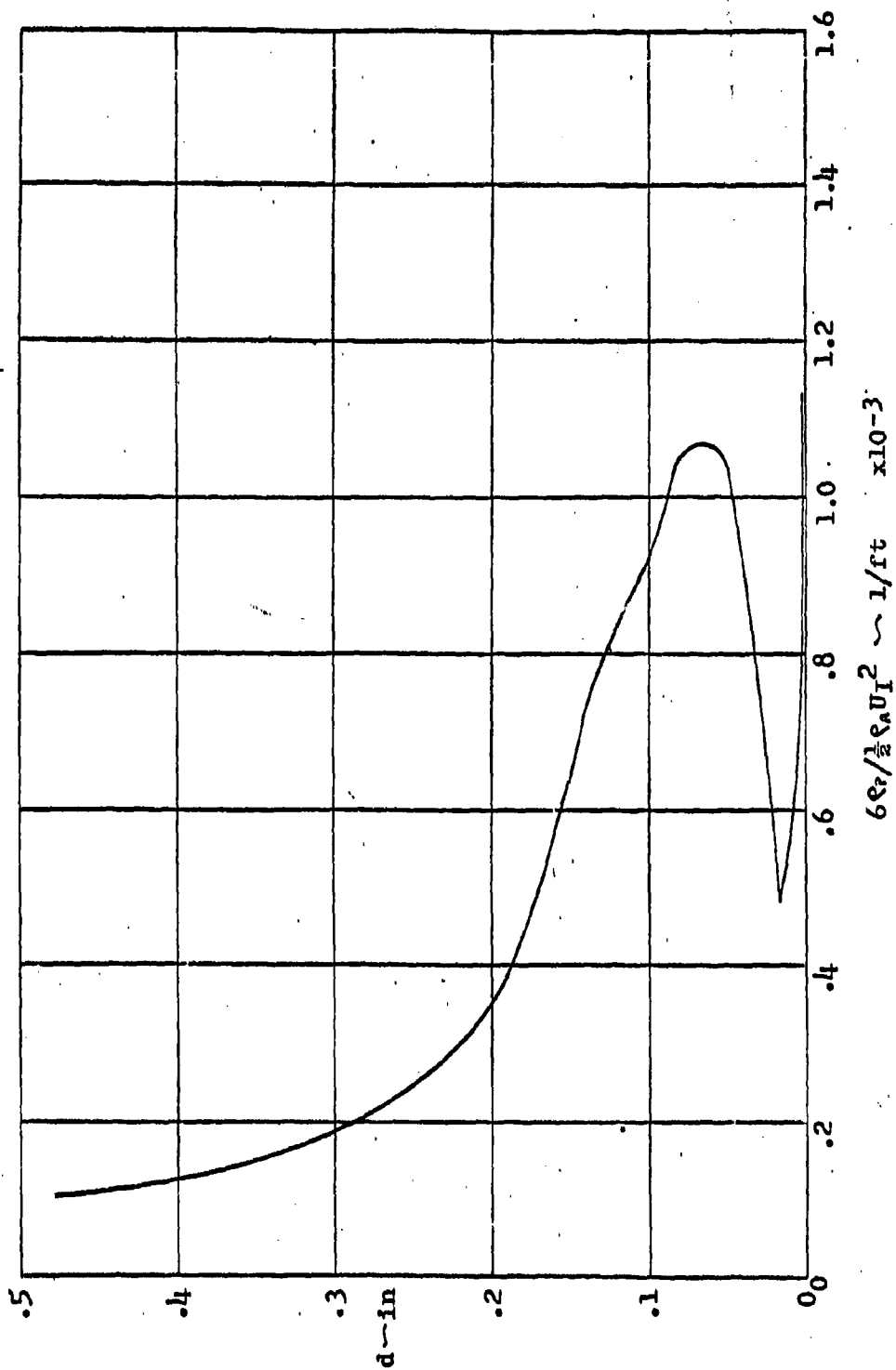


FIGURE 8f

CRITICAL PARTICLE SIZE FOR DRAG ENTRAINMENT

$V_J = 65 \text{ ft/sec}$, $Z/DN = 1$, $R/DN = .5$

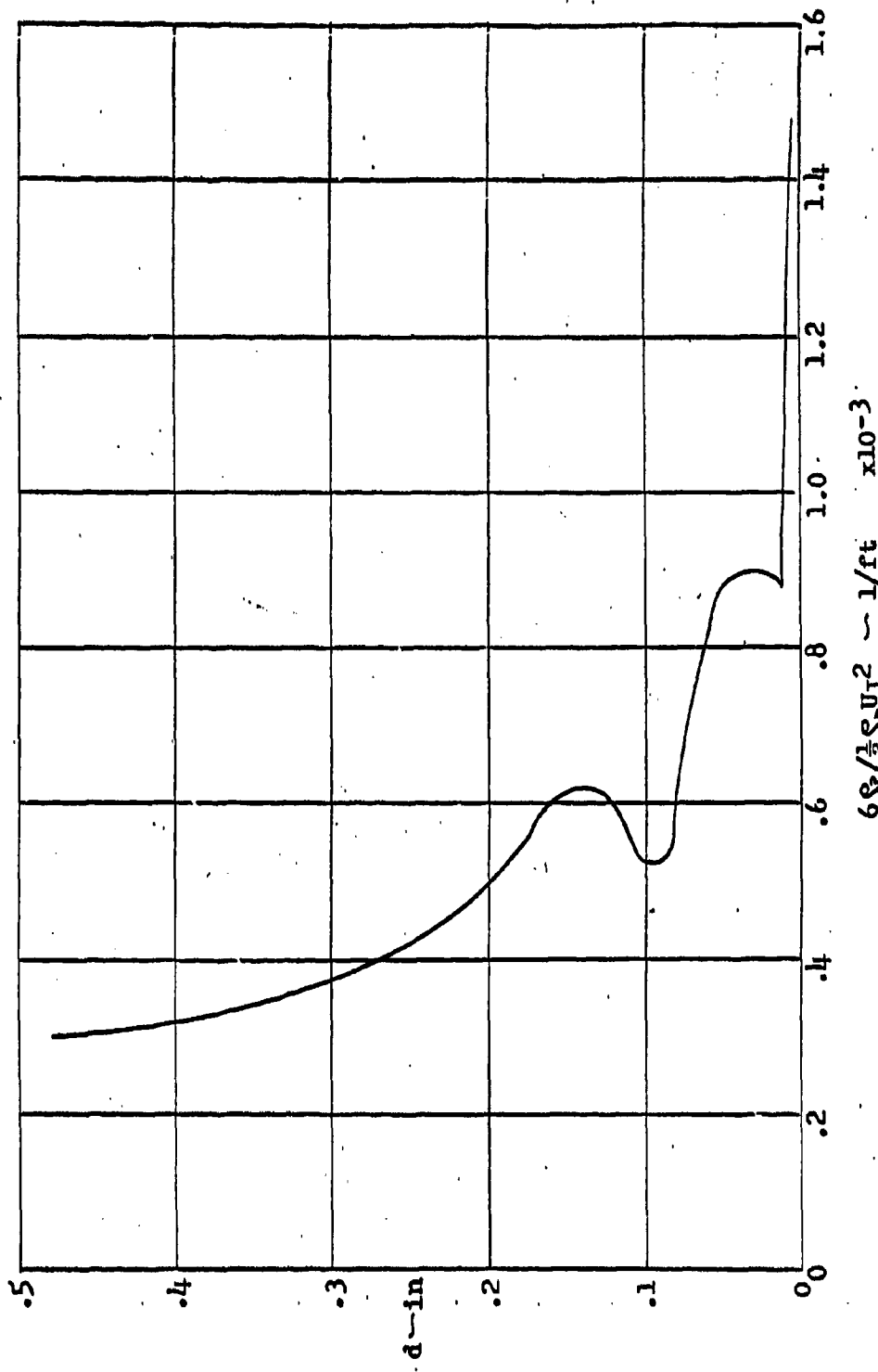


FIGURE 8g

CRITICAL PARTICLE SIZE FOR DRAG ENTRAINMENT
 $V_J = 65 \text{ ft/sec}$, $Z/DN = 1$, $R/DN = 2.0$

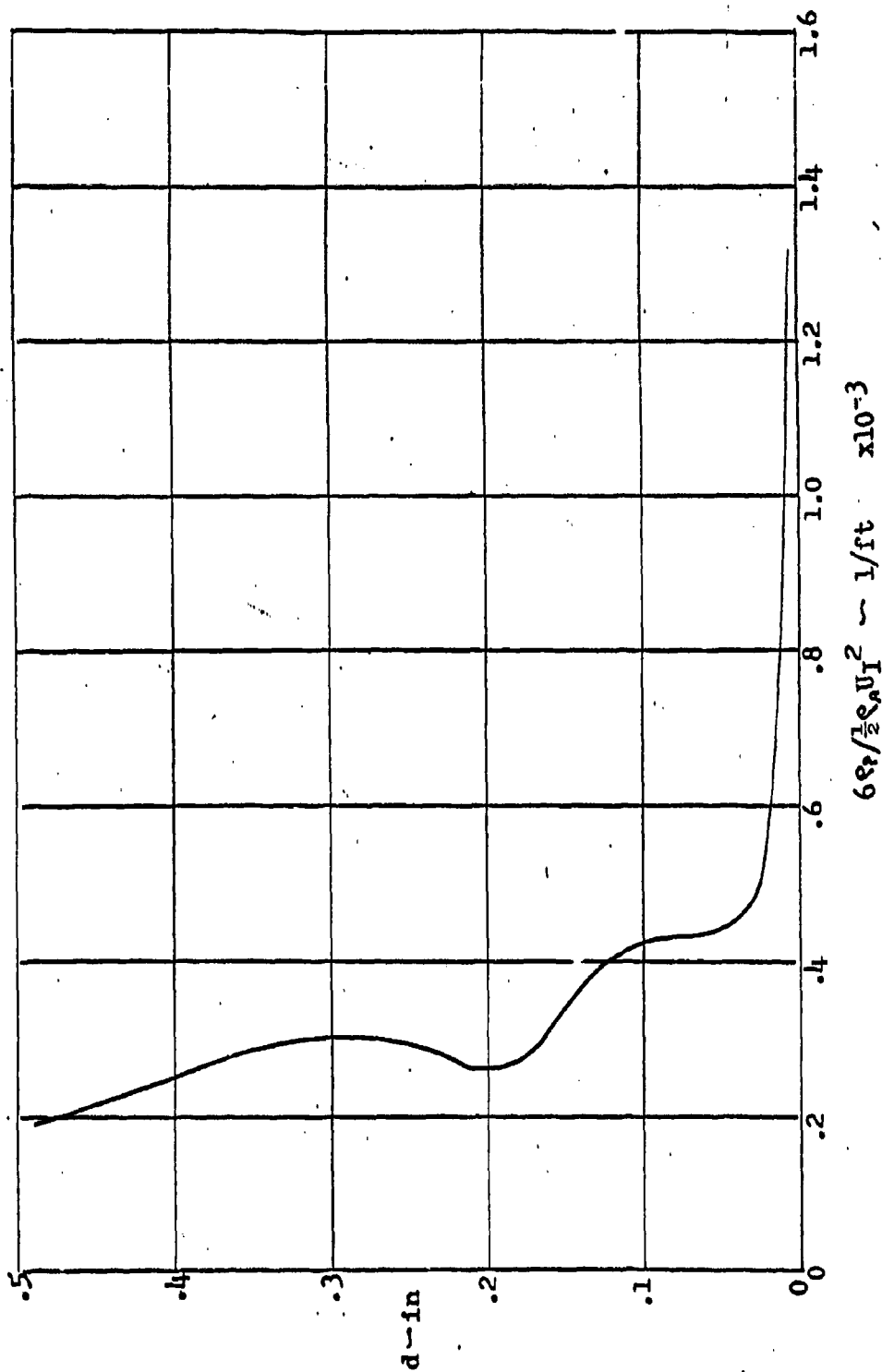


FIGURE 8h

CRITICAL PARTICLE SIZE FOR DRAG ENTRAINMENT
 $V_J = 65 \text{ ft/sec}$, $z/DN = 1$, $R/DN = 4.0$

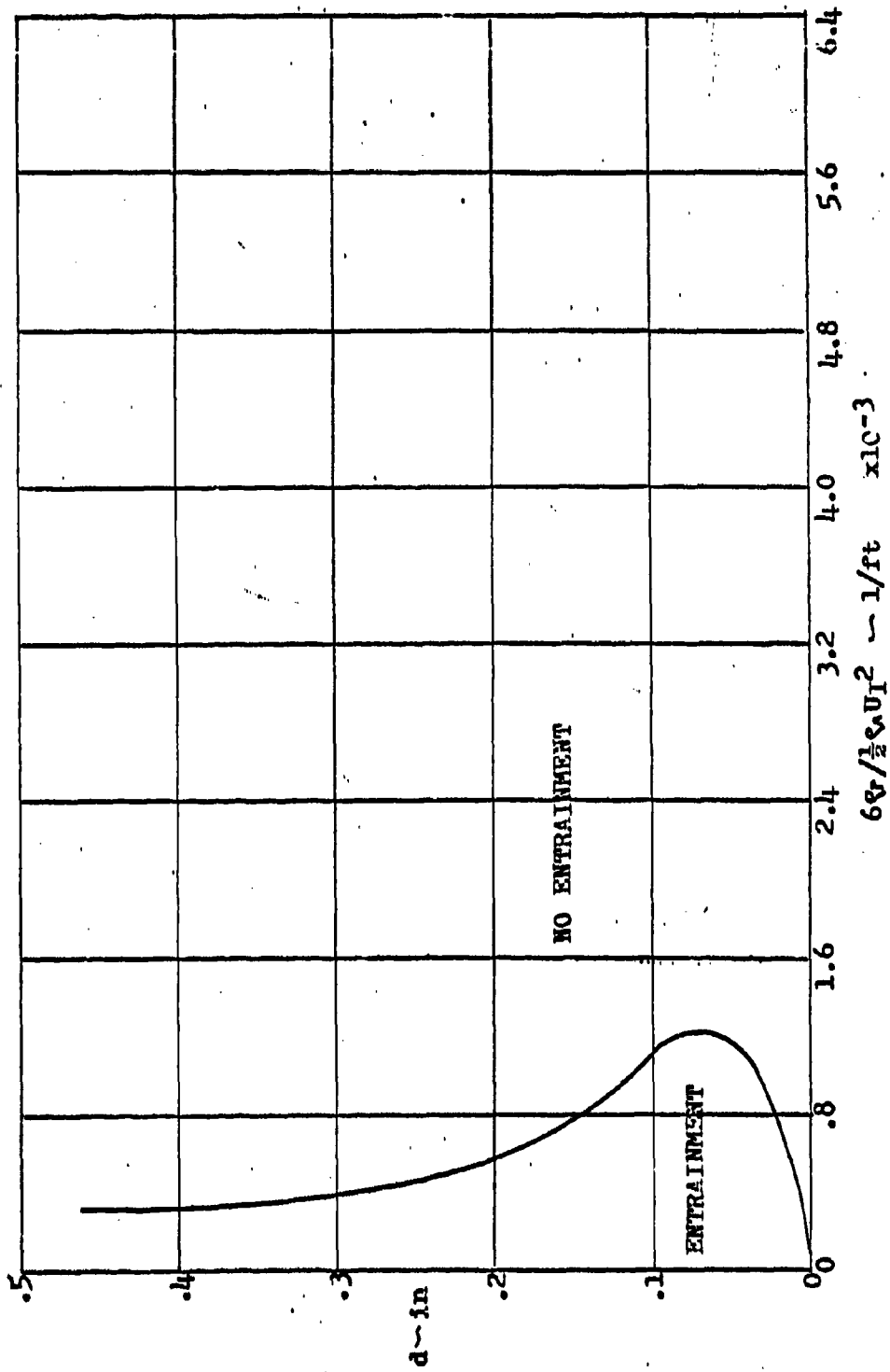


FIGURE 9a

CRITICAL PARTICLE SIZE FOR LIFT ENTRAINMENT
 $V_J = 65 \text{ ft/sec}$, $Z/D_N = 1$, $R/D_N = .05$

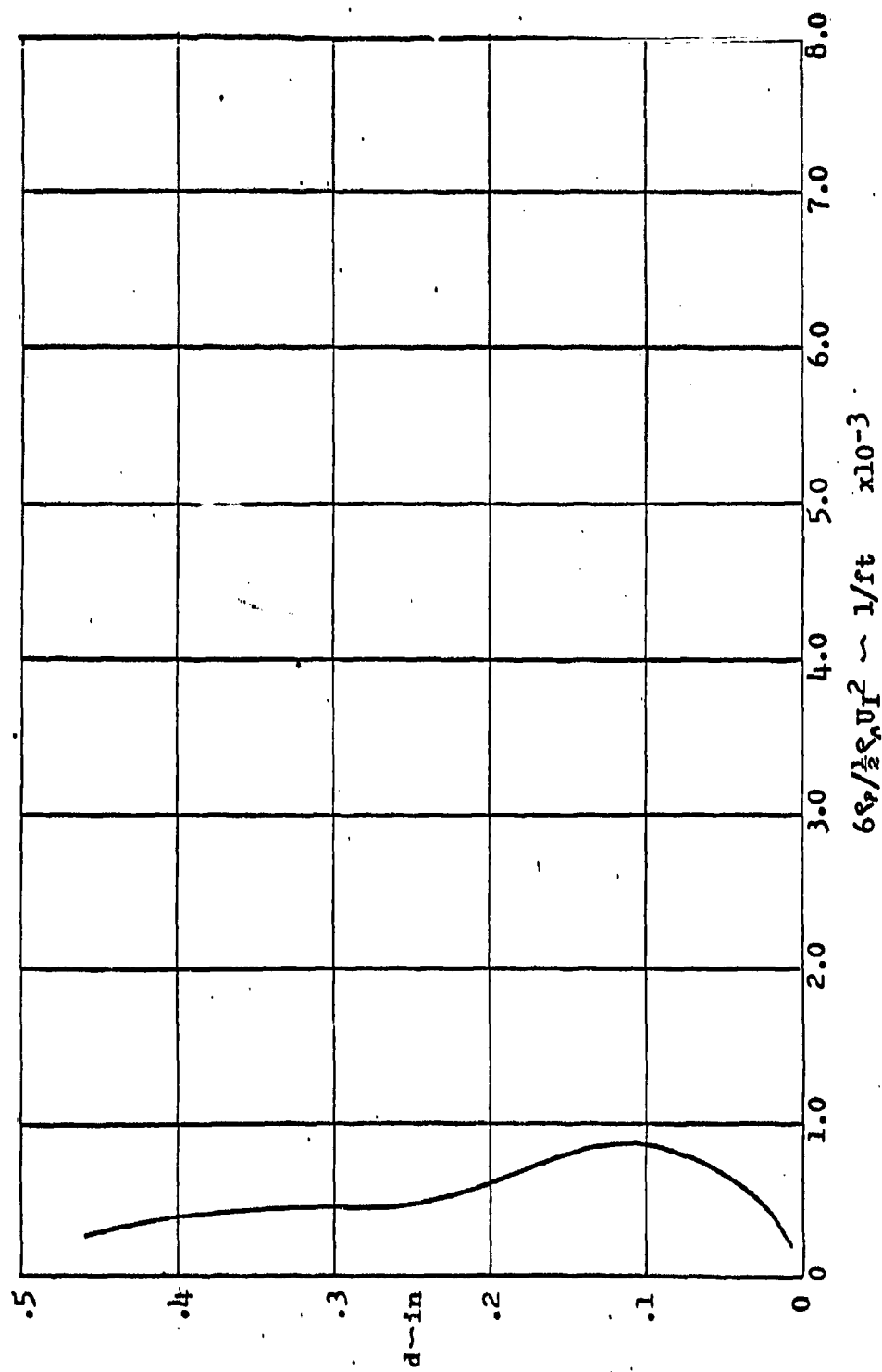


FIGURE 9b

CRITICAL PARTICLE SIZE FOR LIFT ENTRAINMENT
 $V_J = 65 \text{ ft/sec}$, $Z/D_N = 1$, $R/D_N = .1$

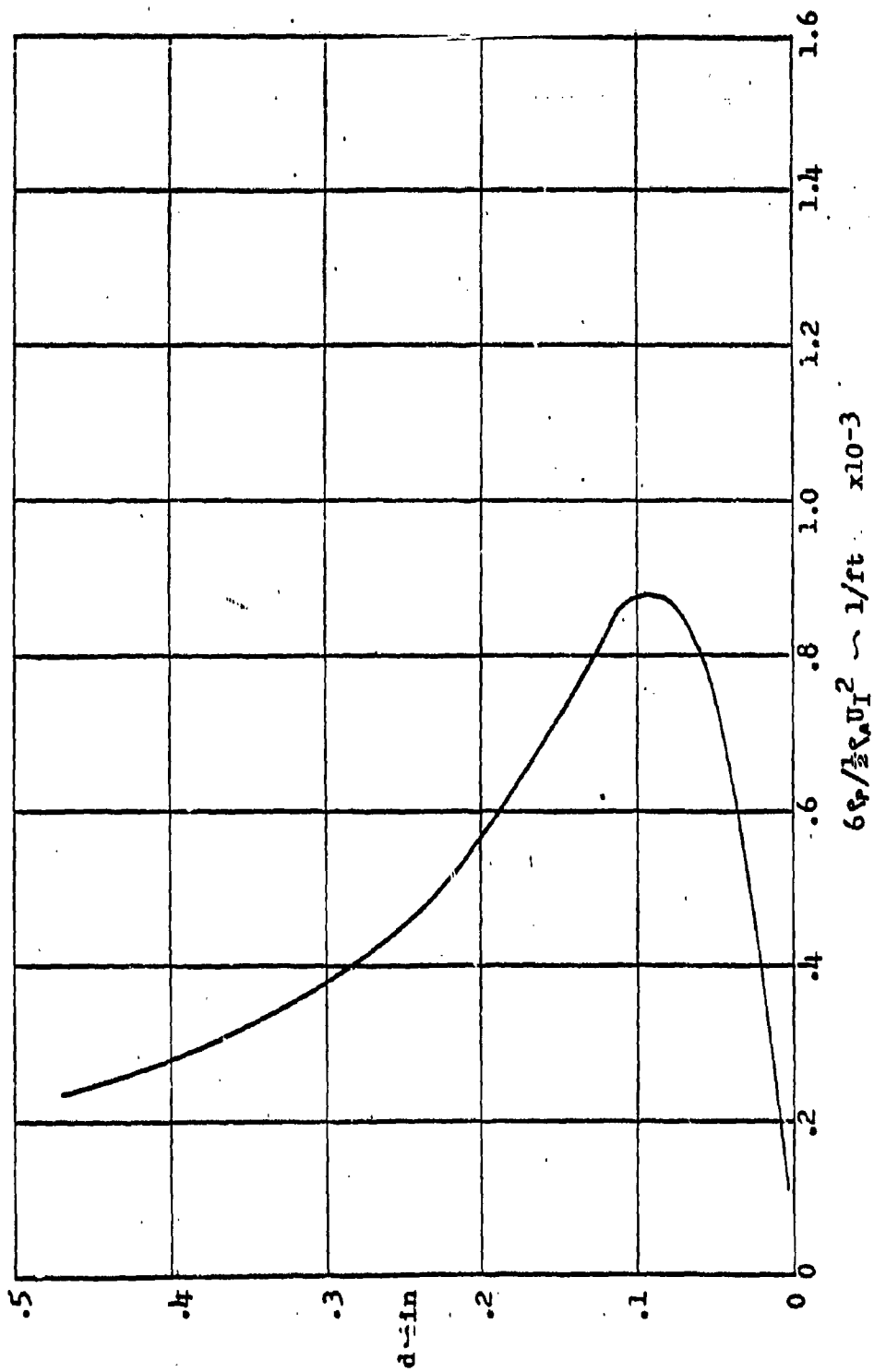


FIGURE 9c
 CRITICAL PARTICLE SIZE FOR LIFT ENTRAINMENT
 $V_J = 65$ ft/sec, $z/D_H = 1$, $R/D_H = .2$

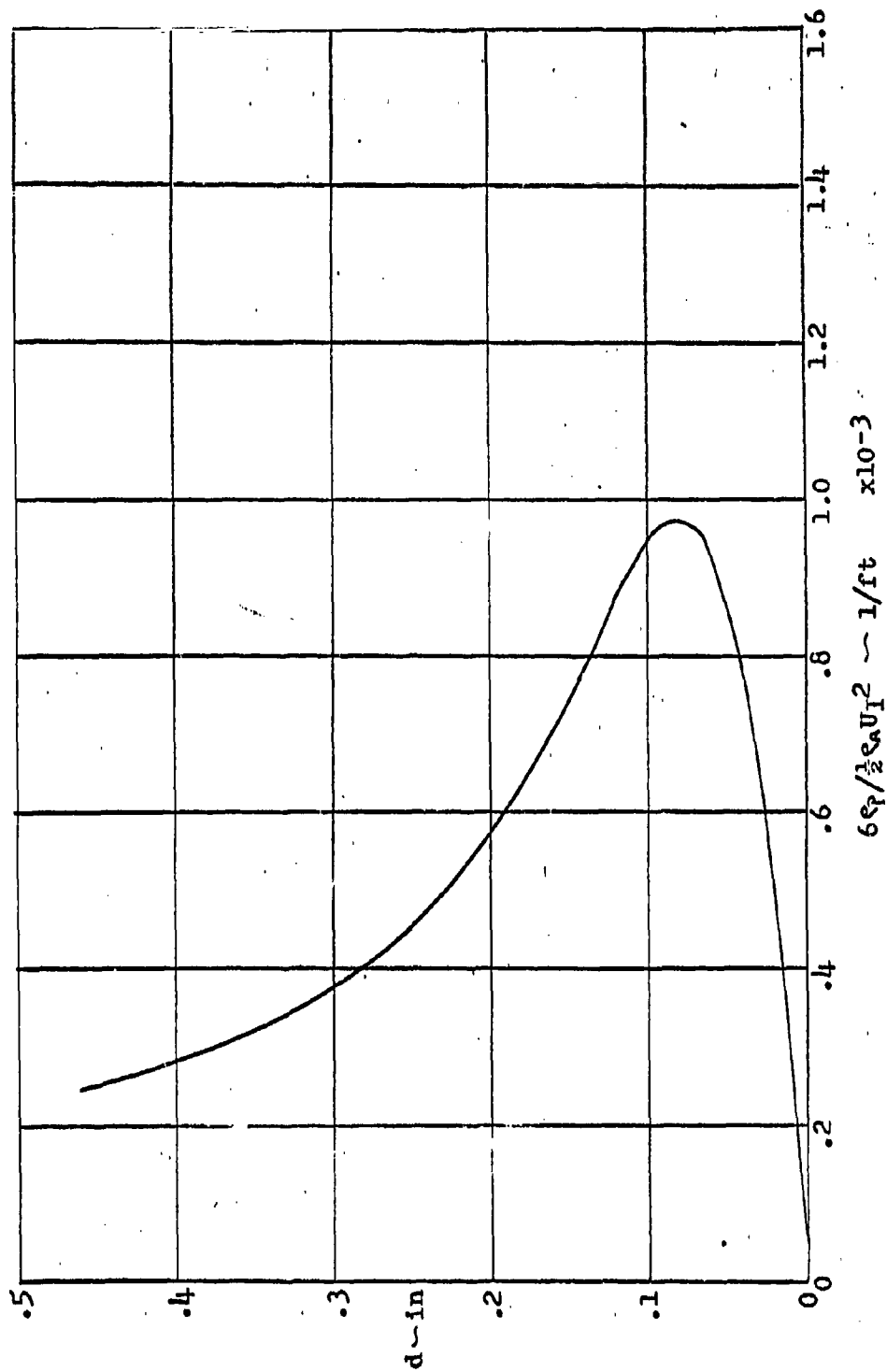


FIGURE 9d

CRITICAL PARTICLE SIZE FOR LIFT ENTRAINMENT

$V_J = 65 \text{ ft/sec}$, $Z/D_N = 1$, $R/D_N = .3$

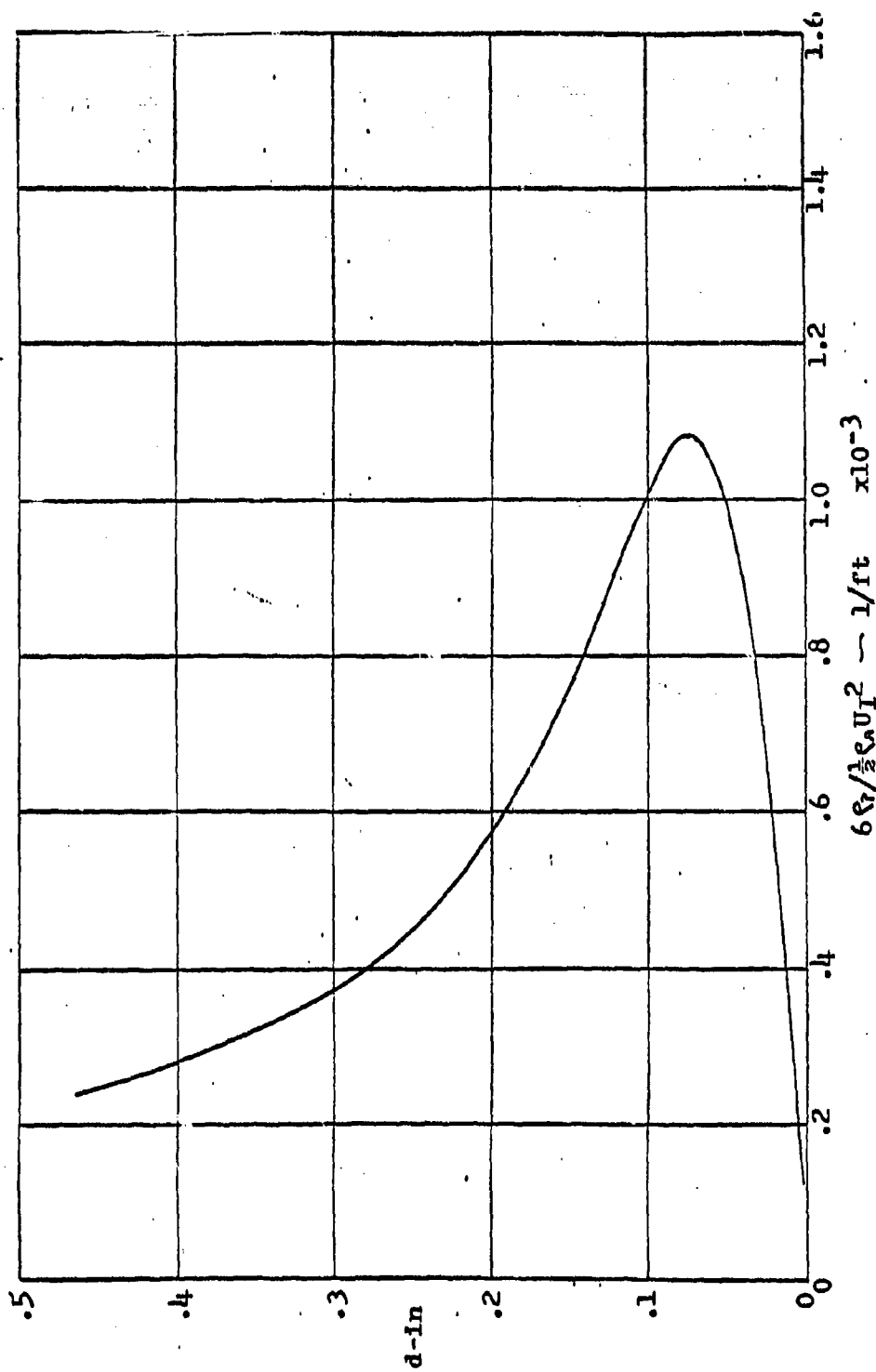


FIGURE 9c
 CRITICAL PARTICLE SIZE FOR LIFT ENTRAINMENT
 $V_J = 65 \text{ ft/sec}$, $Z/D_N = 1$, $R/D_N = .4$

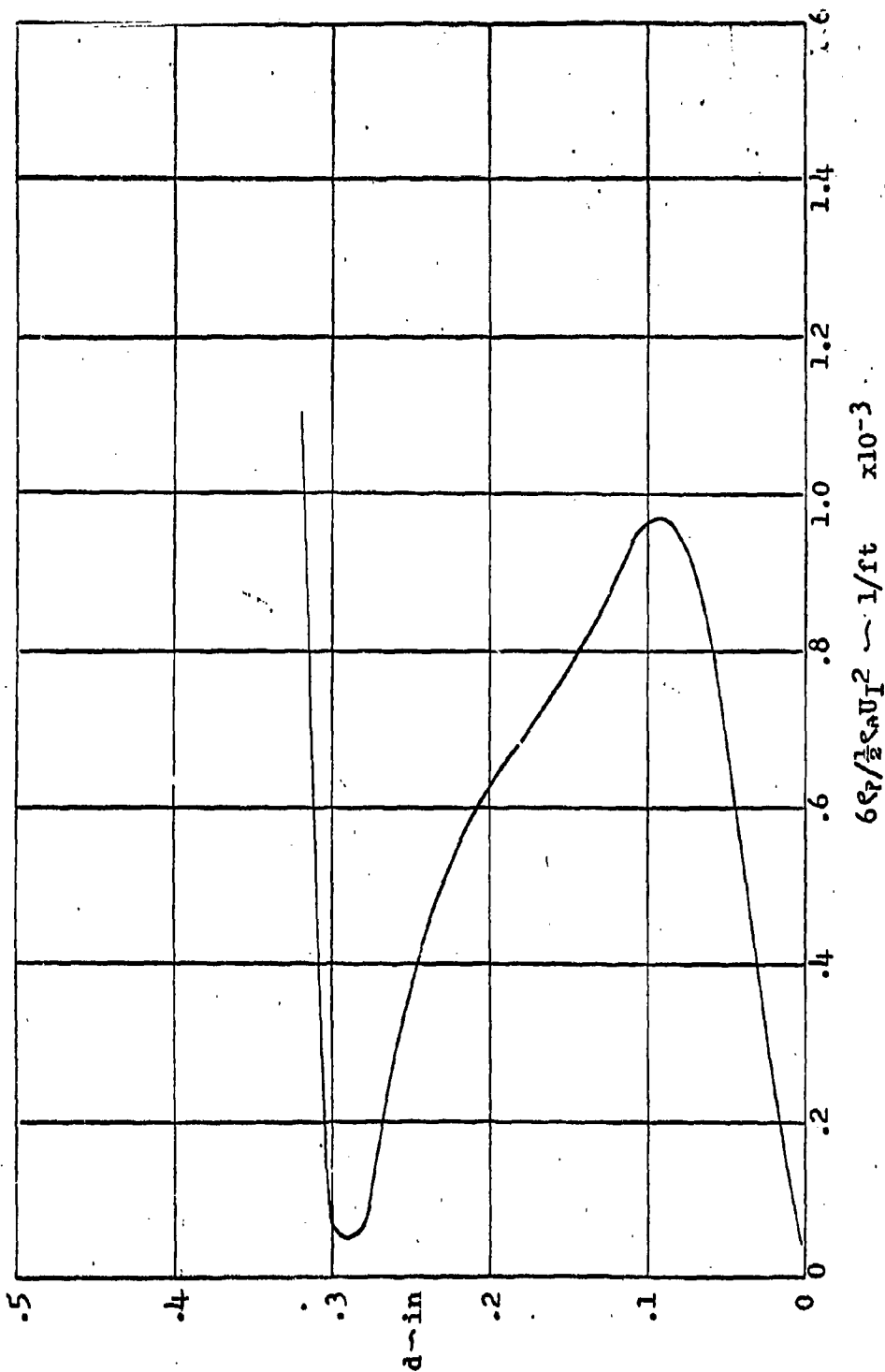


FIGURE 9f

CRITICAL PARTICLE SIZE FOR LIFT ENTRAINMENT
 $V_J = 65$ ft/sec, $Z/D_N = 1$, $R/D_N = .5$

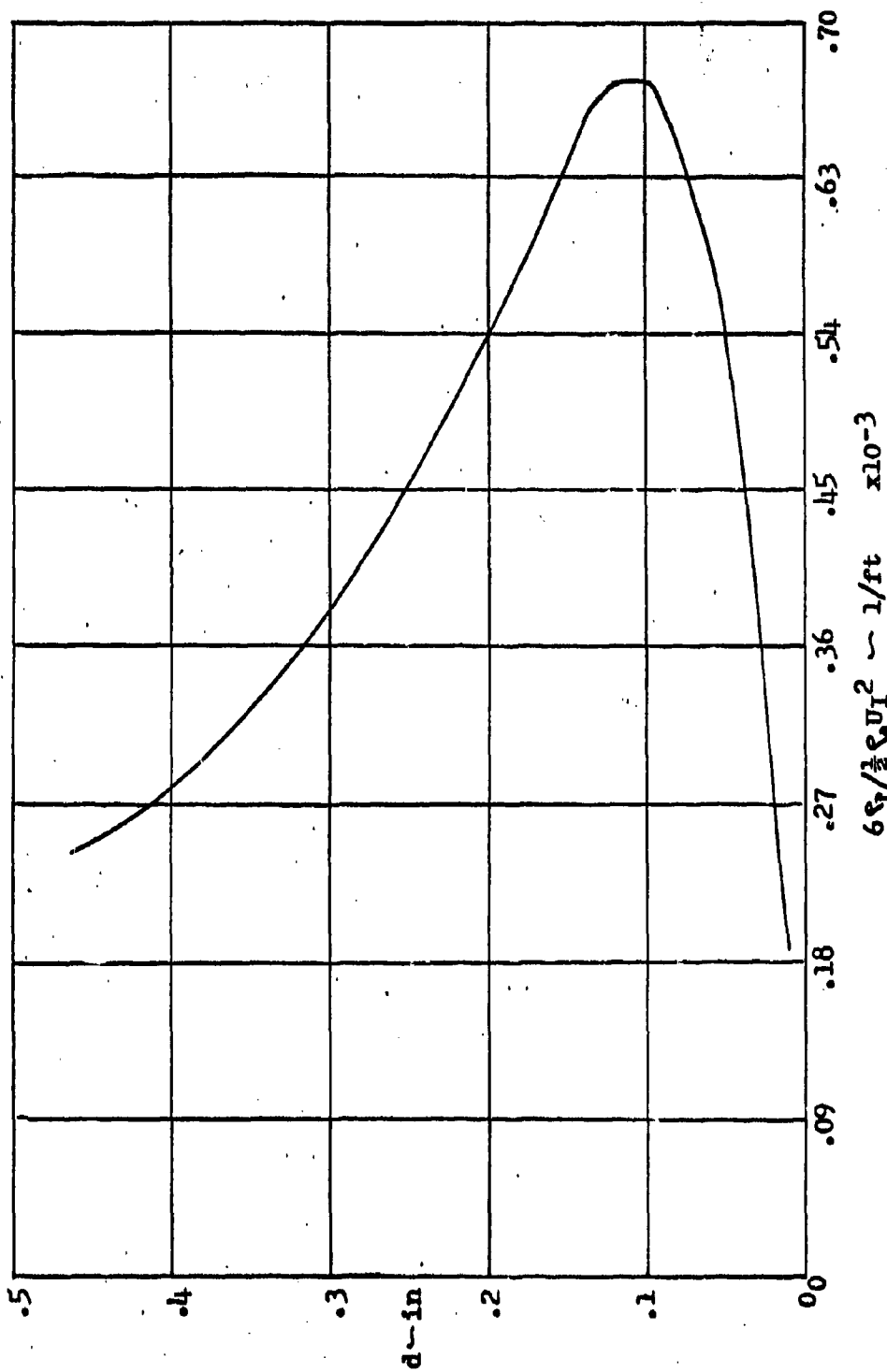


FIGURE 98
 CRITICAL PARTICLE SIZE FOR LIFT ENTRAINMENT
 $V_J = 65$ ft/sec, $Z/DN = 1$, $R/DN = 1.0$

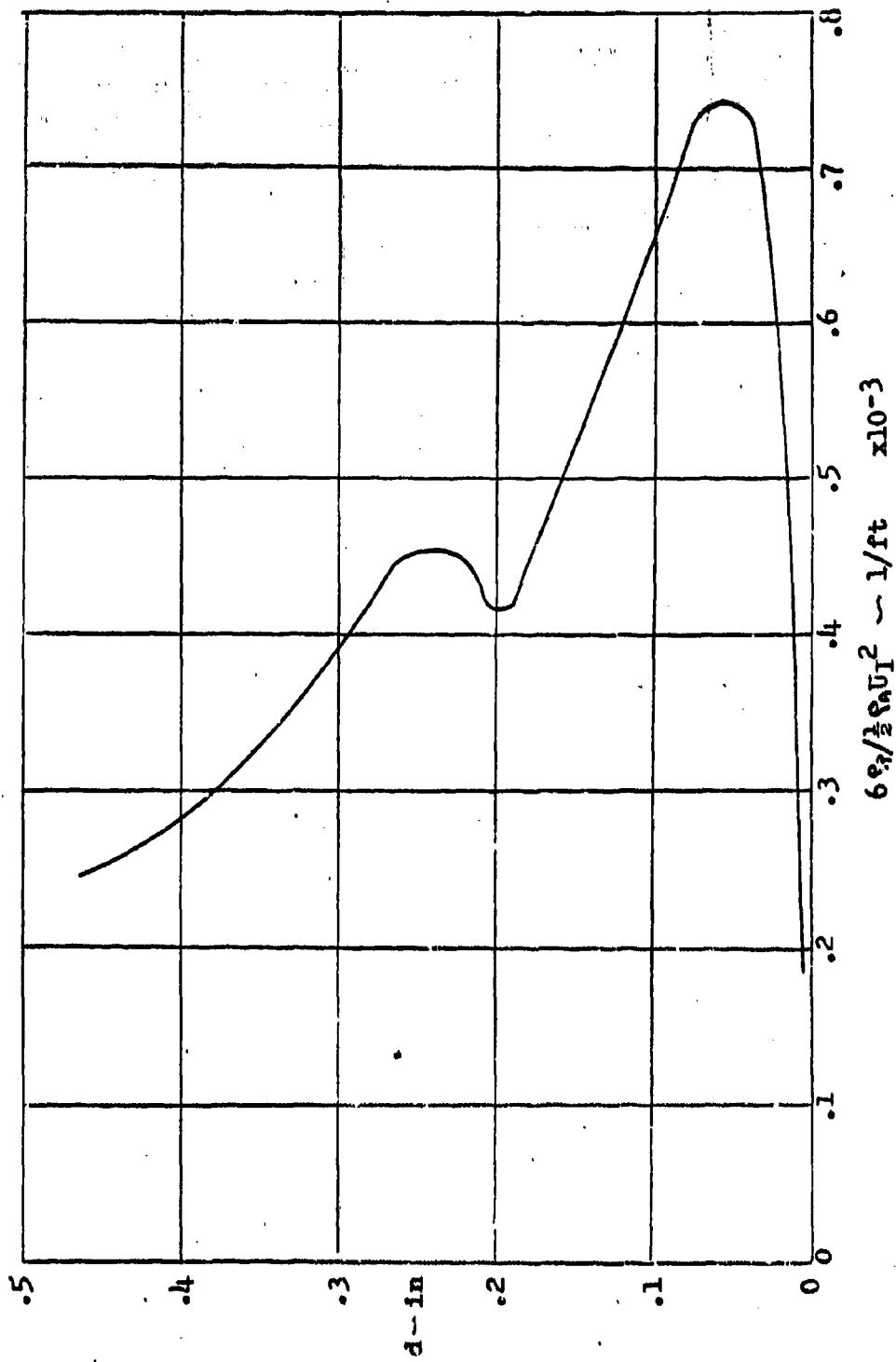


FIGURE 9h

CRITICAL PARTICLE SIZE FOR LIFT ENTRAINMENT
 $V_J = 65$ ft/sec, $z/D_N = 1$, $R/D_N = 1.33$

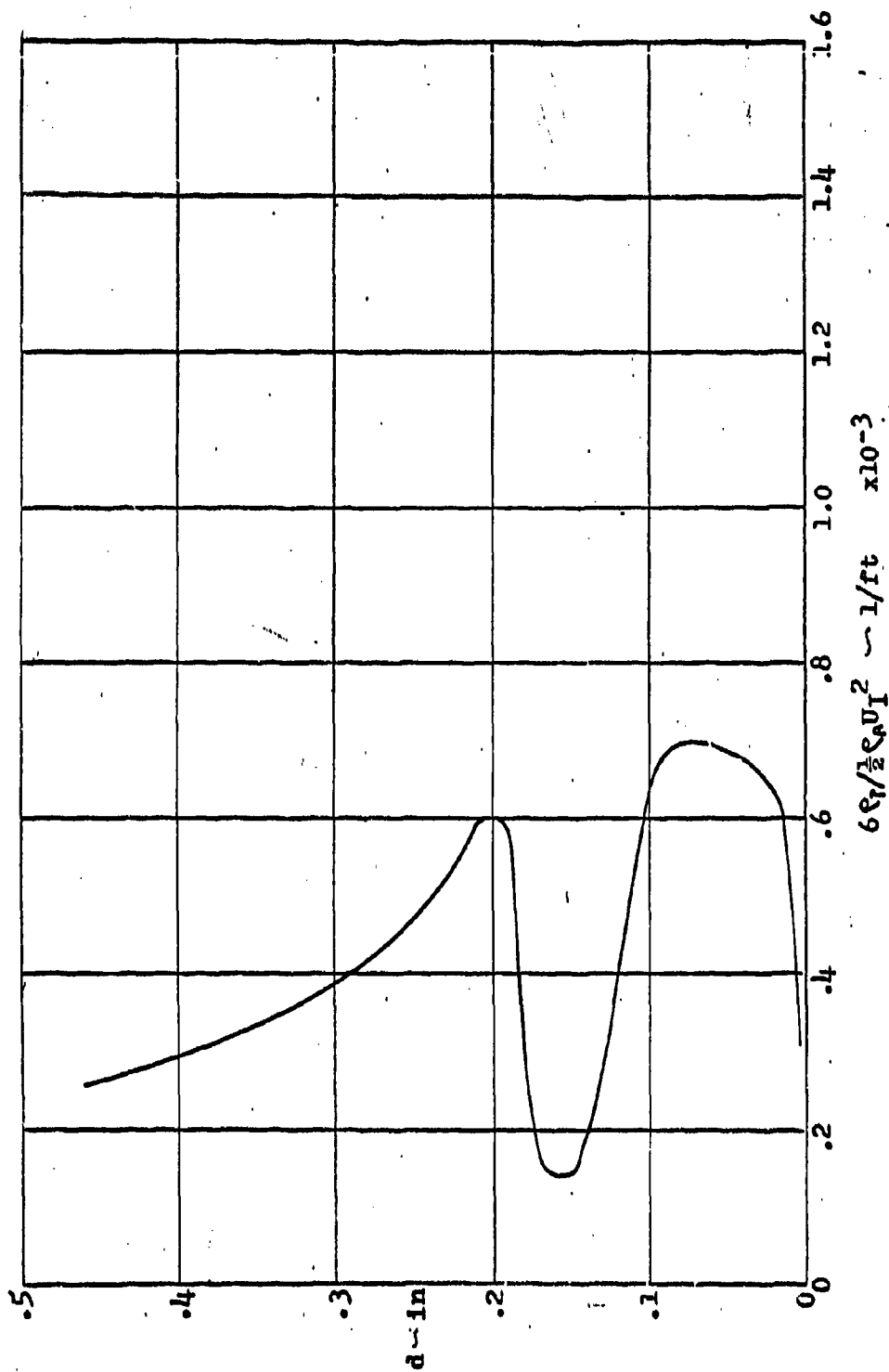


FIGURE 91

CRITICAL PARTICLE SIZE FOR LIPT ENTRAINMENT
 $V_J = 65$ ft/sec, $Z/D_N = 1$, $R/D_N = 2.0$

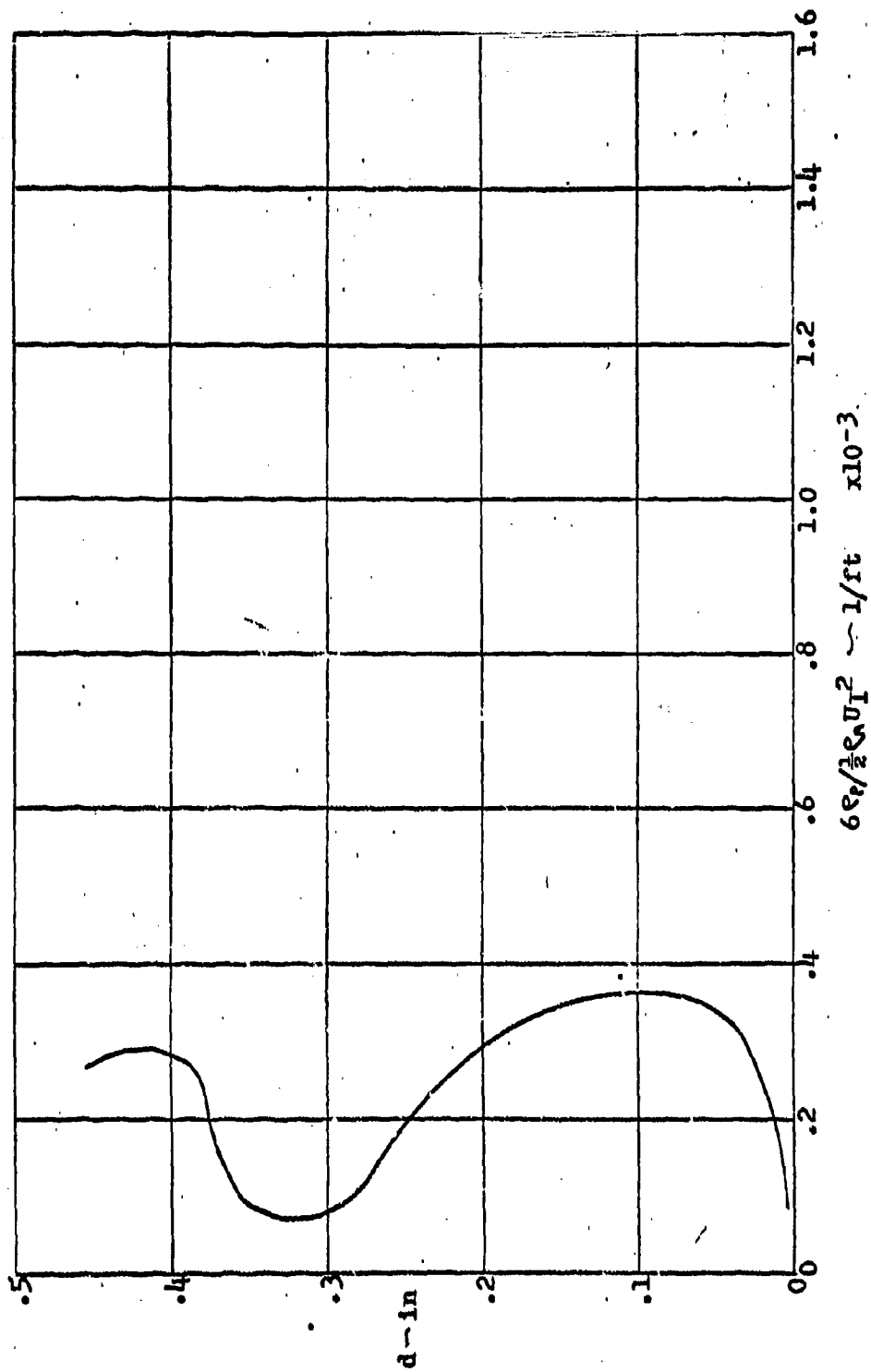


FIGURE 9J

CRITICAL PARTICLE SIZE FOR LIFT ENTRAINMENT
 $V_J = 65$ ft/sec, $Z/D_N = 1$, $R/D_N = 4.0$

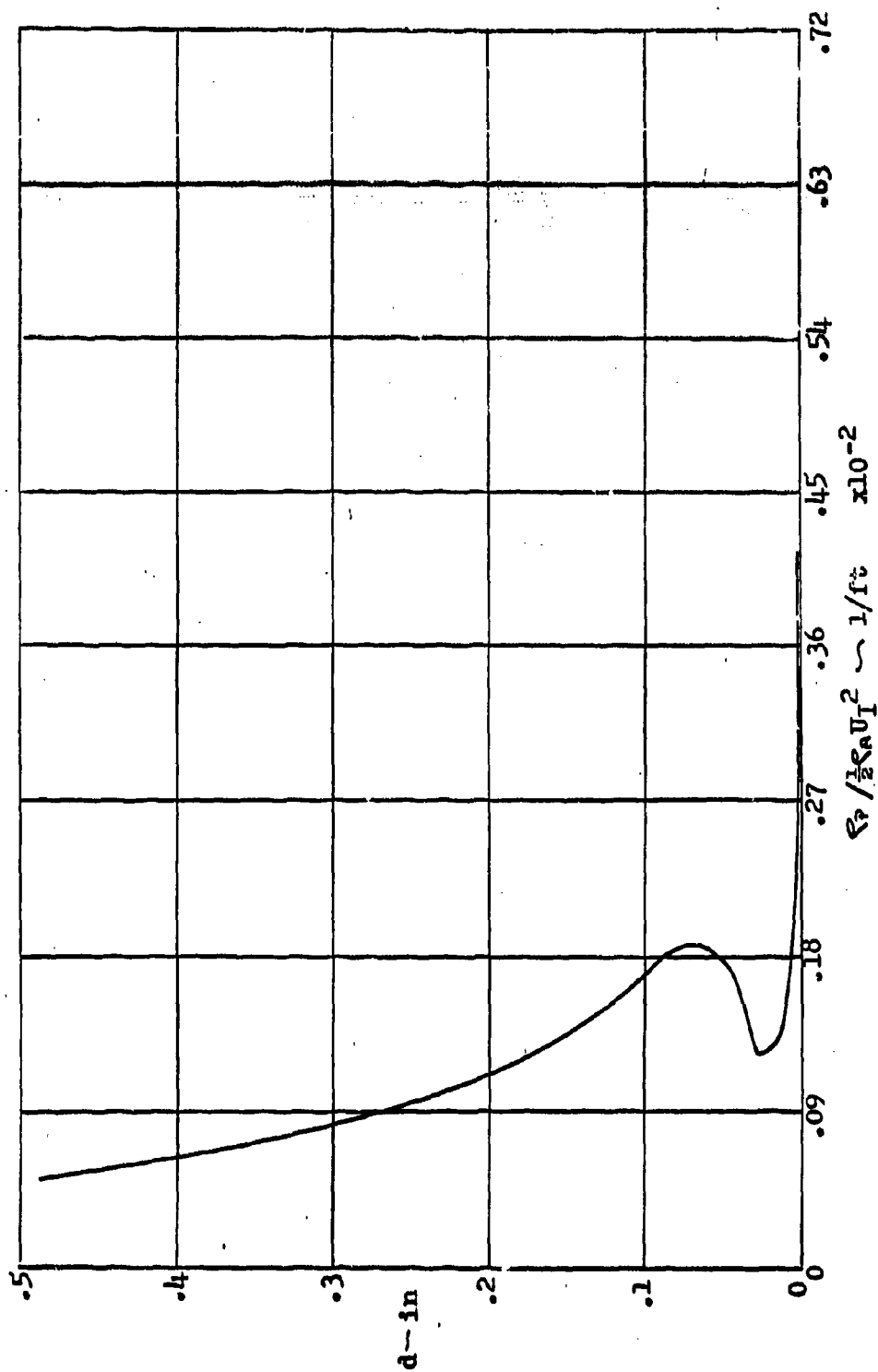


FIGURE 10a
 CRITICAL PARTICLE SIZE FOR DRAG ENTRAINMENT
 $V_J = 65$ ft/sec, $Z/D_N = 4.0$, $R/D_N = 0.5$

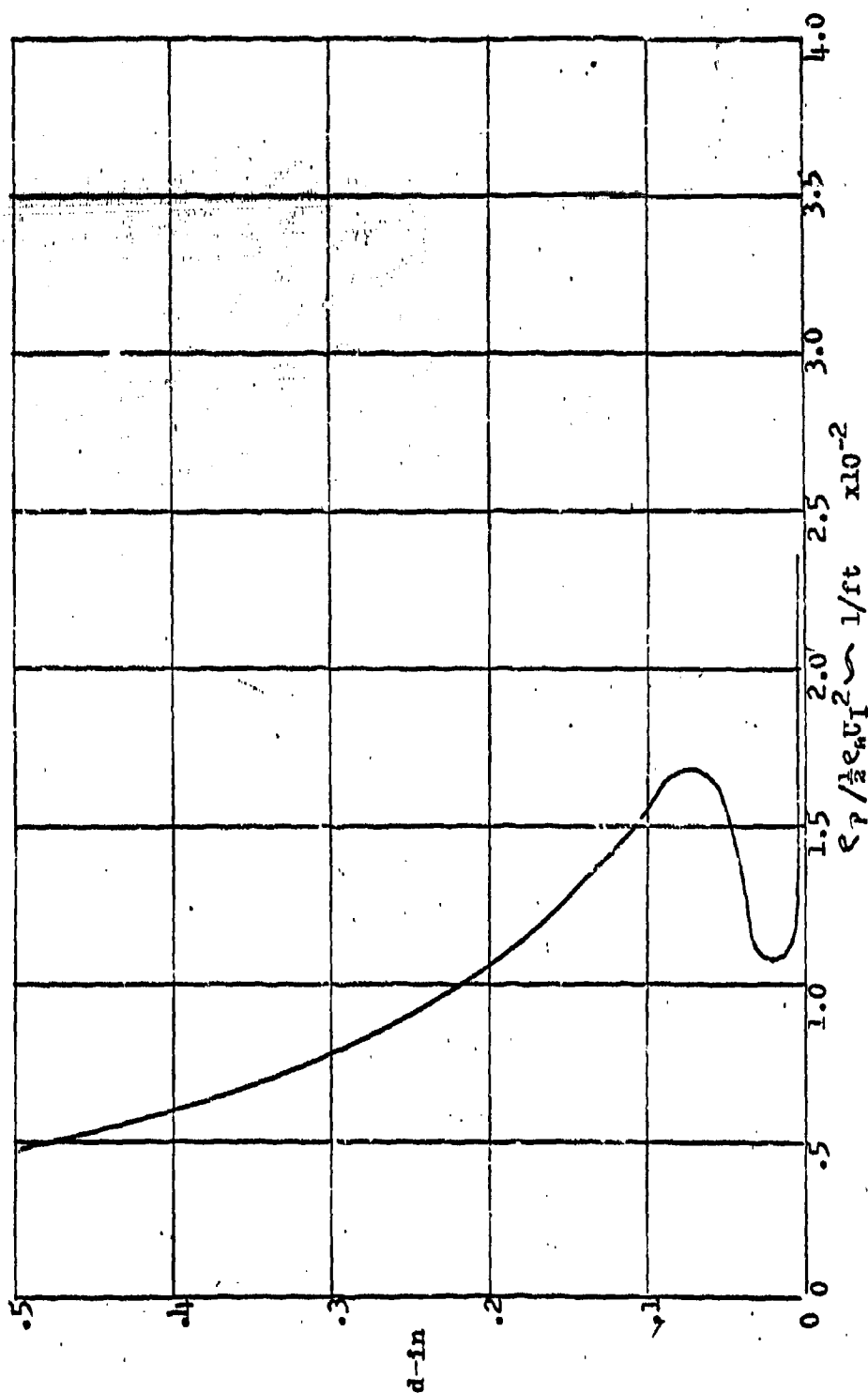


FIGURE 10b
 CRITICAL PARTICLE SIZE FOR DRAG ENTRAINMENT
 $V_J = 65$ ft/sec, $Z/D_H = 4.0$, $R/D_H = .667$

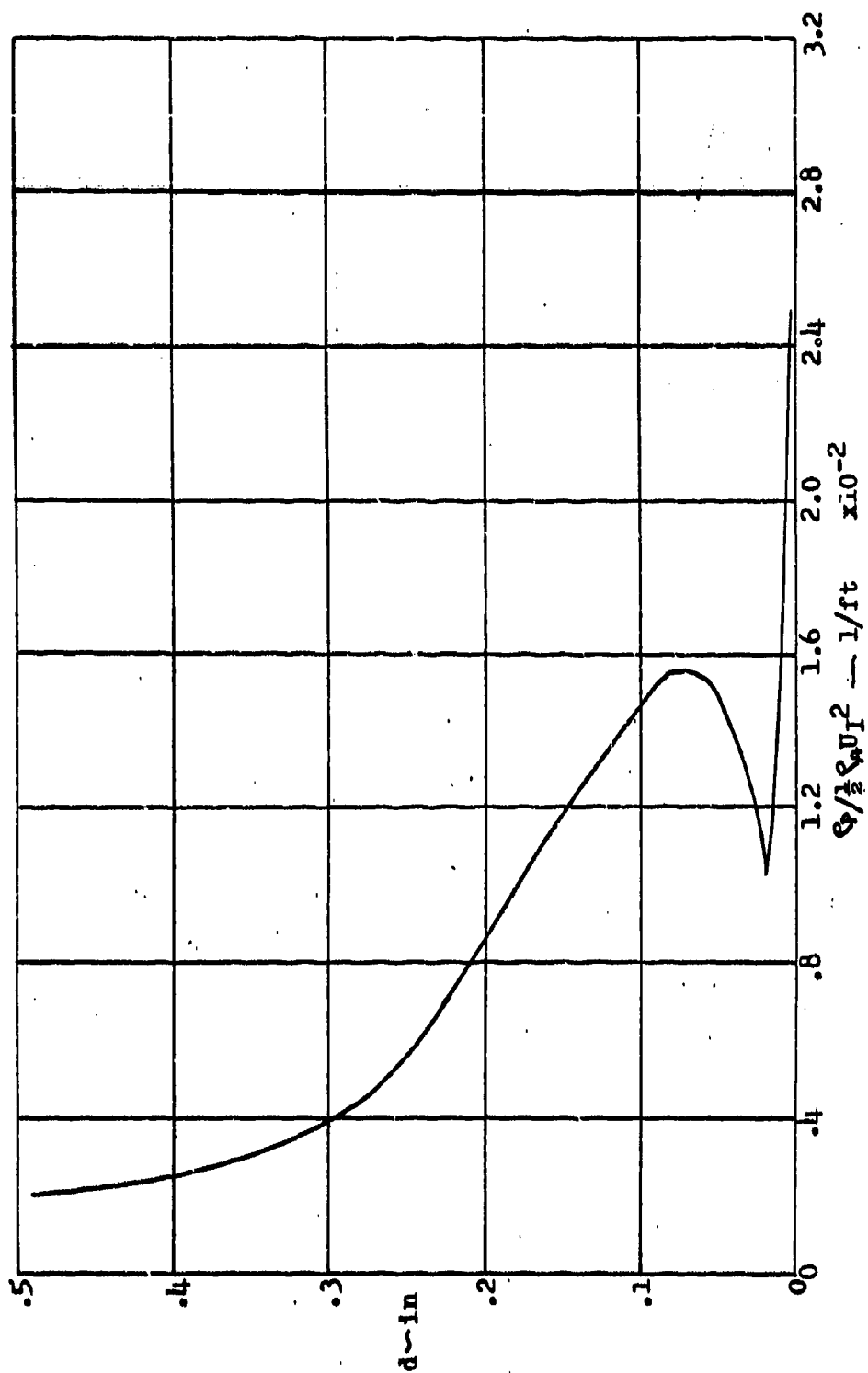


FIGURE 10c

CRITICAL PARTICLE SIZE FOR DRAG ENTRAINMENT
 $V_J = 65 \text{ ft/sec}$, $Z/D_N = 4.0$, $R/D_N = .83$

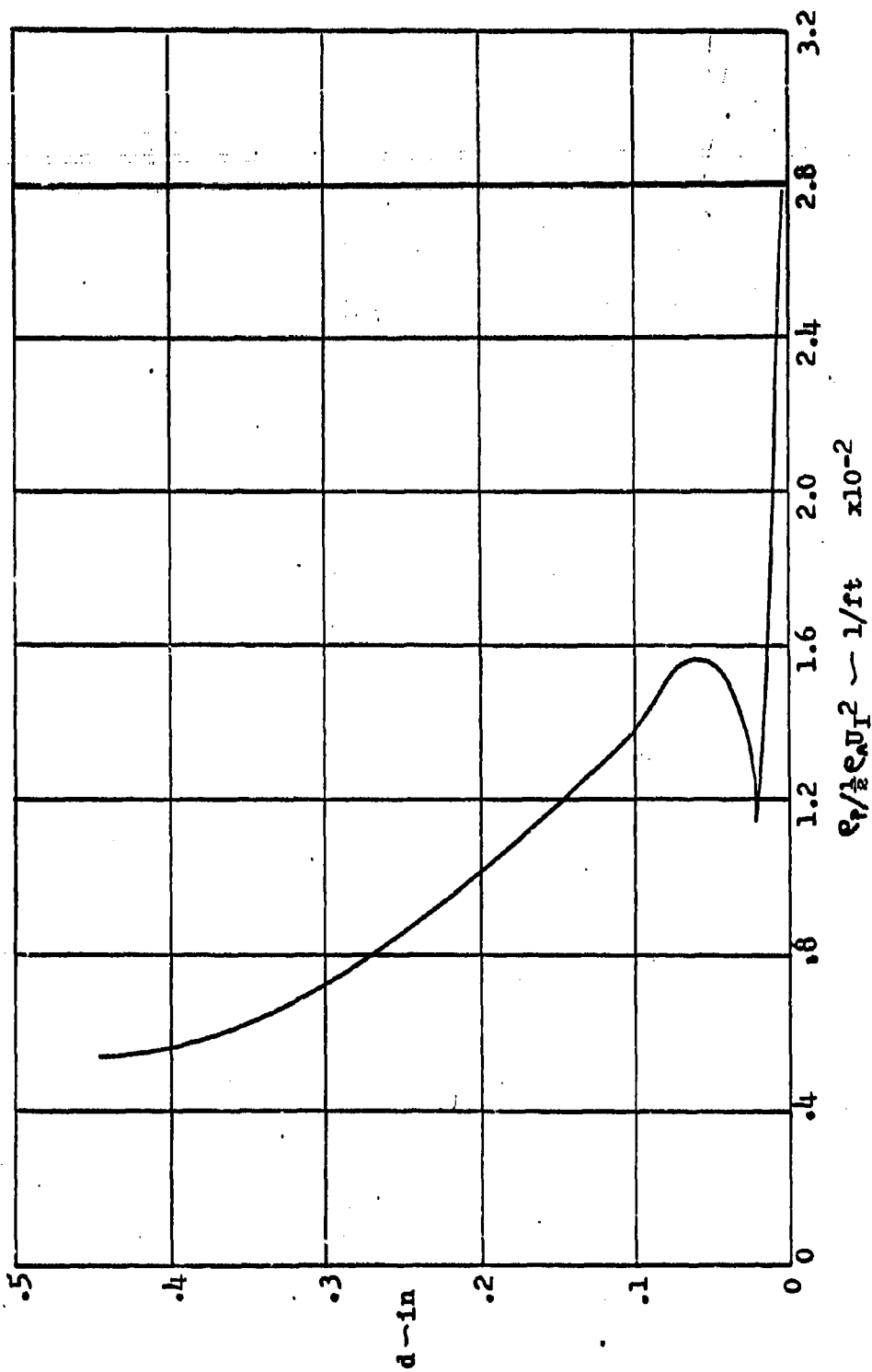


FIGURE 10d

CRITICAL PARTICLE SIZE FOR DRAG ENTRAINMENT
 $v_j = 65$ ft/sec, $z/D_N = 4.0$, $R/D_N = 1.0$

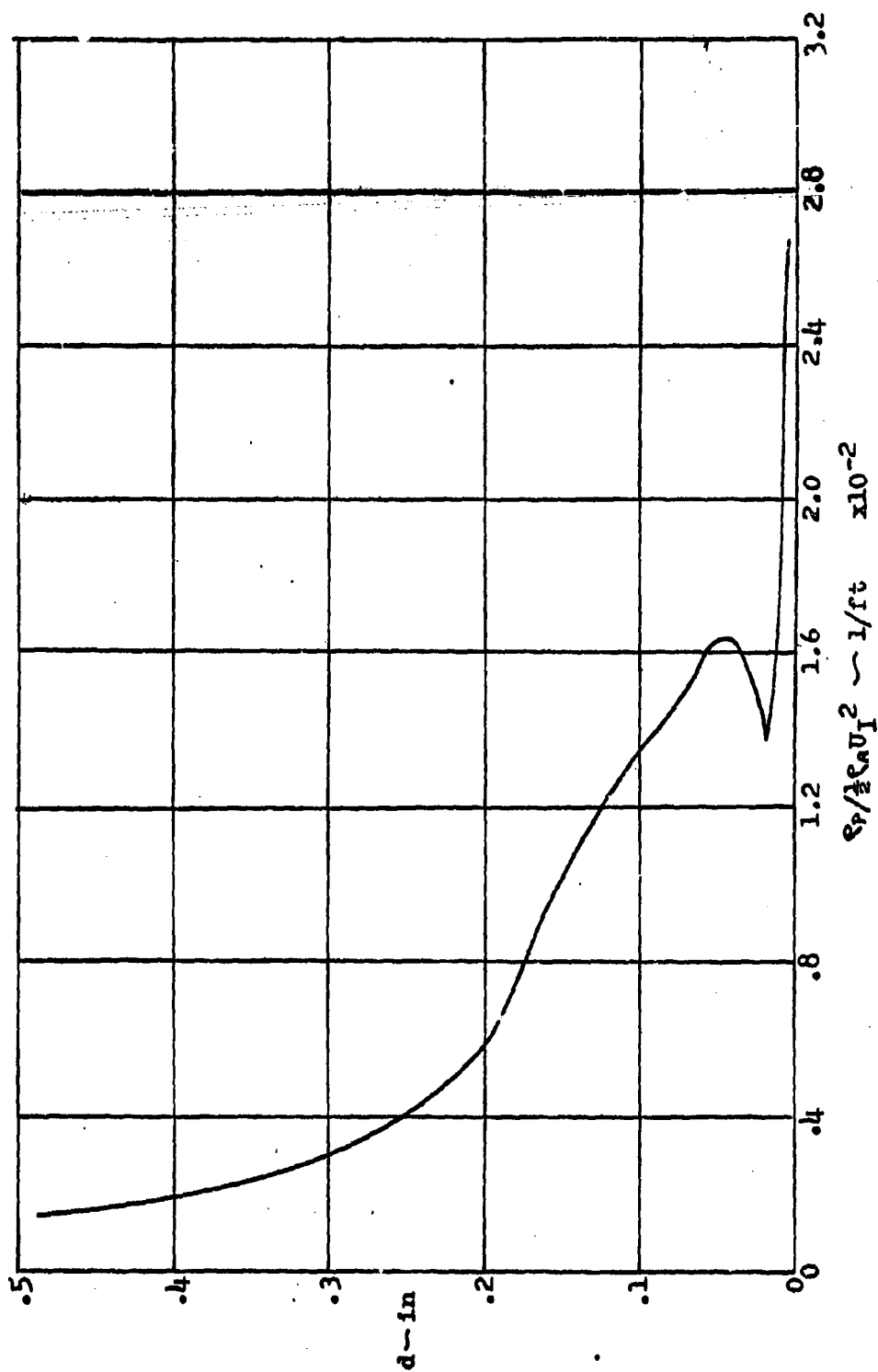


FIGURE 10

CRITICAL PARTICLE SIZE FOR DRAG ENTRAINMENT
 $V_J = 65$ ft/sec, $Z/D_N = 4.0$, $R/D_N = 1.17$

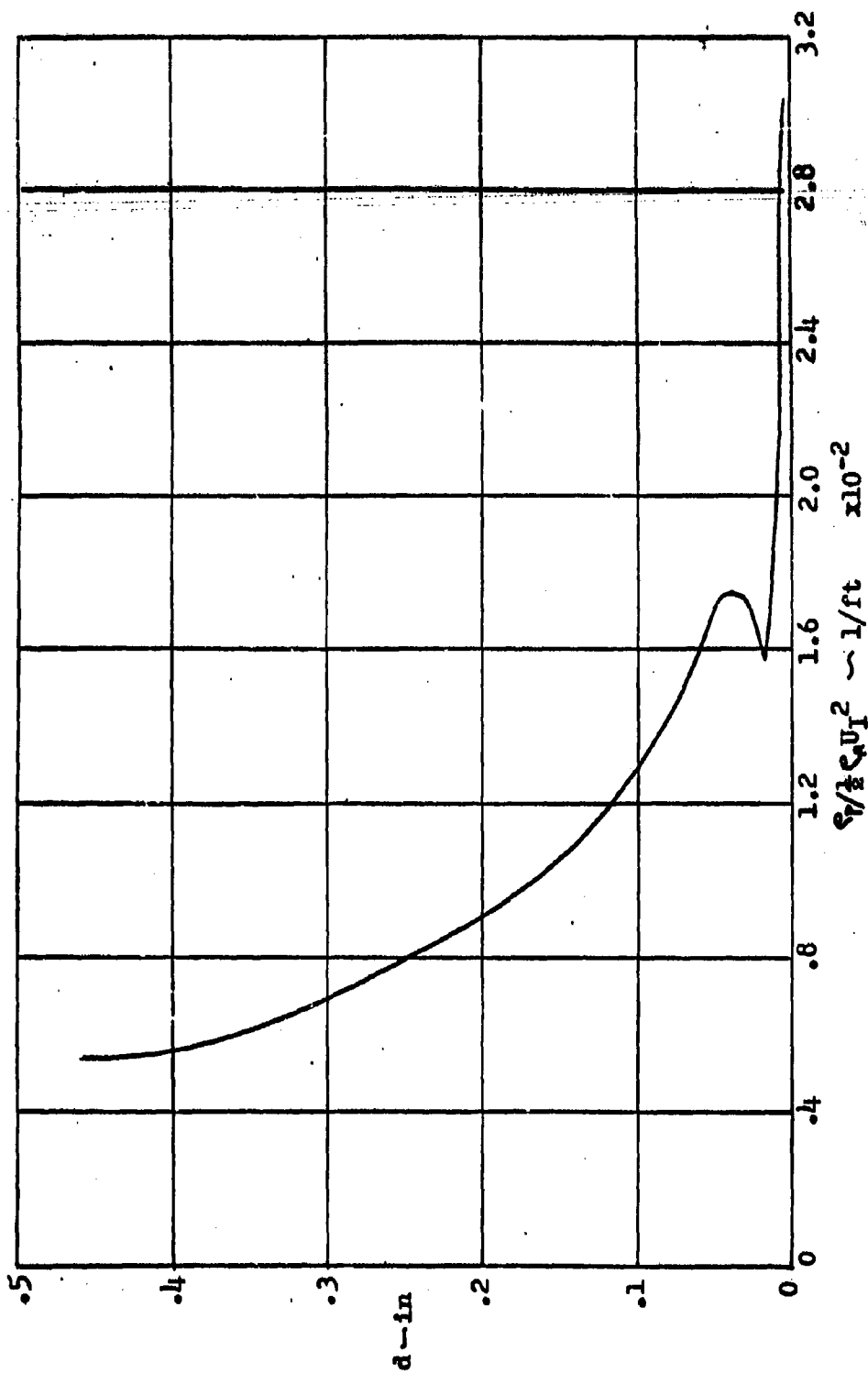


FIGURE 10f

CRITICAL PARTICLE SIZE FOR DRAG ENTRAINMENT

$V_J = 65$ ft/sec, $Z/D_N = 4.0$, $R/D_N = 1.33$

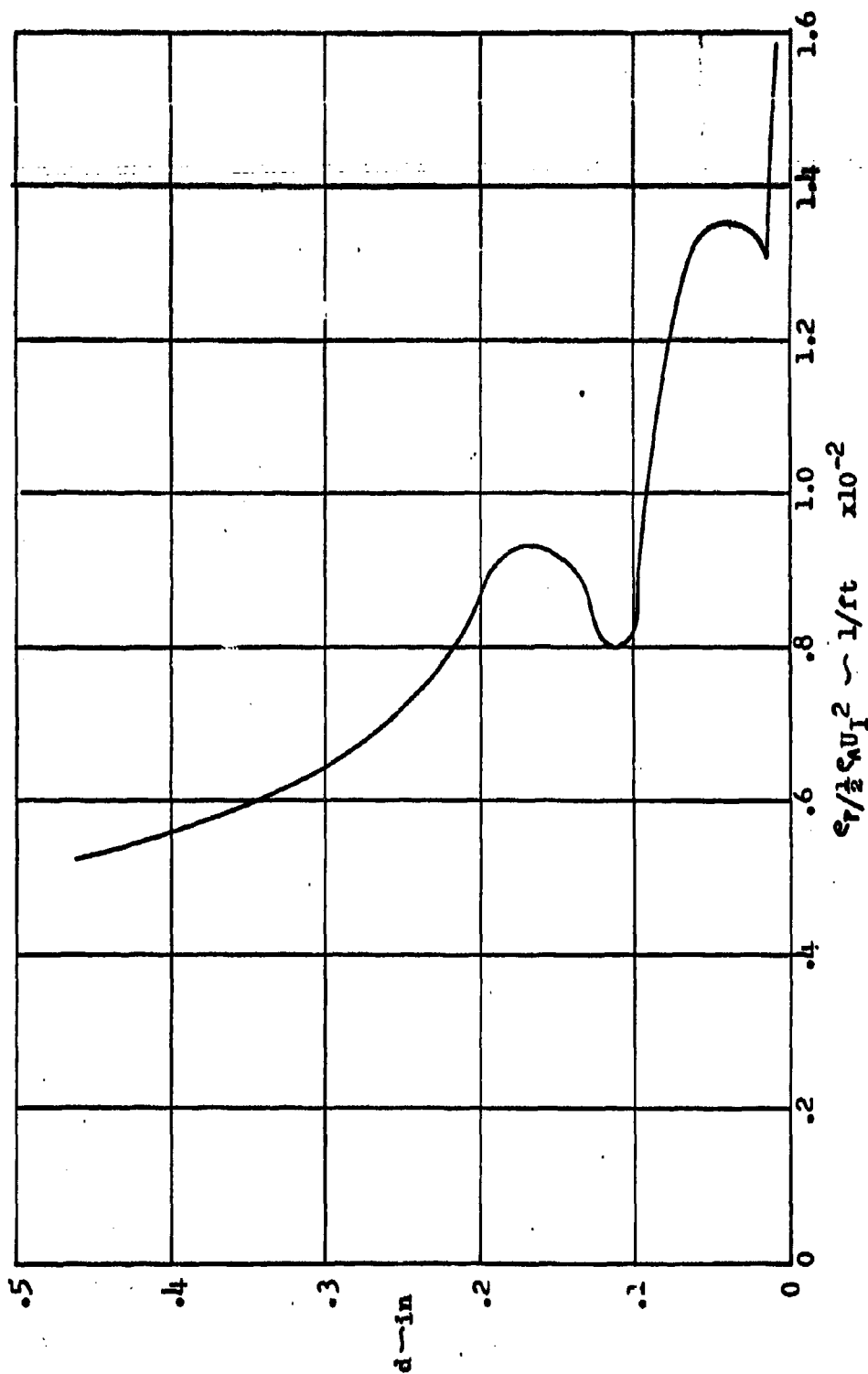


FIGURE 10g

CRITICAL PARTICLE SIZE FOR DRAG ENTRAINMENT
 $V_J = 65$ ft/sec, $Z/D_H = 4.0$, $R/D_H = 2.0$

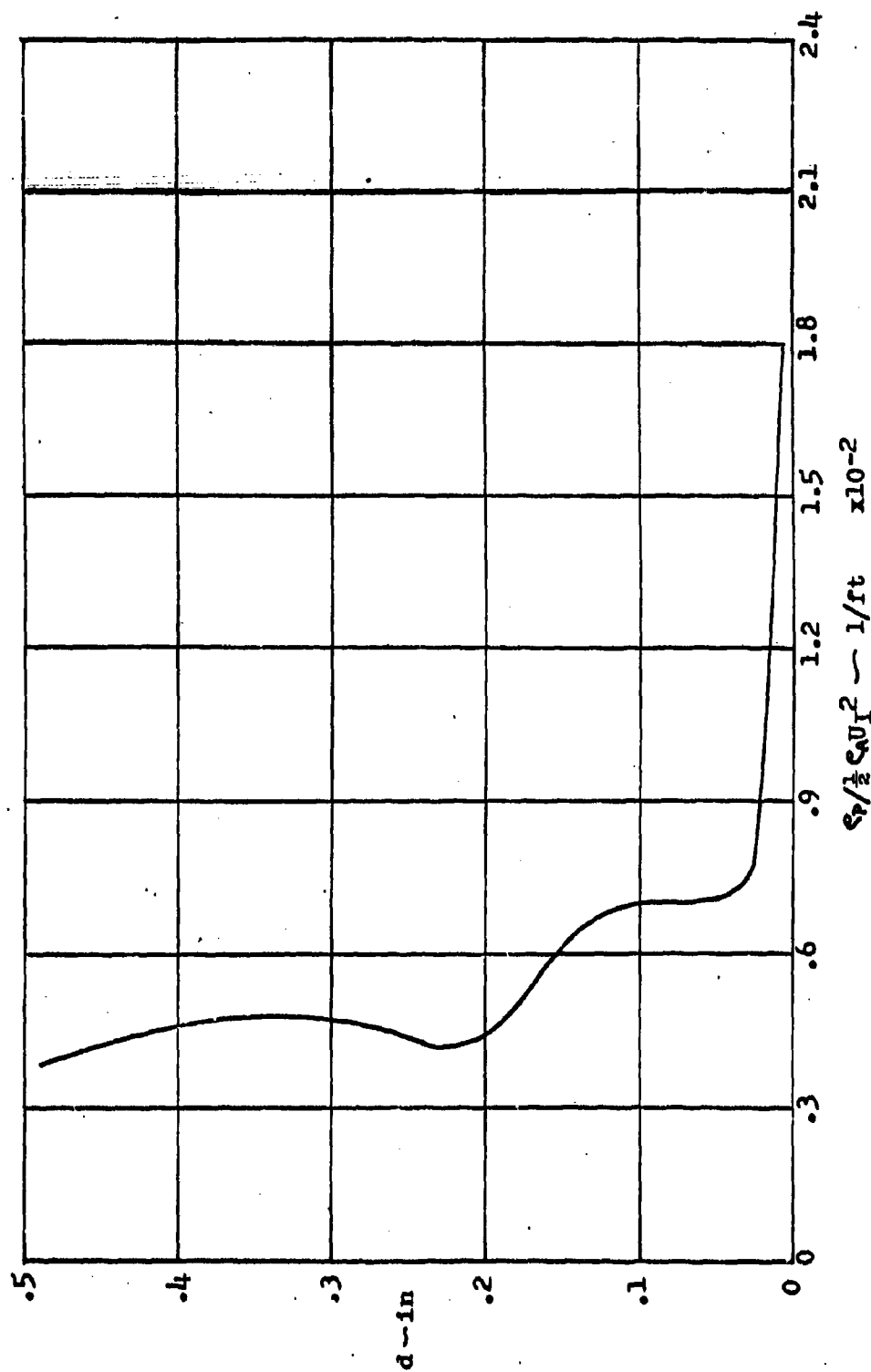


FIGURE 10h
 CRITICAL PARTICLE SIZE FOR DRAG ENTRAINMENT
 $V_J = 65 \text{ ft/sec}$, $Z/D_N = 4.0$, $R/D_N = 4.0$

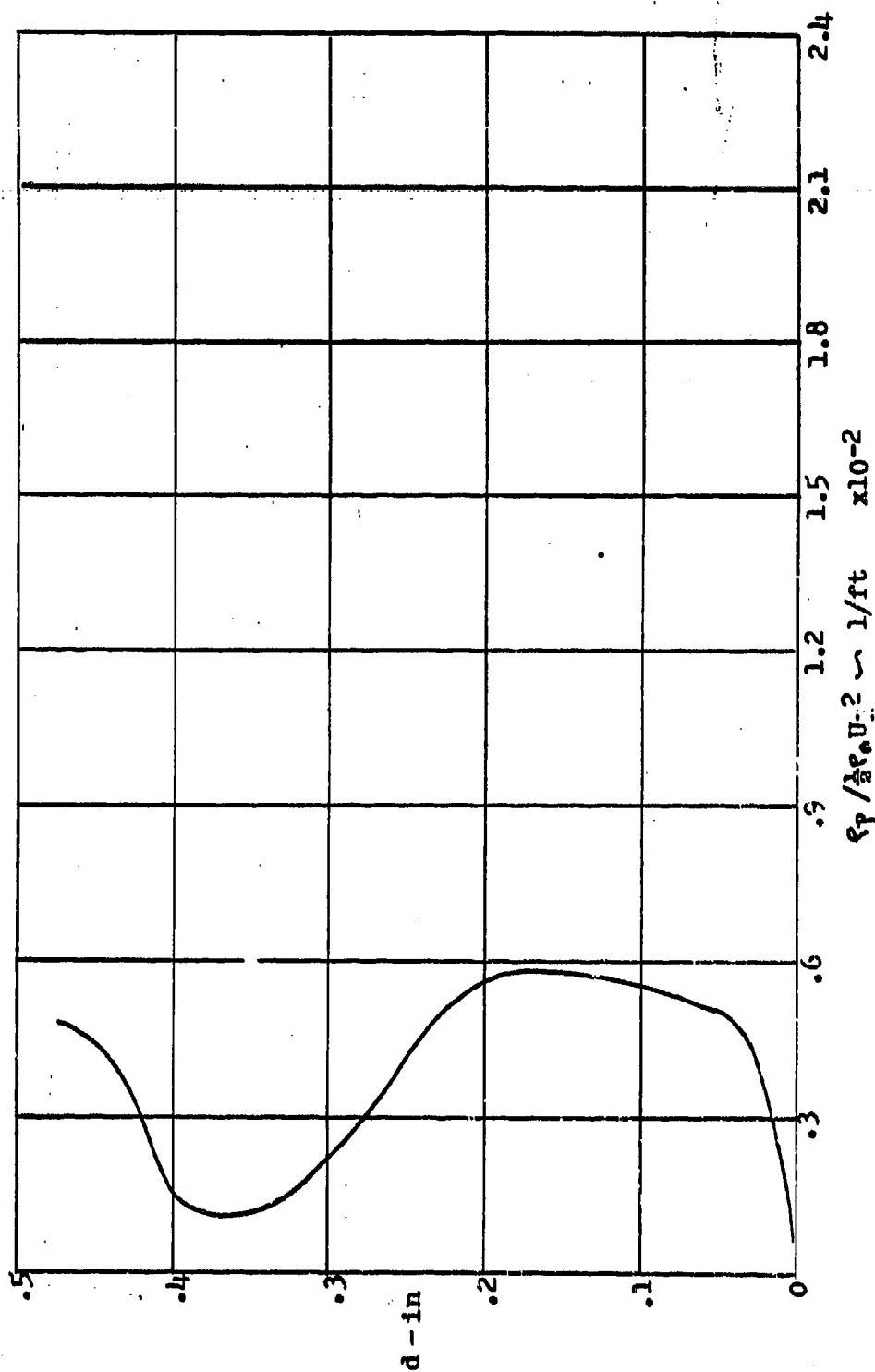
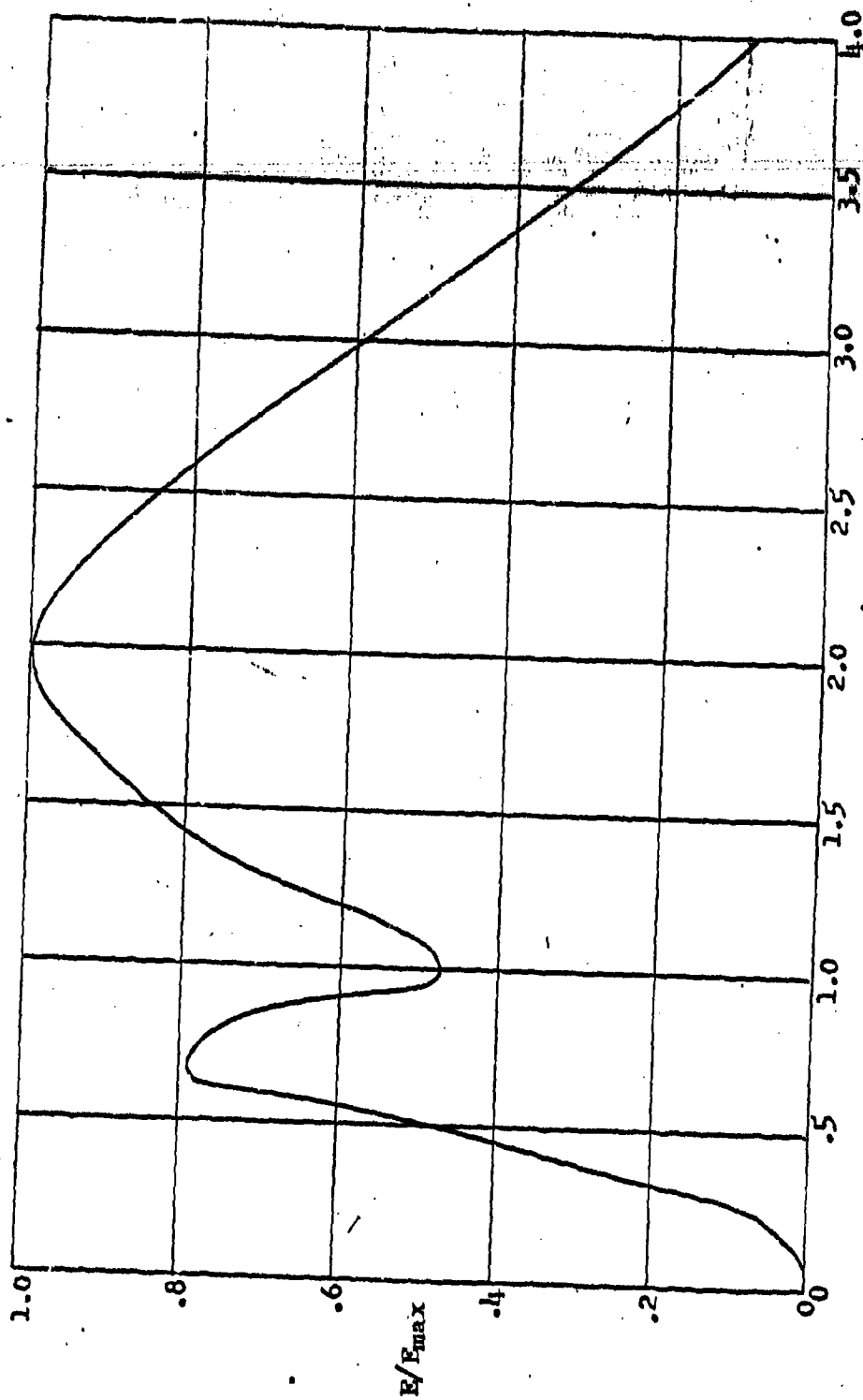


FIGURE 11
 CRITICAL PARTICLE SIZE FOR LIFT ENTRAINMENT
 $V_J = 65$ ft/sec, $Z/D_N = 4.0$, $R/D_N = 4.0$



R/D_N

FIGURE 12a

INCIDENT EROSION RATE
 PARTICLE DIAM. = .003 in, $V_J = 65$ ft/sec, $Z/D_N = .5$

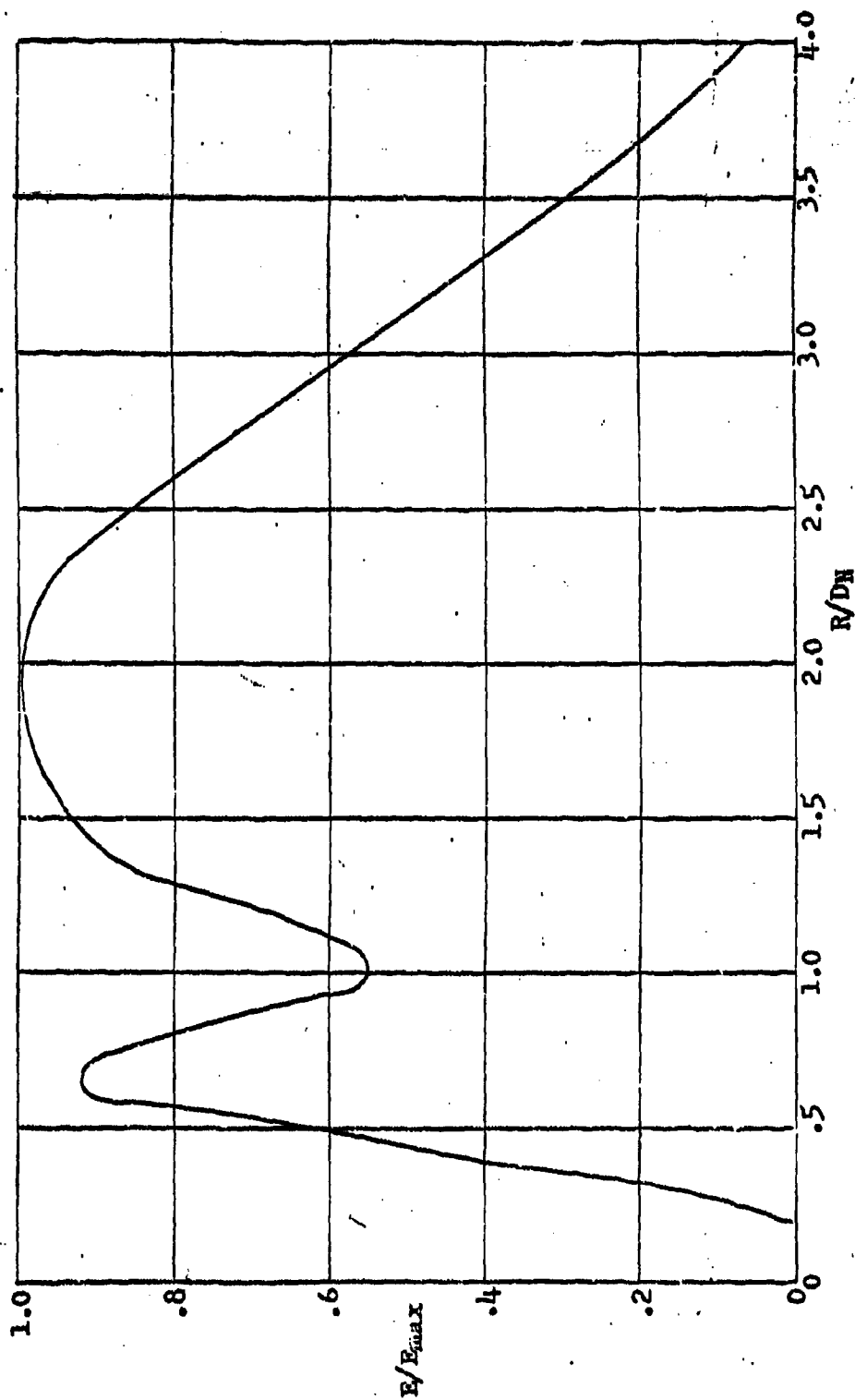


FIGURE 12b

INCIPIENT EROSION RATE
 PARTICLE DIAM. = .007 in, $V_j = 65$ ft/sec, $z/D_N = .5$

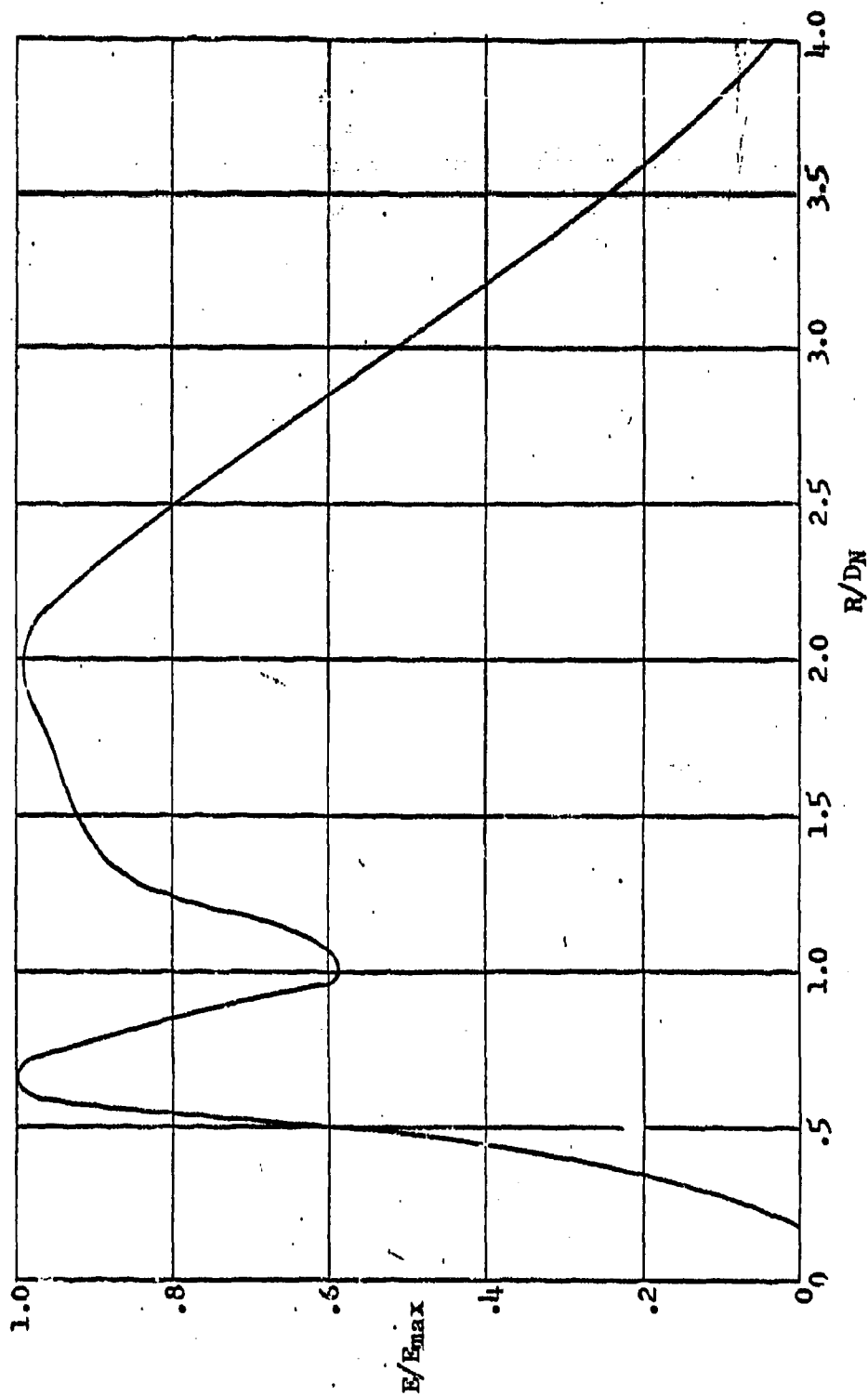


FIGURE 12c

INCIPIENT EROSION RATE
 PARTICLE DIA. $\approx .01$ in, $V_J = 65$ ft/sec, $Z/D_N = .5$

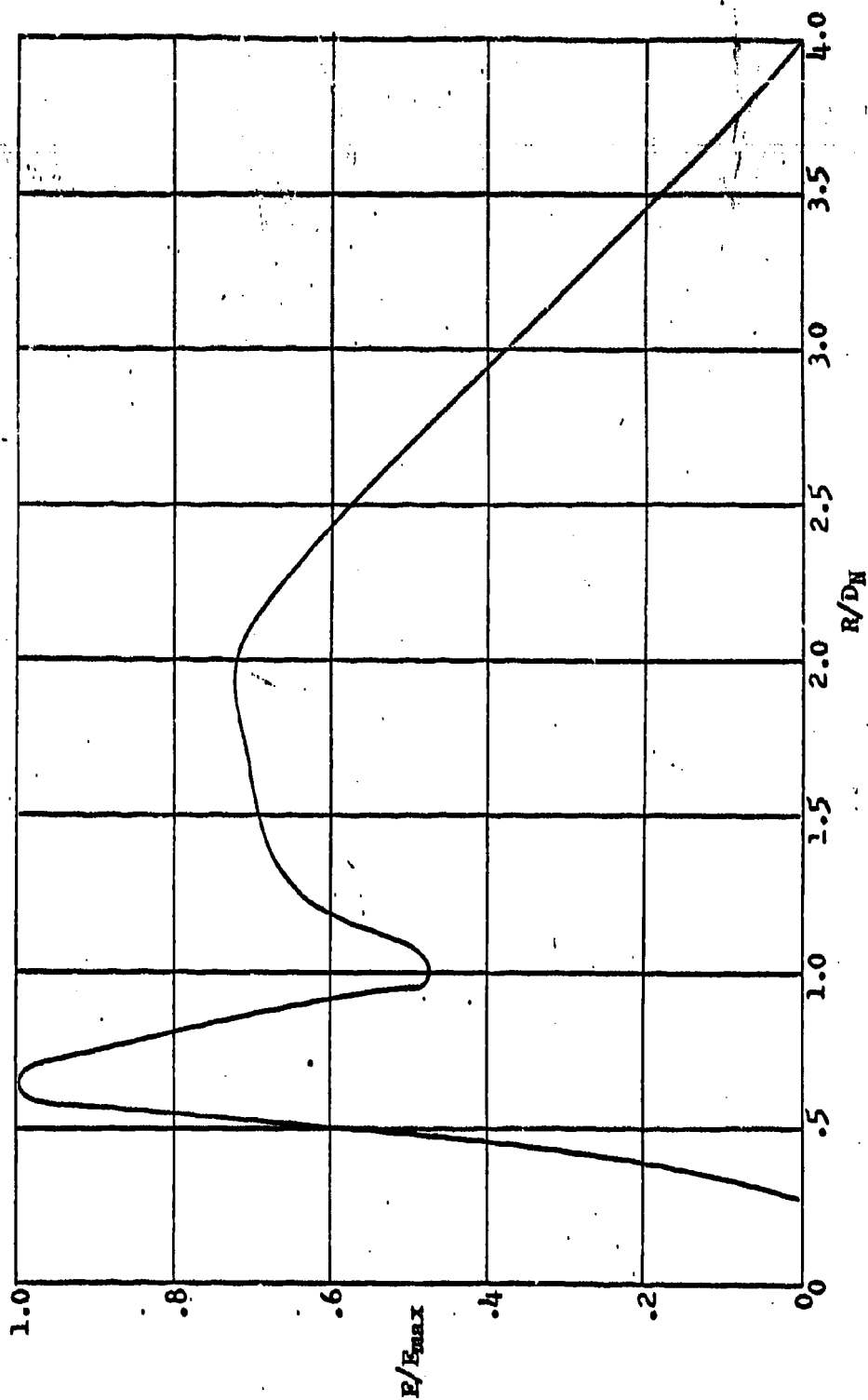


FIGURE 12d

INCIPIENT EROSION RATE
 PARTICLE DIAM. = .02 in, $V_J = 65$ ft/sec, $z/D_N = .5$

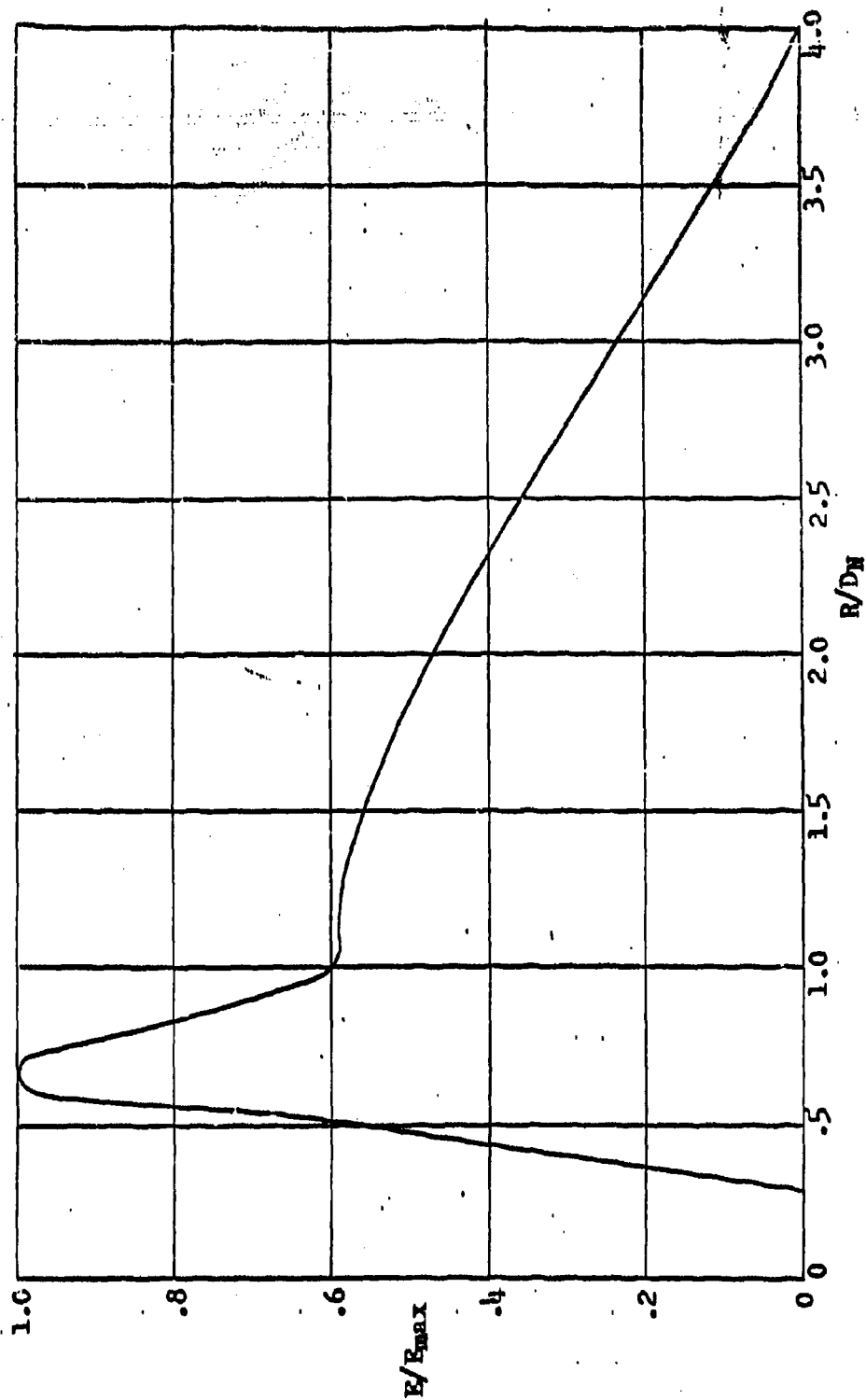


FIGURE 12.

INCIPIENT EROSION RATE
 PARTICLE DIAM. = .04 in, $V_J = 65$ ft/sec, $z/D_H = .5$

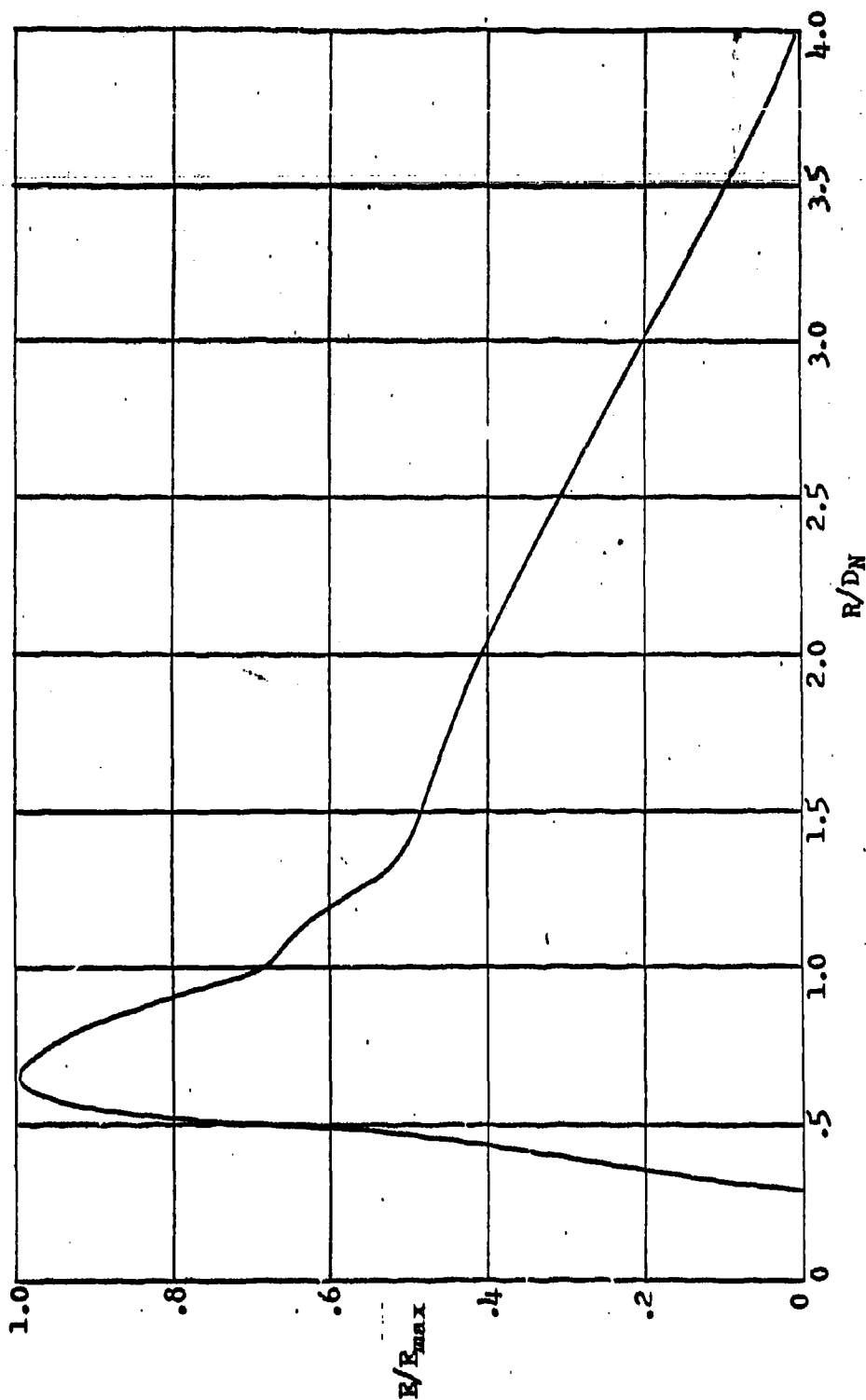


FIGURE 12f
 INCIPIENT EROSION RATE
 PARTICLE DIAM. = .06 in, $V_j = 65$ ft/sec, $z/D_H = .5$

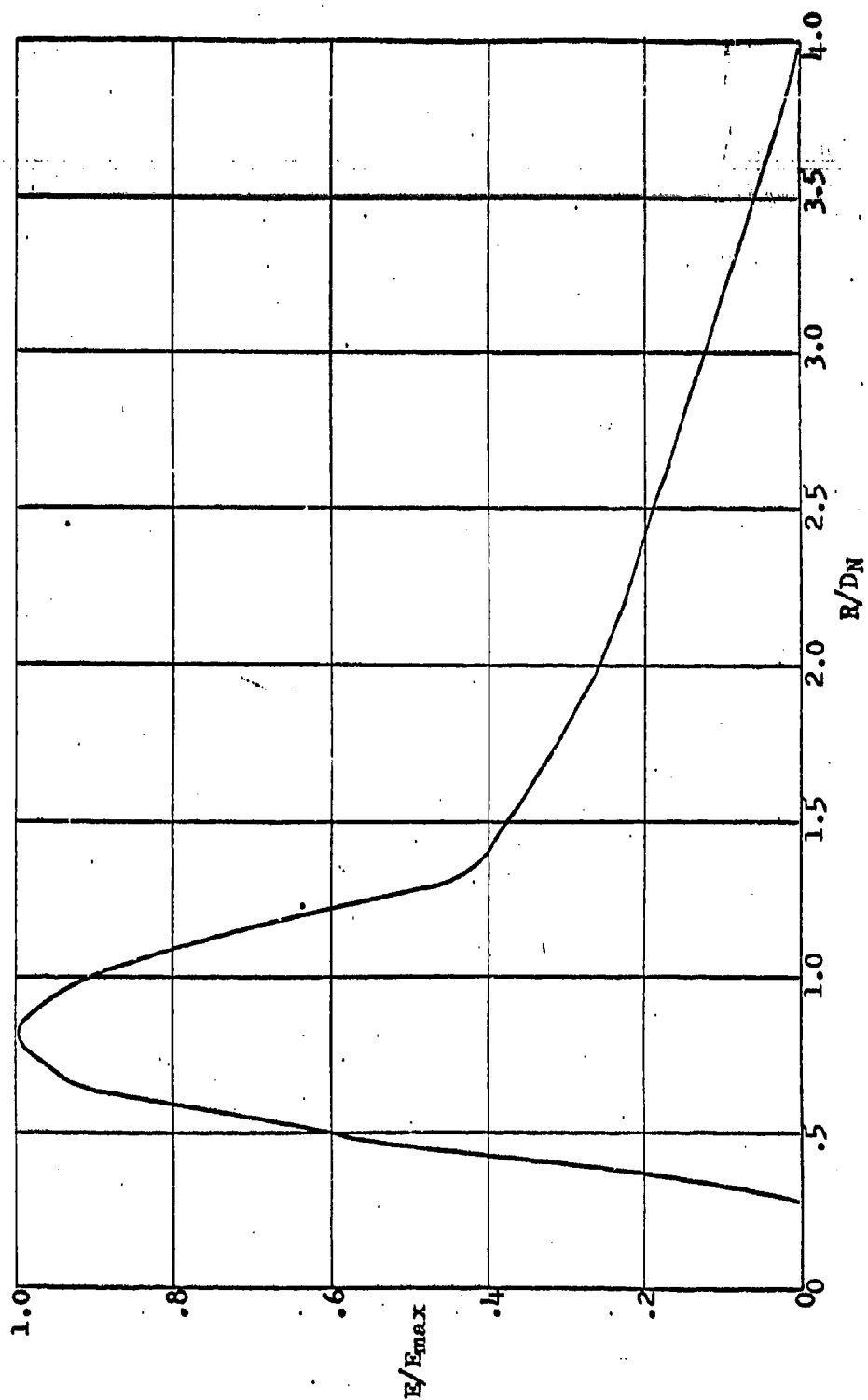


FIGURE 12g

INCIPIENT EROSION RATE
 PARTICLE DIAM. = .125 in, $V_j = 65$ ft/sec, $Z/D_N = .5$

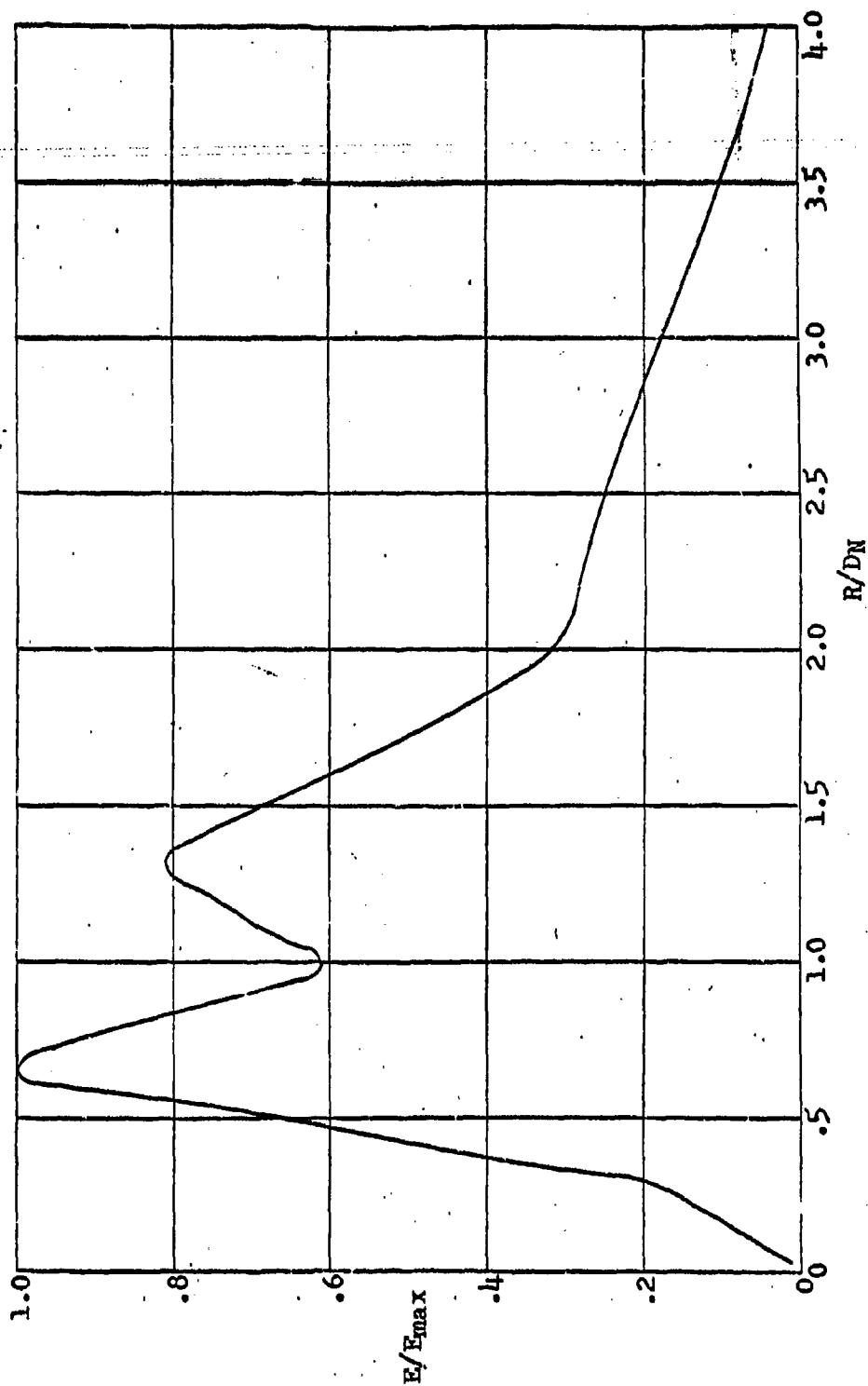


FIGURE 13a
 INCIPIENT EROSION RATE
 PARTICLE DIAM. = .003 in, $V_J = 500$ ft/sec, $Z/D_N = .5$

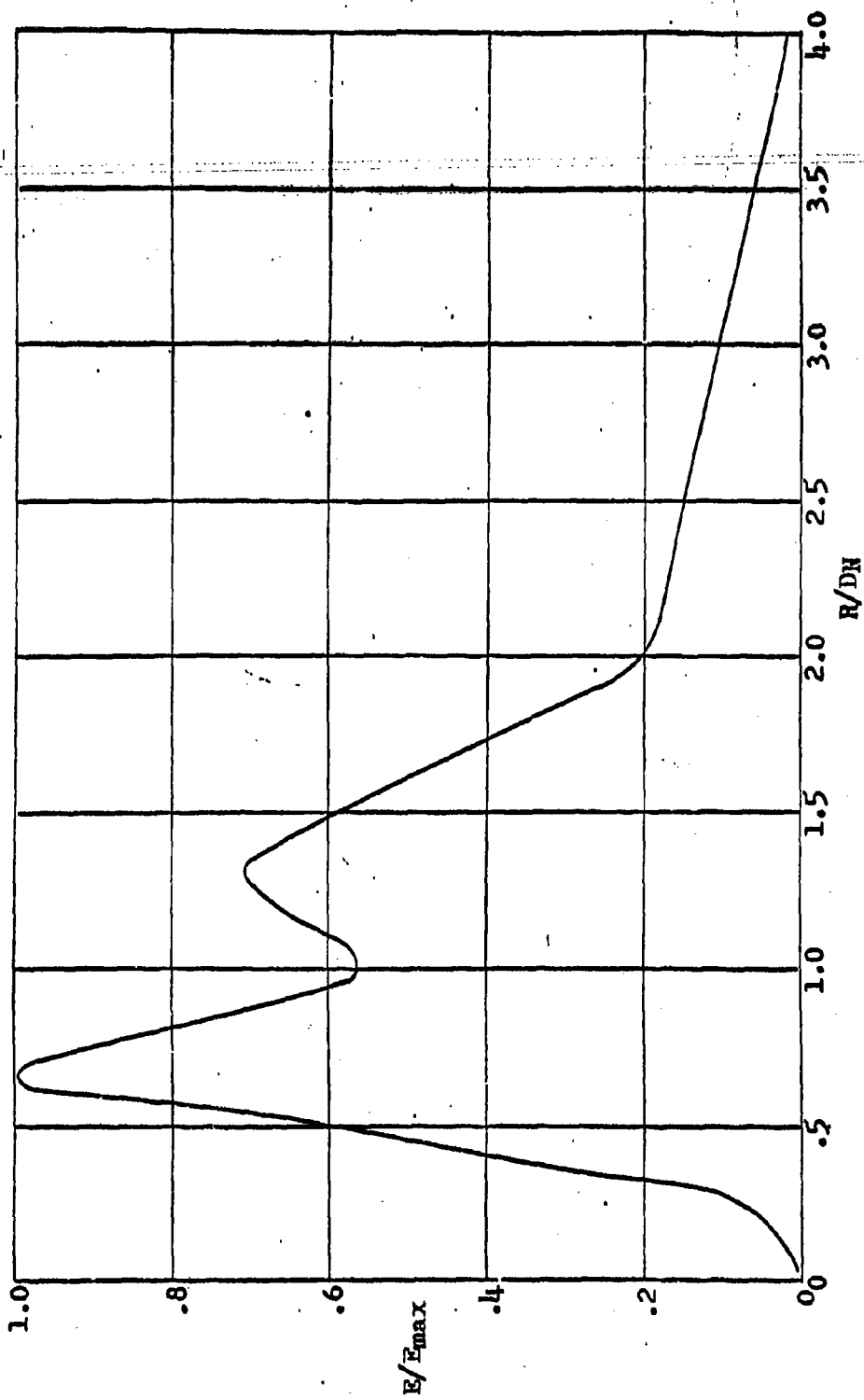


FIGURE 13b

INCIPIENT EROSION RATE
 PARTICLE DIAM. $\approx .007$ in, $V_J = 500$ ft/sec, $z/D_N = .5$

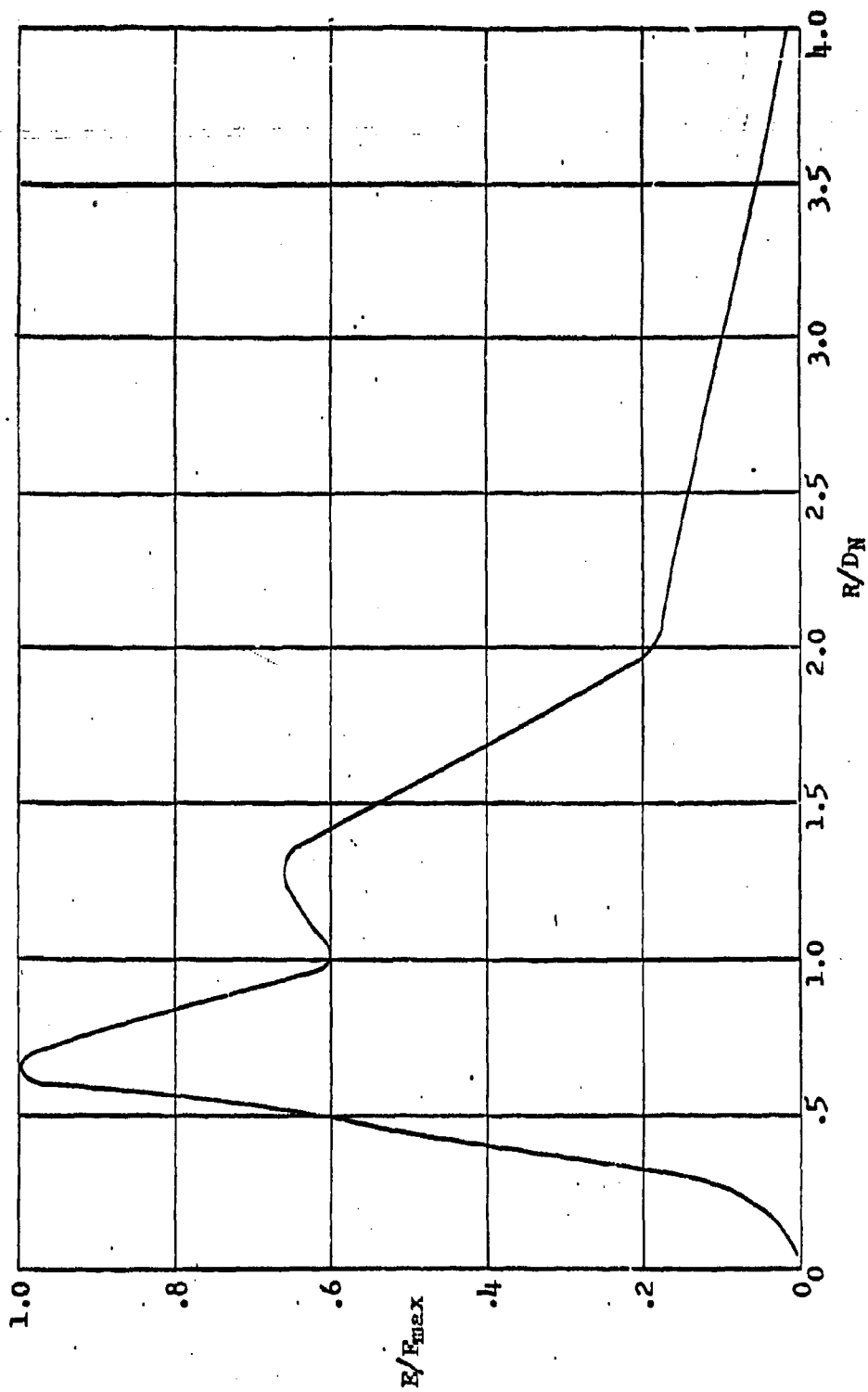


FIGURE 13c
 INCIPIENT EROSION RATE
 PARTICLE DIAH. = .01 in, $V_J = 500$ ft/sec, $z/D_N = .5$

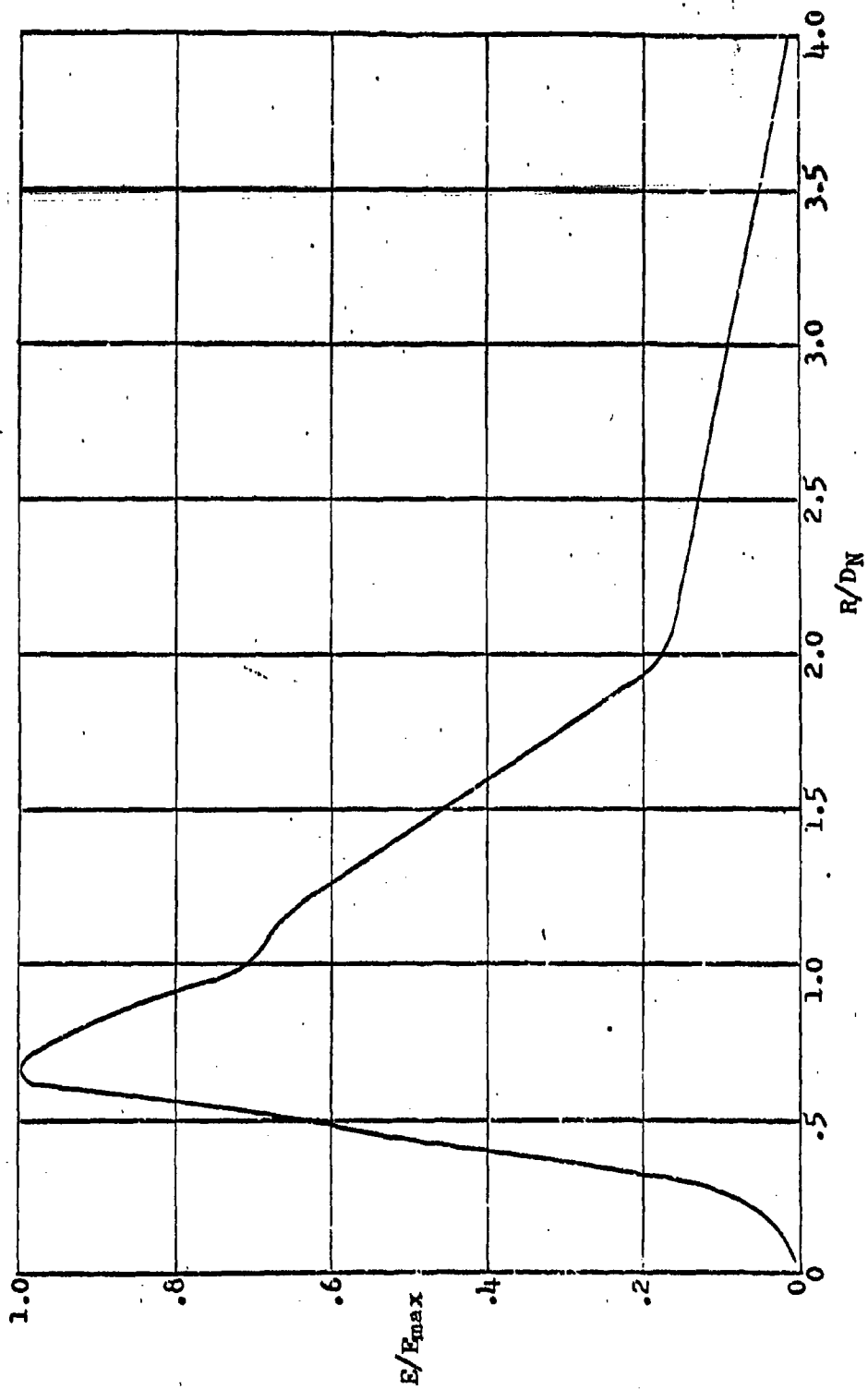


FIGURE 13d

INCIPIENT EROSION RATE
 PARTICLE DIAM. = .02 in, $V_j = 500$ ft/sec, $z_i/DN = .5$

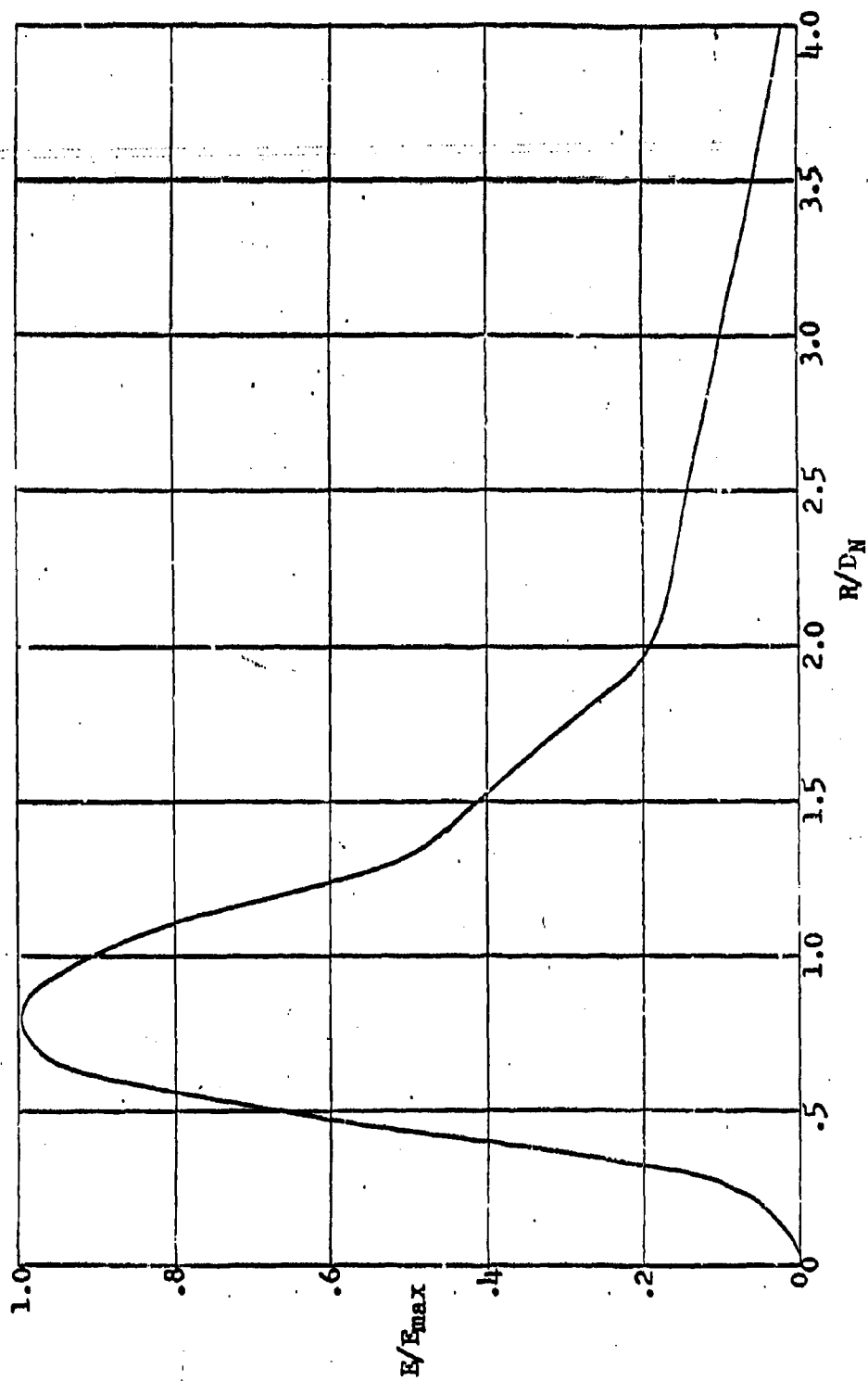


FIGURE 13.
 INCIDENT EROSION RATE
 PARTICLE DIAM. = .04 in, $V_J = 500$ ft/sec, $Z/D_N = .5$

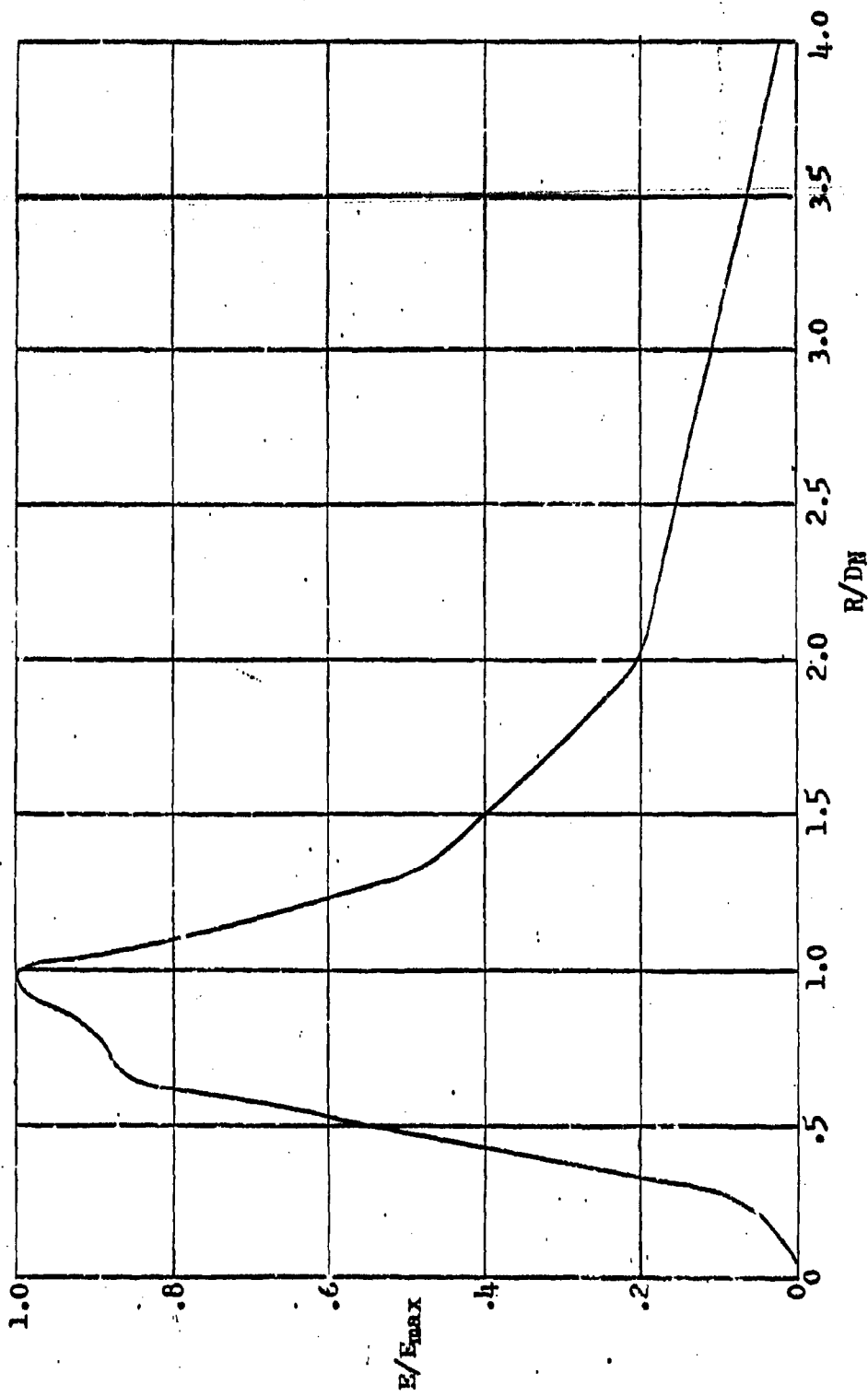


FIGURE 13f

INCIDENT EROSION RATE
 PARTICLE DIAM. = .06 in, $V_j = 500$ ft/sec, $Z/D_N = .5$

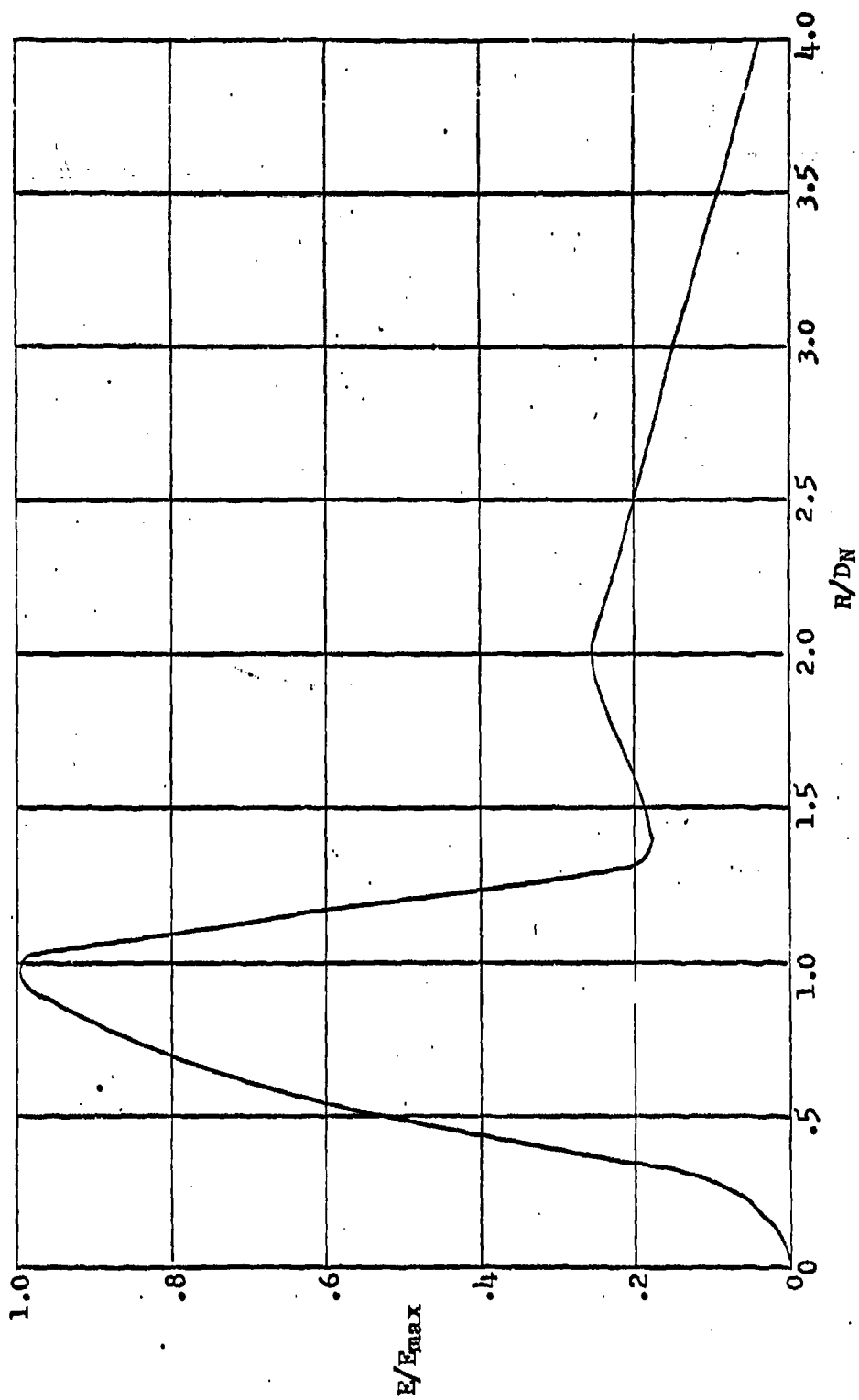


FIGURE 13g
 INCIPIENT EROSION RATE
 PARTICLE DIAM. = .125 in, $V_J = 500$ ft/sec, $Z/D_N = .5$

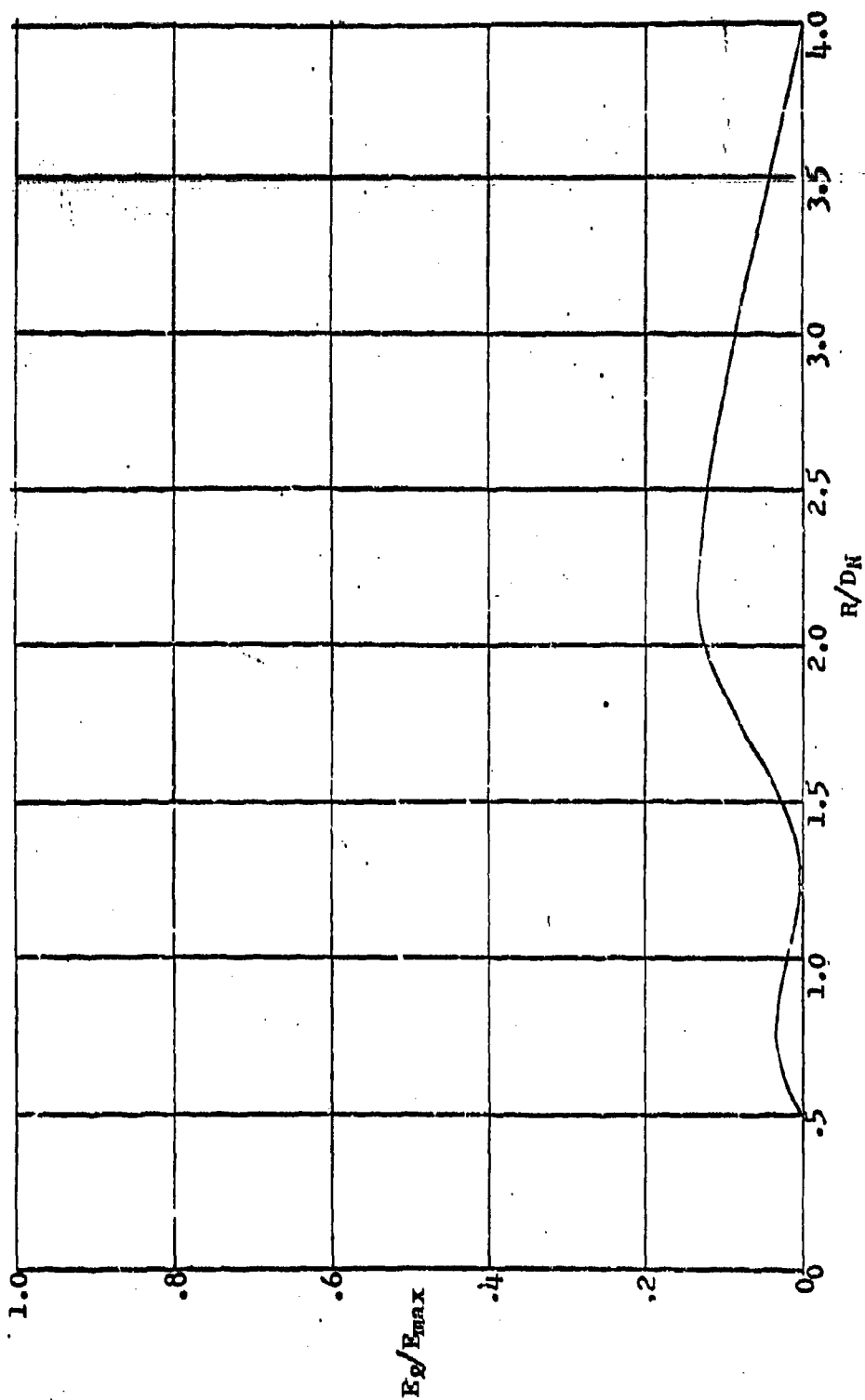


FIGURE 14a

INCIPIENT EROSION RATE FOR LIFT ENTRAINMENT
 PARTICLE DIAM. = .003 in, $V_J = 65$ ft/sec, $z/D_N = .5$

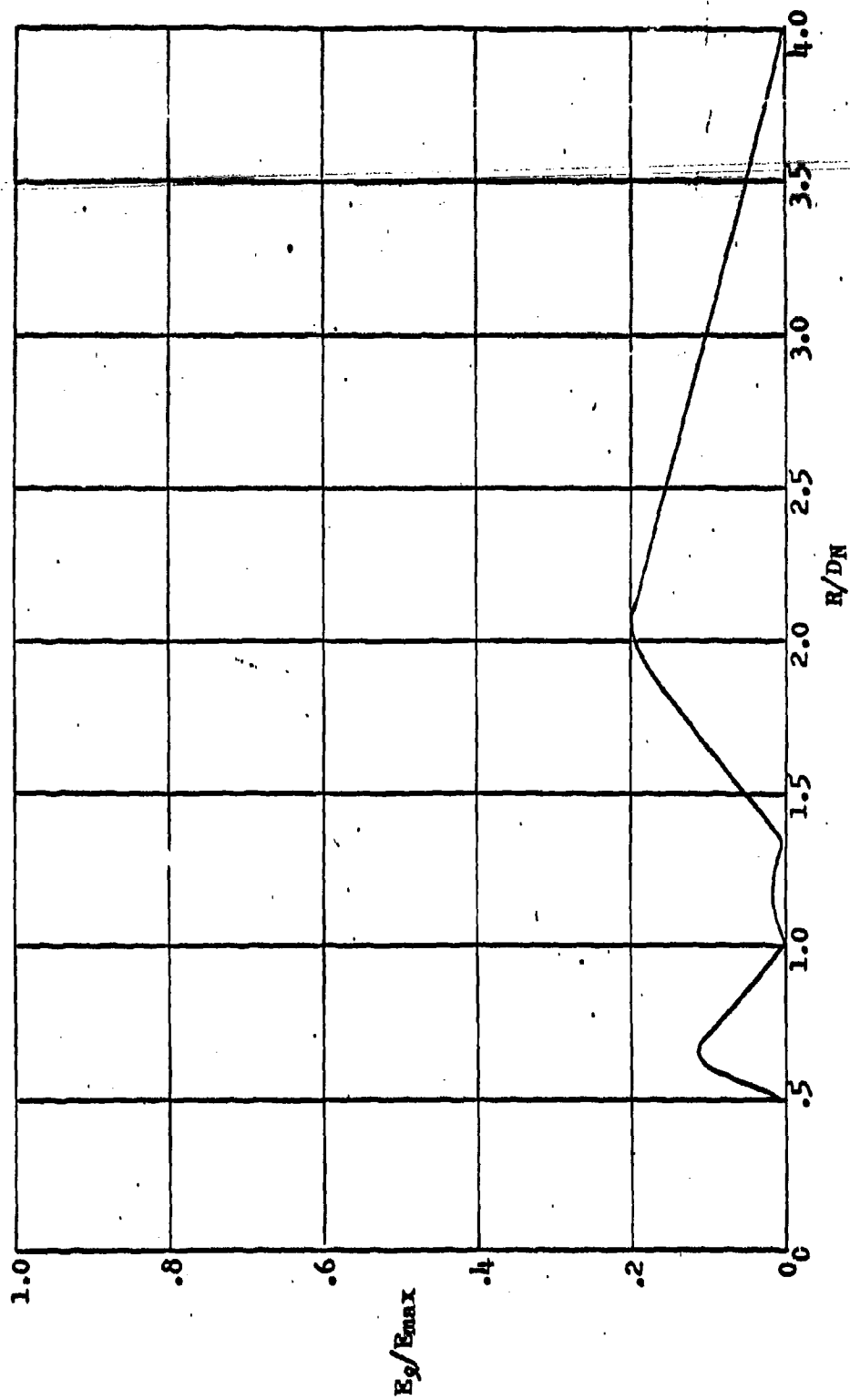


FIGURE 11b

INCIPIENT EROSION RATE FOR LIFT ENTRAINMENT
 PARTICLE DIAM. = .007 in, $V_j = 65$ ft/sec, $Z/D_N = .5$

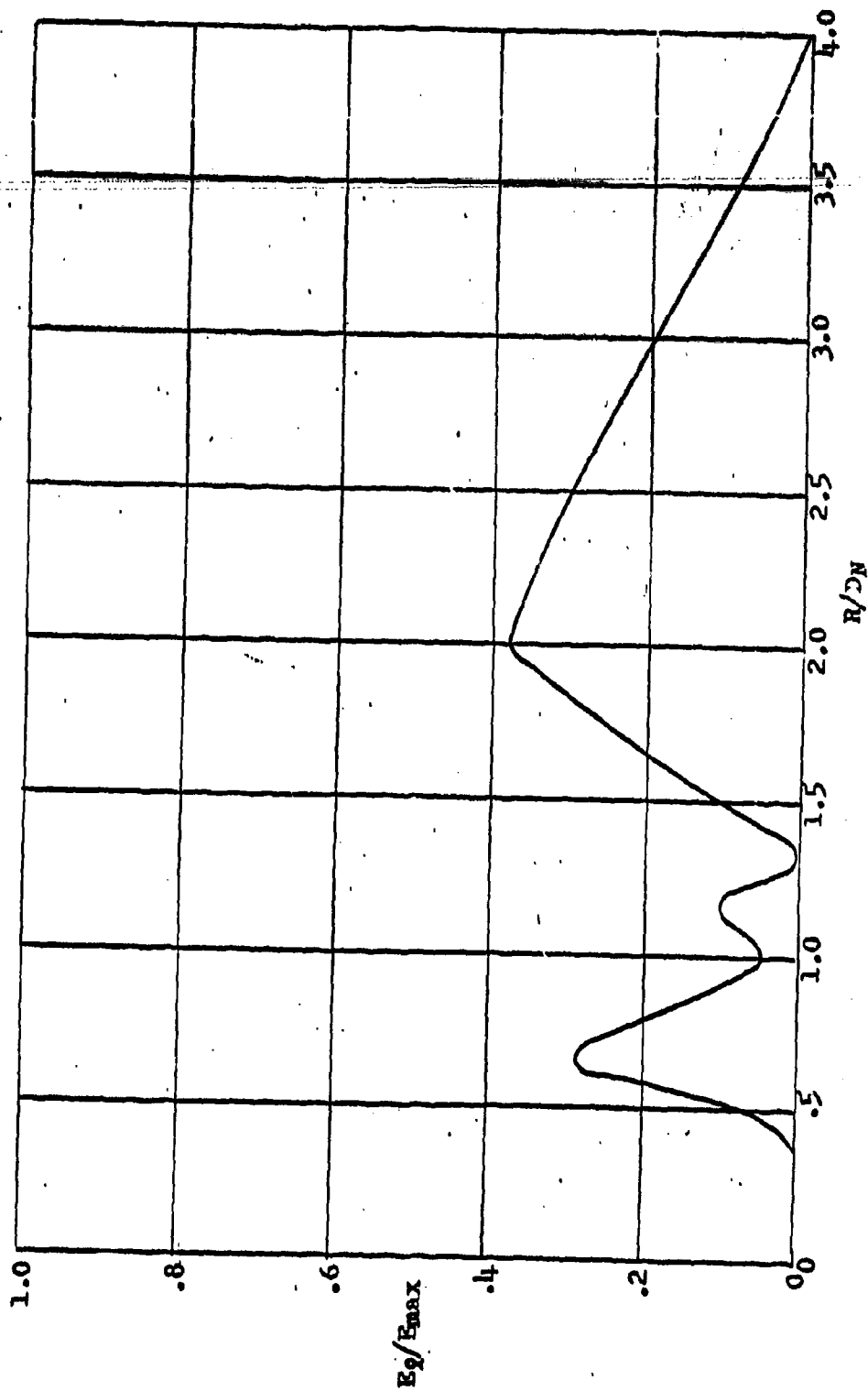


FIGURE 11c
 INCIDENT EROSION RATE FOR LIFT ENTRAINMENT
 PARTICLE DIAM. = .01 in, $V_J = 65$ ft/sec, $Z/D_N = .5$

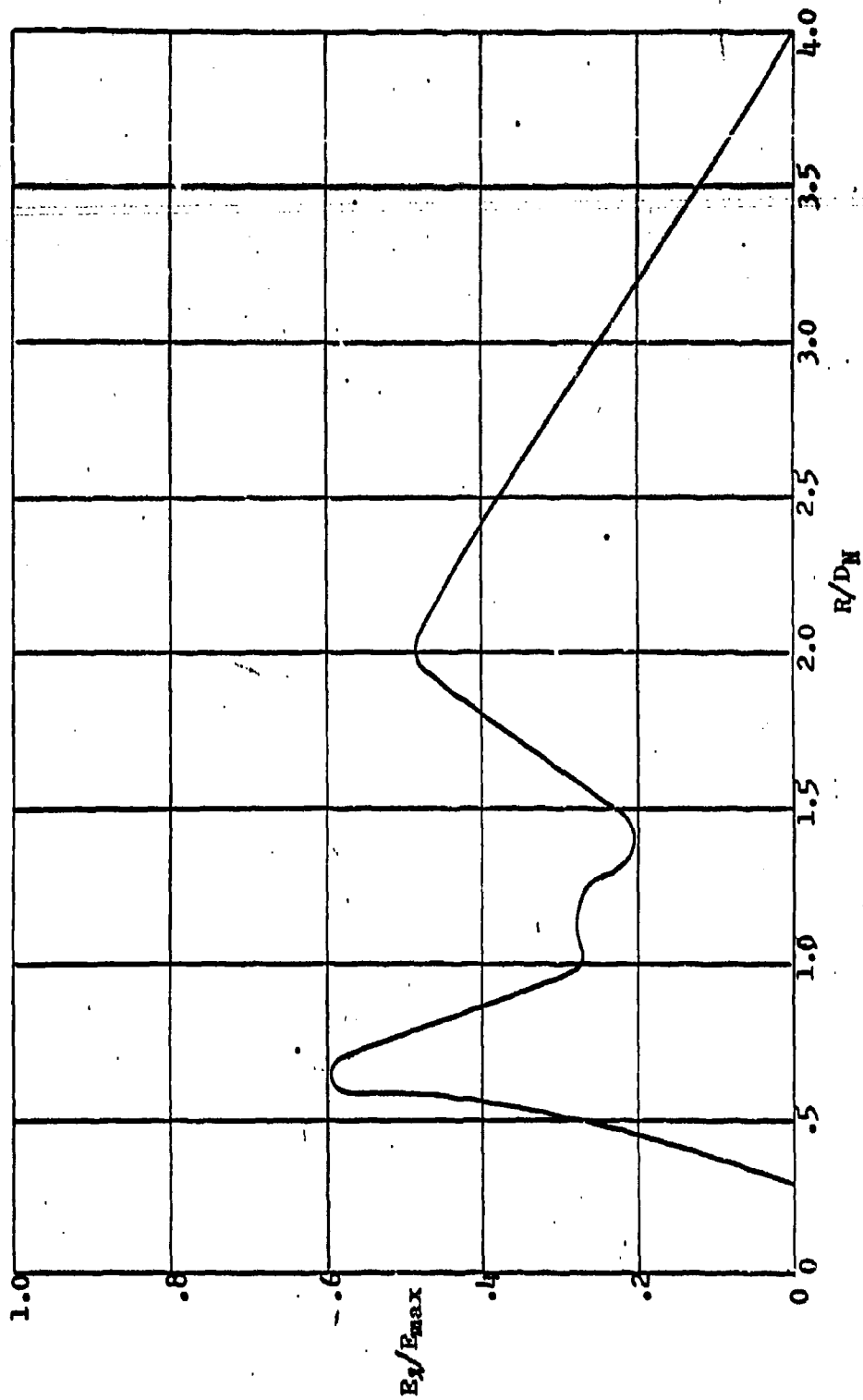


FIGURE 11d

INCIPIENT EROSION RATE FOR LIFT ENTRAINMENT
 PARTICLE DIAM. = .02 in, $V_J = 65$ ft/sec, $Z/D_N = .5$

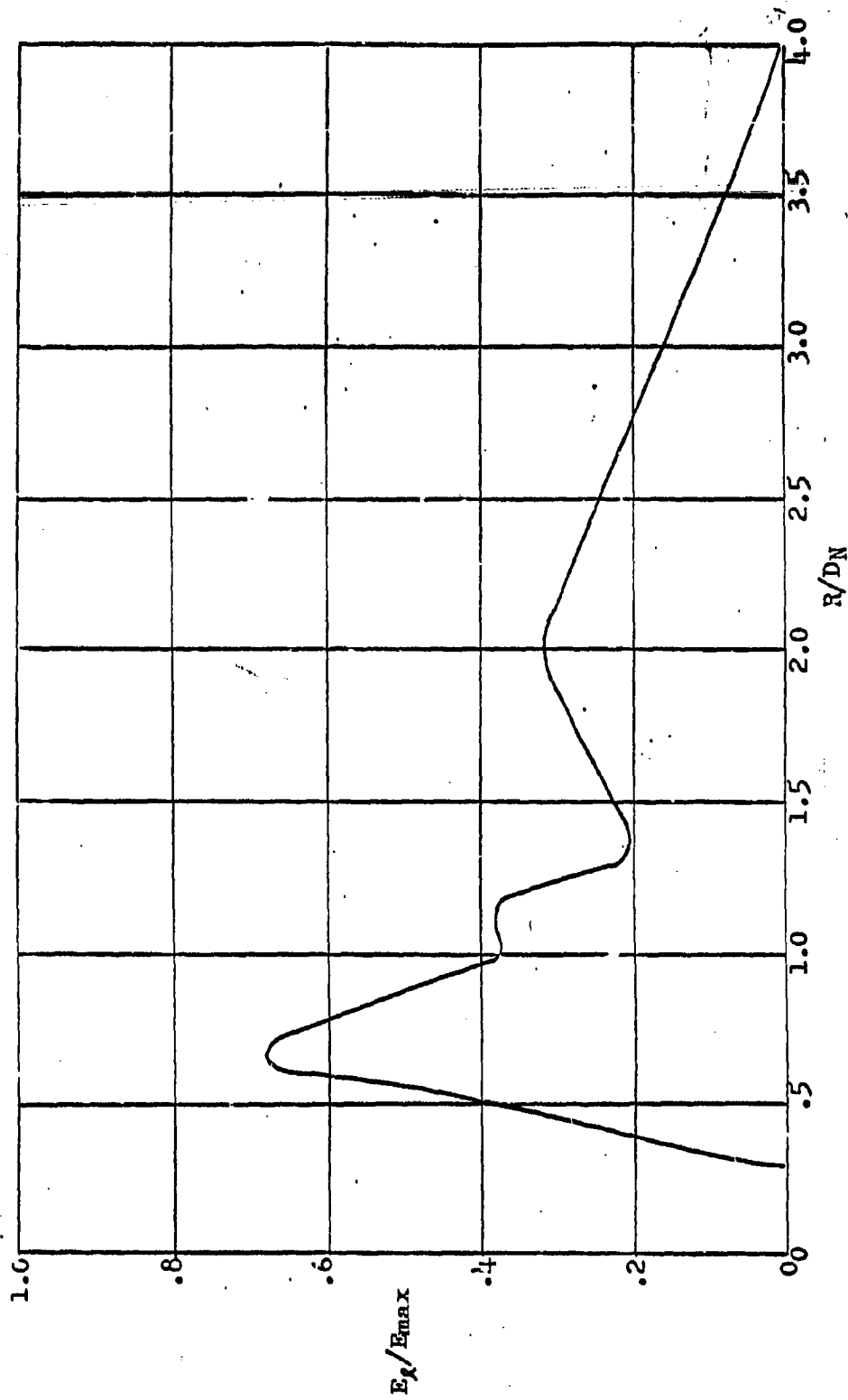


FIGURE 14.0

INCIPIENT EROSION RATE FOR LIFT ENTRAINMENT
 PARTICLE DIAM. = .04 in, $V_j = 65$ ft/sec, $Z/D_N = .5$

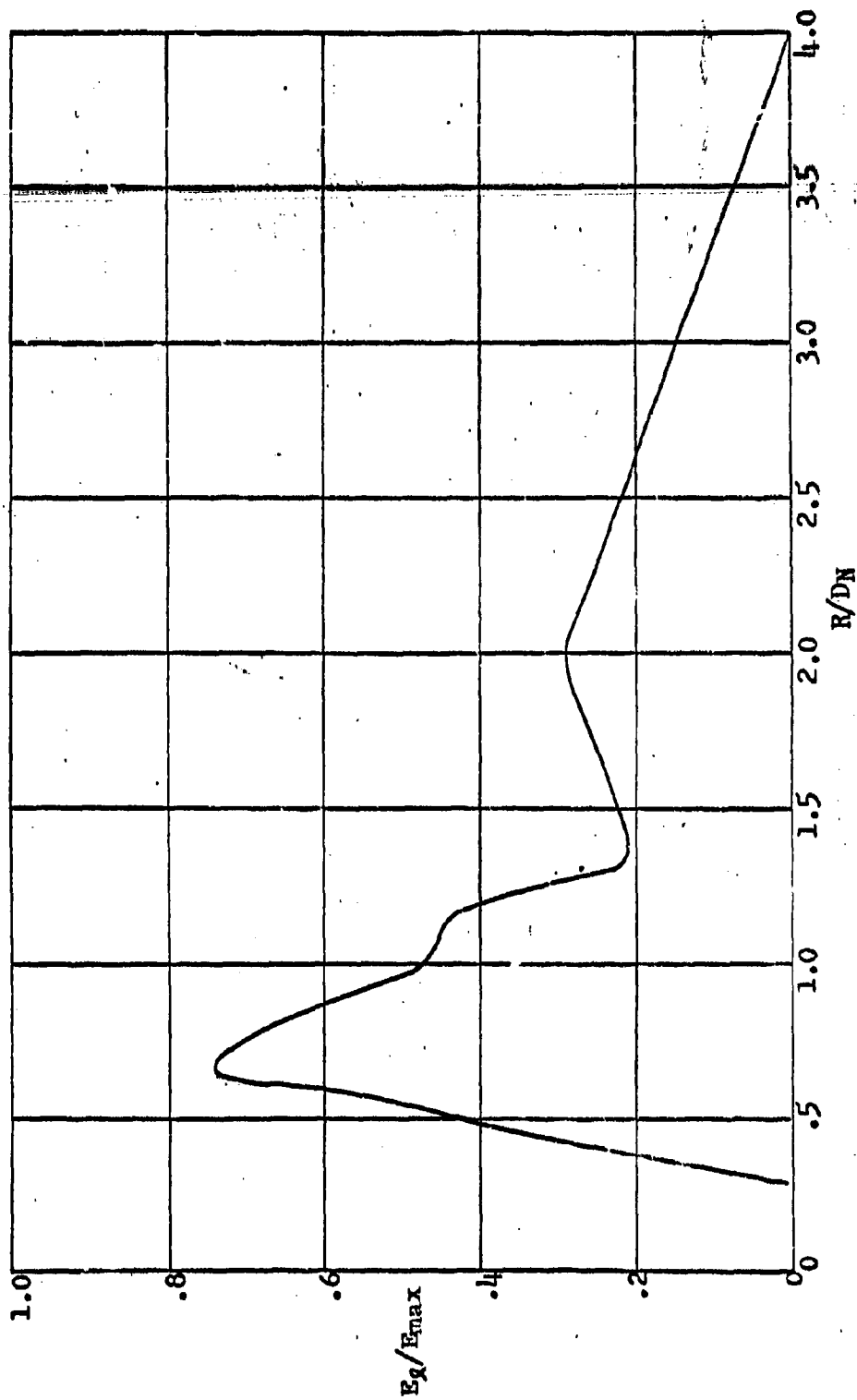


FIGURE 11f
 INCIPIENT EROSION RATE FOR LIFT ENTRAINMENT
 PARTICLE DIAM. = .06 in, $V_j = 65$ ft/sec, $z/DN = .5$

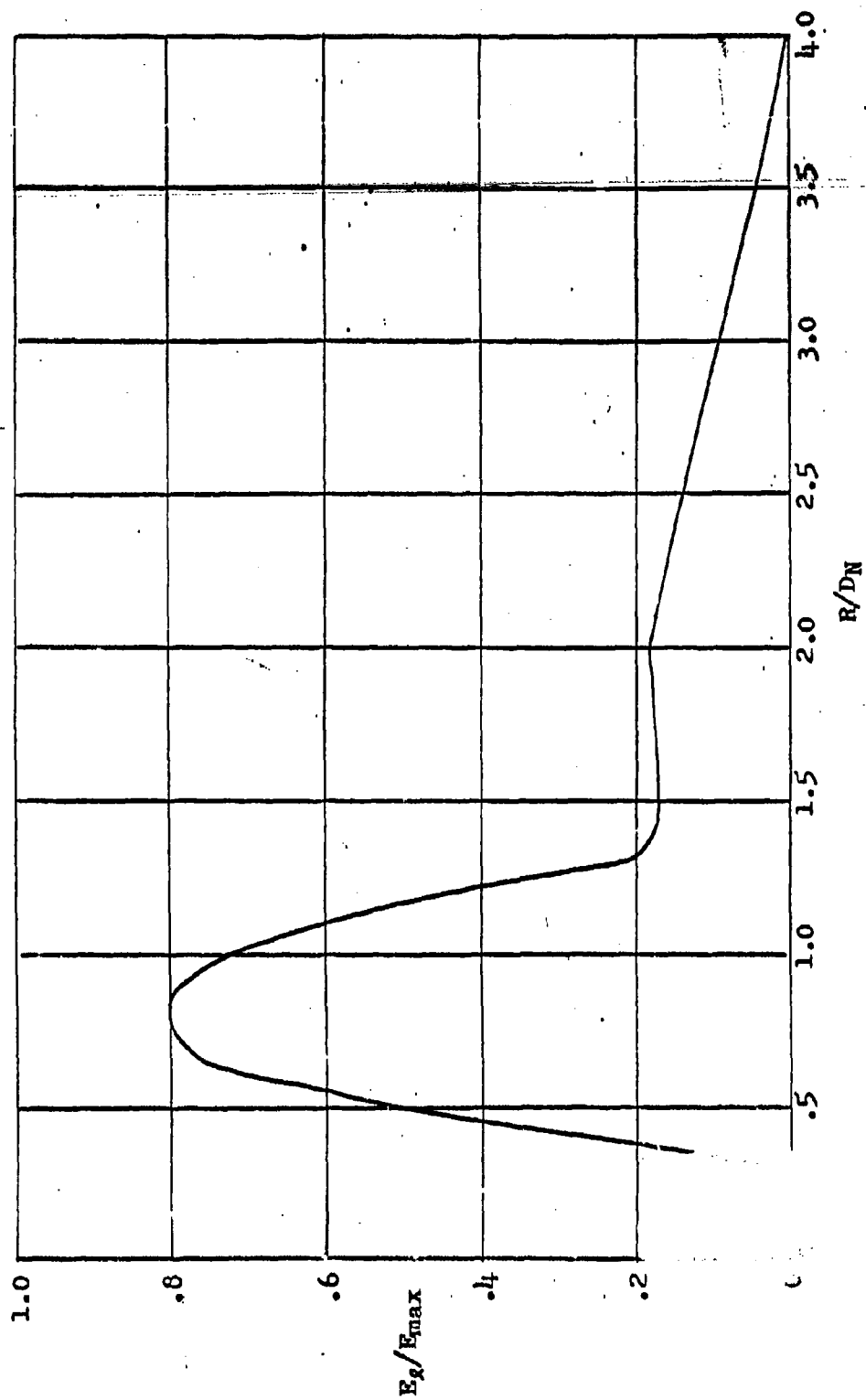


FIGURE 14g
 INCIDENT EROSION RATE FOR LIFT ENTRAINMENT
 PARTICLE DIAM. = .125 in, $v_j = 65$ ft/sec, $z/DN = .5$

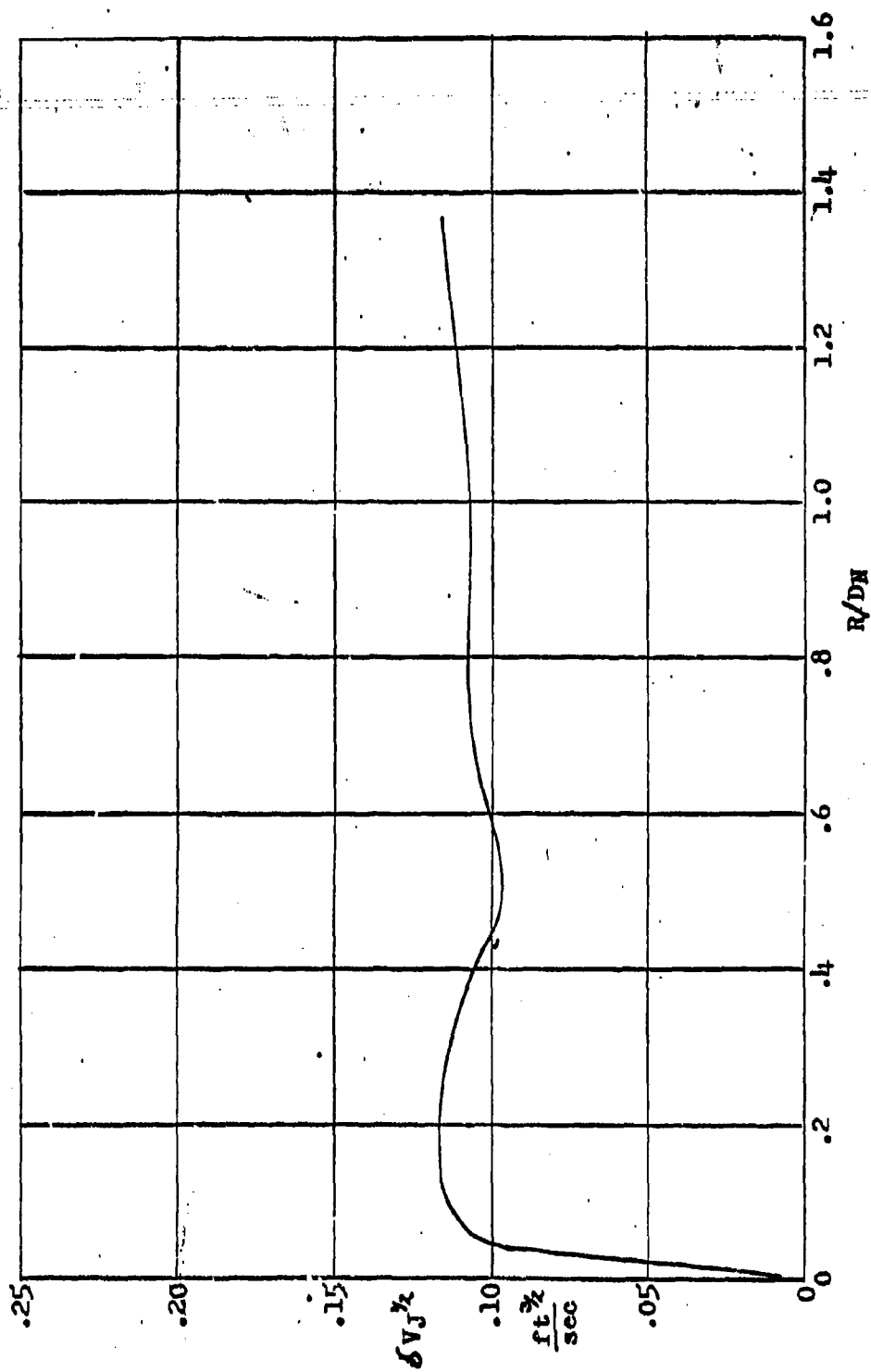


FIGURE 15
LAMINAR BOUNDARY LAYER THICKNESS

BIBLIOGRAPHY

1. AGARD, Ground Proximity and the VTOL aircraft, by P. E. Colin, Report 409.
2. ARC, The steady flow of a viscous fluid past a circular cylinder at Reynolds numbers 40 and 44, by C. J. Appelt. October, 1958. Reports and Memoranda No. 3175.
3. ARC, The forces on a cylinder in shear flow, by A. Thom. July, 1962. Reports and Memoranda No. 3343.
4. Bakke, P. An experimental investigation of a wall jet. Journal of Fluid Mechanics, v. 2, pt. 5, July 1957: 467-472.
5. Daughterty, R. L. and A. C. Ingersoll. Fluid mechanics with engineering applications. McGraw Hill Book Co., Inc., 1954.
6. Department of Mechanical Engineering, Stanford University, The plane turbulent wall jet, part 1. Jet development and friction factor, by G. E. Myers, J. J. Schauer, and R. H. Eustis. June 1961. Technical report no. 1.
7. Glauert, M. B. The wall jet. Journal of Fluid Mechanics, v. 1, pt. 6, December, 1956: 625-643.
8. Hall, I. M. The displacement effect of a sphere in a two-dimensional shear flow. Journal of Fluid Mechanics, v. 1, January, 1956: 142-162.
9. Hoerner, Sigward F. Fluid-dynamic drag, published by the author, 1958.
10. LeClerc, A. Deflection of a liquid jet by a perpendicular boundary. M. S. Thesis, State University of Iowa, 1948.
11. McLachlan, N. W. Bessel functions for engineers. Oxford University Press. 1934.
12. Milne-Thompson, L. M. Theoretical hydrodynamics. The Macmillan Co., 1960.
13. Murray, J. D. and A. R. Mitchell. Flow with variable shear past circular cylinders. Quart. Journal of Mechanics and Applied Mathematics, v. X, pt. 1, February 1957: 13-22.
14. NASA, An investigation to determine conditions under which downwash from VTOL aircraft will start surface erosion from various types of terrain, by R. E. Kuhn. September, 1959. TND-56.
15. NASA, An experimental study of the effect of downwash from a twin-propeller VTOL aircraft on several types of ground surfaces, by T. C. O'Bryan. May, 1962. TND-1239.

16. Pennsylvania State University. Table of Bessel functions to argument 85, by J. W. McClain. September, 1962. Engineering Research Bulletin B-85.
17. Salvadori, M. G. and M. L. Baron. Numerical methods in engineering. Prentice-Hall, Inc., 1952.
18. Schlichting, Herman. Boundary layer theory. McGraw Hill Book Co., Inc., 1960.
19. Smith, A. M. O. Rapid laminar boundary layer calculations by piecewise application of similar solutions. Journal of Aeronautical Sciences, v. 23, no. 10, October, 1956: 901-912.
20. Stiefel, E. L. An introduction to numerical mathematics. Academic Press, 1963.
21. Strand, T. Inviscid-incompressible-flow theory of static two-dimensional solid jets in proximity to the ground. Journal of the Aerospace Sciences, v. 29, no. 2, February, 1962: 170-184.
22. TRECOM, VTOL downwash impingement study, velocity survey, by Hiller Aircraft Corporation. August, 1960. Technical Report 60-58.
23. TRECOM, VTOL downwash impingement study surface erosion tests, by A. Morse. October, 1960. Technical Report 60-67.
24. TRECOM, Study of the VTOL downwash impingement problem, by Cornell Aeronautical Laboratory, Inc., November, 1960. Technical Report 60-70.
25. TRECOM, VTOL aircraft downwash impingement symposium. December, 1960. Technical Report 61-1.
26. TRECOM, Theoretical and experimental studies of impinging uniform jets, by Cornell Aeronautical Laboratory, Inc. April, 1963. Technical Report 63-11.
27. TRECOM, Downwash impingement design criteria for VTOL aircraft, by Dynasciences Corporation. August, 1964. Technical Report 64-48.
28. Vidal, Robert J. Aerodynamic processes in the downwash-impingement problem. Journal of the Aerospace Sciences, September, 1962: 1067-1086.
29. Vidal, Robert J. Corrections and Comments on Aerodynamic processes in the downwash impingement problem. AIAA Journal, v. 1, no. 3. March, 1963: 725.
30. Wentz, C. A. and G. Thodou. Total and form drag friction factors for the turbulent flow of air through packed and distended beds of spheres. American Institute of Chemical Engineers Journal, May, 1963: 358-361.

APPENDIX

FORTTRAN PROGRAMS

LIFT FORCES:

Input.

Program is generated from the polynomials describing the velocity profiles of the boundary layer, for various radial stations.

MM	Number of terms of the polynomial
PCOZ	Coefficients of the polynomial
QSH	Nondimensional shear velocity
VJ	Jet velocity
DN	Nozzle diameter
RG	Radial distance from jet centerline
ZG	Nozzle height above ground
YHVX	Distance to have maximum velocity in turbulent boundary layer
VMX	Maximum velocity in turbulent boundary layer

Intermediate Results and Output

DP	Particle diameter
VI	Inviscid velocity
YND	Nondimensional distance above ground
XND	Nondimensional roots of velocity profile polynomial
DNS	Particle density
DVX	Derivative of polynomial
SDVX	Slope of velocity profile
DUDY	Slope of velocity profile
FLSC	Shear lift (cylinder method)
SLFT	Shear lift (sphere method)
PLFT	Lift due to wall constraint
PLAC	Acceleration of particle in vertical direction

Subroutine Root finds the roots of the velocity profile polynomial

```

SUBROUTINE LIFT( MM,PCOZ, QSH,VJ,DN,RG,ZG,NCC,YHVX,VMX)
DIMENSION DP(10),RP(10), YQU(40),YGB(40),YL(70),YG(70),
1AR(70),VL(70),PCOZ(30),XL(40),FX(30),NLY(5),DVX(30),
2 DGB(5),PCOX(10),R(100),YND(120),XND(120),YND(50),XND(50),
3 VLD(50),YQDD(20)
DP(1)=.06
DP(2)=.04
DP(3)=.02
DP(4)=.01
DP(5)=.007
DP(6)=.125
DP(7)=.003
RGN=RG/DN
ZGN=ZG/DN
PRINT 611, DN
611 FORMAT(/// 22HNOZZLE DIAMETER (FT) = F5.2 )
PRINT 612, VJ
612 FORMAT( 26HNOZZLE VELOCITY (FT/SEC) = F7.1 )
PRINT 400,RGN
400 FORMAT(26HNONDIMEN RADIAL DISTANCE = F20.10)
PRINT 401, ZGN
401 FORMAT(28HNONDIMEN HEIGHTH OF NOZZLE = F20.10)
DO 115 II=1,7
PRINT 403, DP(II)
403 FORMAT(//23HPARTICLE DIAMETER(IN.)= F20.10)
RP(II)=DP(II)/2.
GNU=3.745E-7/2.3769E-3
IF(NCC-25)302,303,302
303 VI=VMX
GO TO 700
302 IF(ZG/DN-.5)640,640,661
661 KZG=ZG/DN
GO TO(640,641,640,643),KZG
640 IF(RGN-.35)60,60,61
61 IF(RGN-.75)18,18,19
19 IF(RGN-1.2)20,20,22
60 VI=VJ*SQRTE(ABSF(1.88*RGN**2-.225*RGN))
GO TO 700
18 VI=VJ*SQRTE(-3.2*RGN**2+5.13*RGN-1.26)
GO TO 700
20 VI=VJ*SQRTE(-2.68*RGN**2+5.48*RGN-1.82)
GO TO 700
22 VI=VJ*SQRTE(2.25*RGN**2-9.45*RGN+8.96)
GO TO 700
641 IF(RGN-.35)60,60,644
644 IF(RGN-1.0)645,645,647
645 VI=VJ*SQRTE(-.0985*RGN**2+1.13*RGN-.241)
GO TO 700
647 VI=VJ*SQRTE(.077*RGN**2-.641*RGN+1.354)
GO TO 700
643 IF(RGN-.40)62,62,654
654 IF(RGN-1.2)655,655,657
655 VI=VJ*SQRTE(-.5*RGN**2+1.2*RGN-.3)

```

```

GO TO 700
557 VI=VJ*SQRTF(.0404*RGNN**2-.318*RGNN+.744)
GO TO 700
62 VI=VJ*SQRTF(.625*RGNN**2+.025*RGNN)
700 ANCL=101.
016 TH=DP(II)/ANCL
NN=ANCL
NA=(NN+1)/2
R(1)=RP(11)
DO 1 K=2,NA
AA=K-1
XLC=AA*TH
1 R(K)=SQRTF(RP(11)**2-XLC**2)
100 IF(NCC-26)901,900,900
901 IF(NCC-25)704,705,900
705 YND(1)=R(1)/YHVX
GO TO 104
704 YND(1)=(R(1)/(12.*DN))*SQRTF(VJ*DN/GNU)
GO TO 104
900 AAA=VI/RG
YND(1)=R(1)*SQRTF(2.*AAA/GNU)/12.
104 XND(1)=0.0
IF(NCC-25)508,504,508
504 IF(YND(1)-.15)500,500,501
500 MM=8
DO 511 IZ=1,MM
511 PCOX(IZ)=PCOZ(IZ)
GO TO 508
501 MM=4
DO 502 I=1,MM
N=I+8
502 PCOX(I)=PCOZ(N)
506 DO 507 KW=1,MM
EX1=MM-KW
FX(KW)=PCOX(KW)*YND(1)**EX1
507 XND(1)=XND(1)+FX(KW)
GO TO 673
508 DO 71 KZ=1,MM
EX1=MM-KZ+1
FX(KZ)=PCOZ(KZ)*YND(1)**EX1
71 XND(1)=XND(1)+FX(KZ)
GO TO 673
105 CALL ROOT(1,MM,PCOZ,XND,YND,NCC)
573 IF(XND(1)-1.0)31,31,32
32 XND(1)=.9999
31 VL(1)=VI*XND(1)
706 ART=0.
DO 43 JZ=1,NA
IF(JZ-1)44,44,45
44 ARE=2.*R(JZ)*3.14159*TH
GO TO 43
45 ARE=4.*R(JZ)*3.14159*TH
43 ART=ART+ARE
SPA=RP(11)**2*4.*3.14159
ADS=SPA-ART
ADS=ADS/SPA
ACOR=1.+ADS
FLS=0.
DO 39 IZ=1,NA
IF(IZ-1)40,40,41
40 FL=-TH/2.*2.3769E-3*R(IZ)*VL(1)**2*OSH/144.
GO TO 39

```

```

41 FL=-TH*2.3769E-3*R(IZ)*VL(1)**2*QSH/144.
39 FLS=FLS+FL
   FLSC=FLS*ACOR
   APPROXIMATE SHEAR LIFT OF PARTICLE BY SPHERE METHOD
130 YGDD(1)=R(1)
   IF(NCC-25)132,77,129
77  YNDD(1)=YGDD(1)/YHVX
   GO TO 133
129 YNDD(1)=YGDD(1)*SQRTF(2.*AAA/GNU)/12.
   GO TO 133
132 YNDD(1)=(YGDD(1)/(12.*DN))*SQRTF(VJ*DN/GNU)
133 SDVX=0.0
   DO 74 KD=1,MM
   MX2=MM-KD
   EX1=MM-KD+1
   IF(NCC-25)75,79,75
79  PCOZ(KD)=PCOX(KD)
75  IF(KD-MM)180,181,180
180 DVX(KD)=EX1*PCOZ(KD)*YNDD(1)**MX2
   GO TO 74
181 DVX(KD)=PCOZ(KD)
74  SDVX=SDVX+DVX(KD)
   IF(SDVX)182,183,183
182 IF(NCC-25)184,183,184
184 SDVX=0.0
   IF(NCC-25)190,183,192
183 DUDY=SDVX*VMX/YHVX*12.
   GO TO 193
192 DUDY=SDVX*SQRTF(2.*AAA/GNU)*VI
   GO TO 193
190 DUDY=SDVX*SQRTF(VJ*DN/GNU)*VI/DN
193 ZON= R(1)/VL(1)*DUDY/12,
   CLF=0.345+0.557*ZON+0.879*ZON**2
   SLFT=CLF*2.3769E-3*VL(1)**2/2.*3.14159*R(1)**2/144.
   PRINT 800
800 FORMAT(14HNONDIMEN SHEAR,5X,17HNONDIMEN VELOCITY,5X,17HLIFT DUE TO
1  SHEAR,5X,17HLIFT DUE TO SHEAR,5X,19HAREA DIFFERENCE 0/0,3X,13HPRO
2FILE SLOPE)
   PRINT 801
801 FORMAT(3X,8HVELOCITY,11X,11HON CYLINDER,12X,10H(CYLINDER),13X,
1  8H(SPHERE)/)
   PRINT 802,QSH,XND(1),FLSC,SLFT,ADS,SDVX
802 FORMAT(6E20.10)
   GO TO 52
5  PRINT 200
200 FORMAT(/5HERROR/)
52  NNT=59
   UN=NNT
603 DGB(1)=0.
   YH=0.
   YLM=NNT-1
   YINC=DP(11)/YLM
   DO 169 J=1,NNT
   IF(J-1)666,111,112
111 YG(J)=0.
   GO TO 169
112 YG(J)=YH+YINC
   YH=YG(J)
169 CONTINUE
   DO 113 K=2,NNT
   YND(1)=0.
   IF(NCC-26)116,902,902

```

```

902 YND(K)=YQ(K)*SQRTF(2.*AAA/GNU)/12.
GO TO 113
116 IF(NCC-25)300,301,902
301 YND(K)=YQ(K)/YHVX
GO TO 113
300 YND(K)=(YQ(K)/(12.*DN))*SQRTF(VJ*DN/GNU)
113 CONTINUE
671 DO 672 NX=1,NNT
XND(NX)=0.
IF(NCC-25)708,720,708
720 IF(YND(NX)-.15)721,721,701
721 MM=8
DO 811 IZ=1,MM
811 PCOX(IZ)=PCOZ(IZ)
GO TO 708
701 MM=4
DO 702 I=1,MM
N=I*8
702 PCOX(I)=PCOZ(N)
DO 707 KW=1,MM
EX1=MM-KW
FX(KW)=PCOX(KW)*YND(NX)**EX1
707 XND(NX)=XND(NX)+FX(KW)
GO TO 672
708 DO 37 KL=1,MM
EX1=MM-KL+1
FX(KL)=PCOZ(KL)*YND(NX)**EX1
37 XND(NX)=XND(NX)+FX(KL)
672 CONTINUE
DO 95 KC=1,NNT
IF(XND(KC))33,35,35
33 IF(KC-1)38,38,51
38 XND(KC)=0.0
GO TO 35
51 XND(KC)=XND(KC-1)
35 IF(XND(KC)-1.0)95,34,34
34 XND(KC)=.9999
95 CONTINUE
FIND AVERAGE VELOCITY
96 SUMV=0.
DO 114 L=1,NNT
VL(L)=VI*XND(L)
114 SUMV=SUMV+VL(L)
VLAV=SUMV/UN
PLIFT=(2.3769E-3/2.)*VLAV**2*3.14167*(3./8.)*RP(11)**2/144.
PLIFT=-PLIFT
VOL=4./3.*3.14159*RP(11)**3
DO 730 MO=1,4
GO TO(731,732,733,734),MO
731 DNS=75.
GO TO 735
732 DNS=90.
GO TO 735

```



```

733 DNS=105,
GO TO 735
734 DNS=125,
735 PWT=DNS/1728.*VOL
PRINT 736, DNS
736 FORMAT(/18HPARTICLE DENSITY = F6.1)
PLTOT* PLIFT-PWT+FLSC
PMAS=PWT/32.16
PLAC=PLTOT/PMAS
IF(PLAC)842,843,843
842 PLAC=0.0
843 PRINT 110
110 FORMAT(/22HAVERAGE LOCAL VELOCITY,3X,16HLIFT ON PARTICLE,3X,
1 26HNET LIFT FORCE ON PARTICLE,4X,21HPARTICLE ACCELERATION)
PRINT 120
120 FORMAT(7X,8H(FT/SEC),7X,22HDUE TO WALL CONSTRAINT,30X,21HIN VERTIC
1AL DIRECTION/)
PRINT 840,VLA,V,PLIFT,PLTOT,PLAC
840 FORMAT(F20.10,E20.10,5X,F20.10,5X,F20.10/)
730 CONTINUE
GO TO 115
666 PRINT 667
667 FORMAT(/5HERROR)
GO TO 668
115 CONTINUE
668 RETURN
END
SUBROUTINE ROOT(NNT,MM,PCOZ,YND,XND,NCC)
DIMENSION YND(70),XND(70),PCOZ(30),DVX(30),FX(30)
DO 210 L=1,NNT
IF(NCC-24)199,199,201
199 IF(YND(L)-.425)200,201,201
201 XND(L)=0.1
106 SFX=0.
SDVX=0.
DO100N=1,MM
MX1=MM-N+1
MX2=MM-N
EX1=MX1
FX(N)=PCOZ(N)*XND(L)**MX1
IF(N-MM)101,102,101
101 DVX(N)=EX1*PCOZ(N)*XND(L)**MX2
GO TO 103
102 DVX(N)=PCOZ(N)
103 SFX=SFX+FX(N)
100 SDVX=SDVX+DVX(N)
RMX=(SFX-YND(L))/SDVX
IF(ABS(RMX)-.01)108,104,104
104 XND(L)=XND(L)-RMX
MLM=1000/MM
IF(XND(L)-2.**MLM)106,204,204
GO TO 210

```

```

108 IF(NCC-24)109,109,210
109 IF(NNT-2)210,210,110
110 IF(XND(L)-1.0)210,203,203
203 IF(YND(L)-2.0)204,204,205
205 XND(L)=.9999
    GO TO 210
204 IF(L-1)304,304,305
304 XND(L)=0.0
    GO TO 210
305 XND(L)=XND(L-1)
    GO TO 210
200 GO TO 210
210 CONTINUE
    RETURN
    END
    END

```

DRAG FORCE:

Input.

Program is generated in the same manner as the lift program.

Intermediate Results and Output.

DELT	Boundary layer thickness
XDEL	at top of boundary layer
FDT	Drag due to pressure force
FFDT	Drag due to friction
PWT	Particle weight
PDAC	Horizontal acceleration of particle

```

SUBROUTINE DRAG(PCOZ,MM,NCC,VJ,RG,ZG,DN,YHVX,VMX)
DIMENSION DP(10),UN(40),RP(10),YGU(40),YGB(40),YL(70),YG(70),
1 AR(70),YND(70),XND(70),VL(70),PCOZ(30),XL(40),FX(30),
2 XDEL(5),YMAX(5),PCOX(10),ARF(70)
DP(1)=.06
DP(2)=.04

```

```

DP(3)=.02
DP(4)=.01
DP(5)=.007
DP(6)=.125
DP(7)=.003
NN=31
RGN=RG/DN
ZGN=ZG/DN
PRINT 611, DN
611 FORMAT(22HNOZZLE DIAMETER (FT) = F5.2)
PRINT 612, VJ
612 FORMAT(26HNOZZLE VELOCITY (FT/SEC) = F7.1 )
PRINT 400, RGN
400 FORMAT(26HNONDIMEN RADIAL DISTANCE = F20.10)
PRINT 401, ZGN
401 FORMAT(28HNONDIMEN HEIGHT OF NOZZLE = F20.10)
DO 115 II=1,7
PRINT 403, DP(II)
403 FORMAT( 23HPARTICLE DIAMETER-IN. = F20.10 )
RP(II)=DP(II)/2.
UNI=NN
TK=RP(II)/(UNI-.5)
YLC=0.
SUMAR=0.
NAT=NN-1
DO 3 N=1,NAT
YL(N)=YLC+TK/2.
AM=N
XL(N)=SQRTF(RP(II) +2-YL(N)**2)
AR(N)=2.*XL(N)*TK
ARF(N)=4.*XL(N)*TK
IF(N-1)8,5,8
5 SUMAR=SUMAR+3.1416/2.*ARF(N)
GO TO 6
8 SUMAR=SUMAR+3.1416*ARF(N)
6 YGU(N)=RP(II)+YLC
YGB(N)=RP(II)-YLC
3 YLC=AM*TK
GNU=.0000003745/.0023769
IF(NCC-25)302,303,302
303 VI=VMX
GO TO 700
302 IF(ZG/DN-.5)640,640,661
661 KZG=ZG/DN
GO TO(640,641,643,643),KZG
640 IF(RGN-.35)60,60,61
61 IF(RGN-.75)18,18,19
19 IF(RGN-1.2)20,20,22
60 VI=VJ*SQRTF(RGN**2+.0175*RGN)
GO TO 700
18 VI=VJ*SQRTF(-3.2*RGN**2+5.13*RGN-1.26)
GO TO 700
20 VI=VJ*SQRTF(-2.68*RGN**2+5.48*RGN-1.82)
GO TO 700
22 VI=VJ*SQRTF(.256*RGN**2-1.48*RGN+2.311)
GO TO 700
641 IF(RGN-.35)60,60,644
644 IF(RGN-1.0)645,645,647
645 VI=VJ*SGRTF(-.0985*RGN**2+1.13*RGN-.241)
GO TO 700
647 VI=VJ*SQRTF(.077*RGN**2-.641*RGN+1.354)
GO TO 700

```

```

643 IF(RGN-.40)62,62,654
654 IF(RGN-1.2)655,655,657
655 VI=VJ*SQRTF(-.5*RGN**2+1.2*RGN-.3)
    GO TO 700
657 VI=VJ*SQRTF(.0404*RGN**2-.318*RGN+.744)
    GO TO 700
62 VI=VJ*SQRTF(.625*RGN**2+.025*RGN)
700 NNT=2*NN-3
    DO29N=1,NNT
        IF(N-NN)24,26,26
24 YG(N)=YGB(NN-N)
    GO TO 27
26 YG(N)=YGB(N-NN+2)
    IF(N-NN)27,27,28
27 AR(N)=AR(NN-N)
    GO TO 977
28 AR(N)=AR(N-NN+2)
977 IF(NCC-26)99,900,900
900 AAA=VI/RG
    YND(N)=YG(N)*SQRTF(2.*AAA/GNU)/12.
    GO TO 29
99 IF(NCC-25)978,301,900
301 YND(N)=YG(N)/YHVX
    GO TO 29
978 YND(N)=(YG(N)/(12.*DN))*SQRTF(VJ*DN/GNU)
29 CONTINUE
672 DO 805 NW=1,NNT
    XND(NW)=0.0
    IF(NCC-25)808,804,808
804 IF(YND(NW)-.15)800,800,801
800 MM=8
    DO 811 IZ=1,MM
811 PCOX(IZ)=PCOZ(IZ)
    GO TO 808
801 MM=4
    DO 802 I=1,MM
802 PCOX(I)=PCOZ(I+8)
806 DO 807 KW=1,MM
    EX1=MM-KW
    FX(KW)=PCOX(KW)*YND(NW)**EX1
807 XND(NW)=XND(NW)+FX(KW)
    GO TO 805
808 DO 809 KY=1,MM
    EX1=MM-KY+1
    FX(KY)=PCOZ(KY)*YND(NW)**EX1
809 XND(NW)=XND(NW)+FX(KY)
805 CONTINUE
75 DO 32 KC=1,NNT
    IF(XND(KC))33,670,670
33 IF(KC-1)72,72,73
72 XND(KC)=0.0
    GO TO 670
73 XND(KC)=XND(KC-1)
670 IF(XND(KC)-1.0)32,32,34
34 XND(KC)=.9999
32 CONTINUE
    IF(II-1)74,74,80
74 IF(NCC-25)78,76,79
79 DELT=4.6*12./SQRTF(2.*AAA/GNU)
    GO TO 80
76 XDEL=0.99
    CALL ROOT(1,MM,PCOX,XDEL,YMAX,NCC)

```

```

DELT=YMAX(1)*YHVB
GO TO 80
78 XDEL(1)=.99
CALL ROOT(1,MM,PCOZ,XDEL,YMAX,NCC)
DELT=YMAX(1)*DN/SQRTF(VJ*DN/GNU)*12.
80 GO TO 31
31 DO35K=1,NNT
35 VL(K)=VI*XND(K)
82 NMID=(NN1+1)/2
RN=VL(NMID)*DP(11)/(12.*GNU)
IF(RN=100.)730,730,731
731 IF(RN=10000.)732,732,733
730 CD=30./(RN*.699)
GO TO 734
732 CD=1.44/(RN*.0396)
GO TO 734
733 CD=1.18
734 FDT=0.
DO36K=1,NNT
FD=2.3769E-3*CD*VL(K)**2*AR(K)/288.
36 FDT=FDT+FD
ARS=4.*3.14159*RP(11)**2
ARD=ARS-SUMAR
ARD=ARD/ARS
ACOR=1.+ARD
CF=.664/SQRTF(RN)
FFDT=0.
DO40M=1,NNT
FFD=2.3769E-3*CF*VL(M)**2*ARF(M)/288.
40 FFDT=FFDT+FFD
CFB=4.*CF
TOL=ABS(CFB*.00001)
CALL CUBE(CFB,TOL,CFB3)
CBD=0.1/CFB3
FBDT=0.
DO 42 MD=1,NNT
FBD=2.3769E-3*CBD*VL(MD)**2*AR(MD)/288.
42 FBDT=FBDT+FBD
PRINT 38
38 FORMAT(/4X,16HPRESSURE DRAG-LB,4X,16HFRICITION DRAG-LB,8X,12HBASE D
1RAG-LB,2X,24HBOUNDARY LAYER THICKNESS,2X,31HSPHERE APPROXIMATION D
2IFFERENCE//)
PRINT 41, FDT,FFDT,FBDT,DELT,ARD
41 FORMAT( 3E20.10,2F20.10)
VOL=4./3.*3.14159*RP(11)**3
DO 720 MO=1,4
GO TO(721,722,723,736),MO
721 DNS=75.
GO TO 724
722 DNS=90.
GO TO 724
723 DNS=105.
GO TO 724
736 DNS=125.
724 PWT=DNS/1728.*VOL
PRINT 725,DNS
725 FORMAT(/18HPARTICLE DENSITY = F6.1)
TOTL=(FDT+FFDT+.707*PWT)*ACOR
PRINT 620, TOTL
620 FORMAT(/34HNET FORCE IN DIRECTION OF MOTION = E20.10)
PMAS=PWT/32.16
PDAC=TOTL/PMAS

```

```
      IF(PDAC)842,843,843
842 PDAC=0.0
843 PRINT 621, PDAC
621 FORMAT(/56HPARTICLE ACCELERATION IN HORIZONTAL DIRECTION (FT/SEC)
1E F20.10)
720 CONTINUE
115 CONTINUE
      IF(NCC-24)668,668,599
599 CONTINUE
668 RETURN
      END
```

SUPPLEMENTARY

INFORMATION

AD-475 412
Naval Postgraduate
School, Monterey,
Calif.
AN ANALYSIS OF GROUND
EROSION CAUSED BY
JET DOWNWASH
IMPINGEMENT.
1965

No Foreign without
approval of Naval
Postgraduate School,
Attn: Code 035,
Monterey, Calif.

No limitation

USNPS ltr,
21 Jan 69